Laser Induced Fluorescence Measurements of Spheromak Plasmas

Thesis by

Steven Edmund Pracko

In Partial Fulfillment of the Requirements

for the Degree of

Doctor of Philosophy

California Institute of Technology

Pasadena, California

2007

(Defended July 25, 2006)

Acknowledgements

The most elementary and valuable statement in science,
the beginning of wisdom, is "I do not know."

—Data, *Star Trek: The Next Generation*

I came to Caltech not knowing much about plasma physics and, as it turns out, knowing even less about myself. As I prepare to leave after all these years, I can say with confidence that I now know a little about plasma physics and a great deal more about who I am. All things considered, I couldn't have asked for a better result.

Although it appears first in these acknowledgements, I waited until after everything else in the thesis was finished before writing about Paul Bellan, because I wanted to take my time in considering what to say. I know with absolute certainty that I would not be graduating from Caltech with a Ph.D. had I joined any other professor's group. Paul granted me far more second chances to get this done than I rightly deserved, and I intend to prove his faith was well placed. While an outside observer can readily see that Paul values good science and good scientists, I know that above all else he wants his students to go on and lead fulfilling lives by following whatever path is right for them. Paul gave me the resources I needed to do my research, he gave me the opportunity to finish what I started, and when necessary he gave me a good swift kick in the rear to prod me into getting out of here.

I am grateful to the members of my defense committee: Noel Corngold, Roy Gould, and Oskar Painter. I thank them for three reasons. One, they all voted to pass me. Two, each asked genuinely insightful questions about the thesis work, and I appreciated the chance to explore those finer details together. Three, they all voted to pass me.

The worst part of experimental physics is that occasionally stuff blows up. The best part of experimental physics is that occasionally stuff blows up real good. (Poor grammar intentional.) If you're lucky, a brilliant engineer will be on hand to put all the

pieces back together again. I was blessed to work with two such individuals at Caltech. Frank Cosso is a living legend, and to this day I still relate anecdotes of his exploits, both professional and personal, to the new people in the group at every opportunity. Dave Felt became a guardian angel fending off the demons of entropy as they conspired to destroy each critical piece of apparatus just before I needed to use it for the very last time to complete this thesis. The laser, the vacuum chambers, the photomultiplier, the Encore amplifier, the capacitor banks—they all thank you, guys, and I thank you.

It's customary to mention the other students and researchers in one's group in this section, but it always bothers me when the names are all cited in one nondescript lump and you never get a sense of who those people are. I would rather give everyone his or her own separate acknowledgement.

I met Professor Raul Stern at the very beginning of my time with the Bellan group, as he had come to work with us that summer. At the time I had no idea who he was or what his importance was in the field in which I was about to be immersed. When he returned a few years later, I was able to appreciate fully the boon I had been granted to avail myself of his wisdom. The 1001 tips and tricks he shared for how to pull an LIF signal out of thin air cannot be learned in any book. To extend the science fiction theme started at the beginning of these acknowledgements, I count myself extremely fortunate to have been instructed by the Master Yoda of LIF.

If Raul Stern is Yoda, that makes Steve Sanders my Obi-Wan Kenobi, guiding me as I took my first steps into a larger world. Steve gave me my first lessons in how to operate and maintain the LIF equipment and explained how to identify a good signal.

Jimmy Yee was one of the first people to welcome me into the group at a time when I didn't know many people at Caltech and hadn't really taken the time to speak with anyone. In addition to teaching me how to make spheromaks in the laboratory, Jimmy also showed me that one can spend a considerable amount of time at Caltech and still move on to a successful career in a field outside science.

Freddy Hansen once saved my life. If not for his ability to speak French, however limited, I have no doubt that I would still be stranded in Quebec City, desperately trying to convince people to take pity on the wealthy American movie star. (That's my emergency plan in case I'm ever stranded in a foreign country where I don't speak the language—pretend that I'm a wealthy American movie star.) I admire Freddy for the balance he has been able to strike between his work and his social life. Let me take this opportunity to apologize publicly once again for the whole "Mr. Computer Monitor on Which Freddy is Writing His Thesis meet Mr. Bar Magnet" incident. However, in my defense, that was both a) a valuable scientific exercise to prove that a beam of non-neutral plasma can be deflected by a variable magnetic induction and b) funny.

In the acknowledgements of his thesis, Carlos Romero thanked me for helping him to understand American culture. However, he failed to mention that we discovered many of the cartoons he saw as a child in Mexico were the very same ones I watched growing up in Chicago. Isn't syndication wonderful? I've been fortunate to count Carlos as a good friend and colleague for many years. As he struggled through the writing and revising of his thesis, I imparted to him the same words of advice over and over: If you want to get out of here, shut up and do it the way Paul wants. Now that I've gone through the process, it's more apparent than ever that I was absolutely right.

Scott Hsu built the coplanar gun that made Chapter 4 possible, and since Chapter 4 accounts for nearly half of the entire thesis, I suppose that makes his contribution a relatively significant one. Much of my understanding of the physics underlying the formation and evolution of spheromaks in our experiments comes directly from Scott's work. Because of Scott, I also had the opportunity to be interviewed in person by a very lovely and very intimidating FBI agent. Never forget that you owe your security clearance to me.

Sett You kept the proud tradition of spheromak experiments rolling right along after Scott, and in so doing he provided me with those last few points of physical interpretation that have given my work at least the hint of usefulness. Maybe one day some other graduate student will make that multiple gas LIF experiment happen. Sett also motivated the group to adopt a central server for storing all our data, which made my job that much easier when it came time to pull together numbers for the thesis. I only regret that I didn't have enough time to teach him proper English. The last letter of the alphabet is not "zed."

Eli Jorne never paid his half for the framed Snoop Dogg/Tupac Shakur poster that graces the wall of our office, and because of that I find it hard to say anything nice about him. On the other hand, he did build the power supply that I later commandeered for the portable plasma device, so perhaps that makes us even in the great cosmic scheme of things. In all seriousness, Eli made it entertaining to come to the office every day, and he introduced us to Don Wheatley, who always had the parts we needed for our experiments.

I know Deepak Kumar has been waiting extremely impatiently to read what I have to say about him here. Some might consider it a tad presumptuous to assume that you're going to mentioned in a person's acknowledgements, but I'm willing to let that slide. Without a doubt Deepak has been the target of the most ribbing in our office, and he has always been a good sport and taken it in the spirit of friendship with which it was intended. For that, he earns my respect. Deepak is an excellent researcher in the lab and a diligent student, and I've enjoyed observing as his interests have branched out from plasma physics to include karate and the fearsome Robot-Truck.

I owe Shreekrishna Tripathi many times over for the assistance he provided in the lab and in dealing with our ornery computers, but even more so for the warmth of his friendship. It is because of his knowledge of IDL keywords that the plots in this thesis came out looking just right. Whether through the sharing of amusing anecdotes about life in the villages of India or through the hospitality he and his wife showed in opening up their home to have the group over for dinner, Shreekrishna has always been a source of positive energy to elevate everyone's spirits.

Thanks to Gunsu Yun, I am fully capable of serving as the head of a household in eastern South Korea, but perhaps the details of that assertion are best left within the circle of those who already know. I am grateful to Gunsu for donating his time to run the spectrometer to provide the data on page 104. That's not just a spectrum—it's a work of art. I've found Gunsu's work ethic in the lab, as well as his thoroughness and attention to detail, to be without equal.

I'll resist the temptation to make the cheesy joke about how fitting it was that the first female graduate student to join the Bellan group full time is named Eve. As soon as Eve Stenson inherited the solar prominence experiment, she put her own personal gymnast's touch on it; the gas valves that used to lie horizontally now stand up straight and look like they're doing handstands. Eve is also continuing the tradition of Bellan group members becoming involved with the Caltech Graduate Student Council. I truly hope she doesn't wind up sticking around there for quite as long as I did.

It is with deepest regret that I must inform Auna Moser that she needs to carry her keys with her all the time from now on, because I won't be around to unlock the office door anymore. This was a big problem at first, but she's gotten better. Maintaining my sanity at Caltech always relied heavily upon having someone else in the office who could keep up with at least some of the ‘80s pop culture references that form the basis of my language. It turns out that not many Techers were raised on a steady diet of MTV like I was. Thankfully, Auna was there at the end to fill that gap, even though she inexplicably does not possess the proper level of appreciation for Mötley Crüe. (Work on that, Auna.) Even though she's one of the newest members of the group, Auna is already blowing up high voltage power supplies like an old pro.

If I ever need a guitarist to play “Stairway to Heaven,” I know I can call on Rory Perkins. Unfortunately, if I ever need a guitarist to play any other song that's ever been written, I'm going to have to look somewhere else. Many times Rory would come into the office and say he had a good feeling that one of us was going to do some Nobel Prize calibre work that day. I'm going to go out on a limb and make the bold prediction that, if any Bellan alumnus or alumna ever does win a Nobel, it'll be Rory. Don't let me down.

There are far too many Caltech staff and administrators to thank individually, so I'll give them a collective acknowledgement here. Whether it was wading through bureaucratic red tape on my behalf or making sure that money got to where it needed to be, they've been a tremendous support system. I'll now break my own rule and thank all the Bellan group administrative assistants with whom I worked: Greg Dunn, Eleonora Chetverikova, Mary Metz, and Connie Rodriguez. Extra special thanks to Professor Michael Hoffmann and Natalie Gilmore in the Graduate Office for services rendered.

I dedicate this thesis to my family, because they have dedicated so much of their lives to me. My sister has always done her best to keep me grounded and to never let me get too full of myself, a common malady among academics. So many of the qualities that make me who I am come straight from my parents. After my devilishly handsome good looks, the most valuable trait I inherited is an indomitable tenacity that many people at Caltech came to know... and fear. There were points in this journey where the easy choice, and perhaps the most advisable choice, would have been to give up, but that is not in my nature. If I had wanted easy, I wouldn't have come to Caltech. This challenge is finally over, and I'm hungry for the next one.

Mission accomplished.

Only in America.

Abstract

This thesis reports the results of investigations intended to further the understanding of the formation and evolution of spheromak plasmas via the use of laser induced fluorescence (LIF) measurements of laboratory plasmas. LIF is a spectroscopic technique in which laser radiation induces atomic energy level transitions in a target species within a specified volume.

LIF experiments have been performed on Ar II plasmas produced in a spheromak confinement configuration. The term spheromak refers to a class of plasmas whose internal magnetic fields satisfy a particular topology, the details of which are presented as they relate to the formation and evolution of plasmas generated in this work. LIF measurements made on these spheromak plasmas suggest that 20 eV Ar II ions have been produced at densities of 10^{21} m^{-3}.

LIF experiments studying plasmas generated by a second spheromak device are discussed. The planar electrodes in this new device produce spheromaks with a distinct central column of plasma whose evolution is related to α, an important parameter in the theory of force-free Taylor states, where the internal magnetic field $\mathbf{B}$ of the plasma satisfies $\nabla\times\mathbf{B}=\alpha\mathbf{B}$. Experiments have been conducted with the probing laser oriented both parallel to and perpendicular to the axis of symmetry of the spheromak. Ion parameter estimates calculated from LIF measurements are found to agree with those obtained from other diagnostics, including passive spectroscopy and high speed photography.

Details are presented concerning the design and operation of a portable device capable of generating plasma discharges. The motivation for the construction of this device is to provide a convenient plasma source that may be used to calibrate the laser and photodetection systems used in LIF experiments.

The Ar II ion temperature and density values reported in this work are believed to be among the first such measurements performed on plasmas produced in a spheromak confinement configuration. Suggestions are offered for several modifications that could be made to the experiment that might serve to increase the amount of information that can be gained during each plasma discharge and thus augment the future value of the experiment.

Table of Contents

List of Figures

Chapter 1
Introduction

This thesis reports the results of investigations intended to further the understanding of the formation and evolution of spheromak plasmas via the use of laser induced fluorescence (LIF) measurements of laboratory plasmas.

Chapter 2 introduces the physical principles that form the basis of the laser induced fluorescence diagnostic. LIF is an active spectroscopy technique in which laser radiation is used to induce atomic energy level transitions in a target species within a specified volume. LIF has applications in a variety of fields, including plasma physics, where it is frequently employed in the study of ion temperature and/or density (Stern 1975, for example). A discussion is presented of how the combination of these plasma parameters, electromagnetic fields applied to the plasma, and even the probing laser itself can affect the fluorescent emission spectrum of the plasma and how measurement of this spectrum provides information about plasma behavior.

Chapter 3 reports the results of an LIF experiment that has been performed on Ar II plasmas produced in a spheromak confinement configuration. The term spheromak refers to a class of plasmas whose internal magnetic fields satisfy a particular topology, the details of which are presented as they relate to the formation and evolution of plasmas generated in this experiment. Electrostatic breakdown of plasma occurs between two coaxial cylindrical electrodes; MHD $\mathbf{J}\times\mathbf{B}$ forces then propel the plasma into a large vacuum chamber where it is intercepted by the probing laser that induces fluorescent emission. Fluorescent light from the plasma is ultimately collected by a photomultiplier tube located outside the vacuum chamber. A noteworthy feature of this work is that the plasma discharge has been synchronized with a pulsed laser system; the method by which this is accomplished may be of interest in other applications requiring the interaction of two such independent sequences of time-critical events. The spectral line broadening models discussed in Chapter 2 are fitted to the data collected in this experiment relating the intensity of emitted fluorescent light from the plasma to the wavelength of the probing laser. This analysis includes a discussion of the Voigt model that assumes the presence of broadening effects associated with both ion temperature and ion density. The LIF measurements performed on these spheromak plasmas suggest that 20 eV Ar II ions have been produced at densities of approximately 10^{21} ions/m^3.

Chapter 4 continues the discussion of experimental results, focusing on LIF measurements conducted on plasmas that are generated by a second spheromak device. The primary difference between this new device and that used in the experiments described in Chapter 3 is the electrode configuration used in the electrostatic breakdown of gas to form plasma. The planar geometry of the electrodes employed in this new device produces spheromaks with a distinct central column of plasma whose evolution is related to α, an important parameter in the theory of force-free Taylor states (Taylor 1974). In force-free states, including spheromaks, relaxation to a minimum-energy magnetic topology requires that the internal magnetic field **B** of the plasma satisfy $\nabla\times\mathbf{B}=\alpha\mathbf{B}$.

The LIF experiments performed on plasmas produced by this planar spheromak gun have benefitted from experience acquired during the investigations conducted on the previous coaxial spheromak device. Several improvements have been made to the experimental apparatus that are intended to promote plasma discharge repeatability and to enhance the quality and magnitude of measured induced fluorescence signals. LIF measurements of ion parameters have been made with the probing laser beam oriented both parallel to and perpendicular to the axis of symmetry of the spheromak, exploiting the spatial resolution and orientation-sensitivity offered by the LIF diagnostic. An ~30 km/s ion propagation velocity is measured along each of these directions, suggesting that the plasma may be freely expanding into the vacuum chamber after it emerges from the plasma gun. Ion parameter estimates provided by LIF are found to agree with those obtained from other diagnostics, including passive spectroscopy (measuring ion density) and visible light photography by a high speed framing camera (measuring ion propagation velocity).

Chapter 5 describes the design and operation of a portable device capable of generating plasma discharges. The motivation for the construction of this device is to provide a convenient plasma source that may be used to calibrate the laser and emitted light detection systems used in the spheromak LIF experiment. Details of the assembly of the portable device are presented, along with typical operating characteristics. A discussion of the results of preliminary experiments aimed at detecting an LIF signal from Ar II plasmas produced in this device notes how the operating regime of the device might be enhanced to produce stronger fluorescence signals without sacrificing the device's portability. The compact size of the device (~30 cm length, ~5 kg weight) and its modular design create the possibility that the device could be used in a variety of other applications.

Finally, Chapter 6 summarizes the results presented in this thesis. The Ar II ion temperature and density values reported in this work are believed to be among the first such measurements performed on plasmas produced in a spheromak confinement configuration. Certain characteristics of the present experiment limit the degree of understanding of spheromak behavior that may be drawn from these findings. Suggestions are offered for a number of modifications that could be made to the experiment that might serve to increase the amount of information that can be gained during each plasma discharge and thus augment the future value of the experiment.

1.2 References

R.A. Stern and J.A. Johnson III, "Plasma ion diagnostics using resonant fluorescence," *Phys. Rev. Let.*, **34(25)**, 1548 (1975).

J.B. Taylor, "Relaxation of toroidal plasma and generation of reverse magnetic fields," *Phys. Rev. Let.*, **33(19)**, 1139 (1974).

Chapter 2
Laser Induced Fluorescence

2.1 Introduction

The investigations described in this thesis involve the application of a laser induced fluorescence (LIF) diagnostic to study argon spheromak plasmas produced by two plasma generating devices. A brief overview of LIF theory and methodology will be useful in understanding the subsequent discussion of these experiments; therefore, this chapter presents a summary of salient principles.

2.2 Laser Induced Fluorescence

Laser induced fluorescence is a sensitive spectroscopic technique that may be implemented in a variety of fields, including plasma physics. LIF utilizes laser radiation to selectively excite a particular electron energy level transition in a target species. This feature of LIF endows the diagnostic with an important advantage over passive spectroscopy, in which measurements entail the integration of all light along the line-of-sight of the detector: The region of plasma probed by laser induced fluorescence can be made arbitrarily small by adjusting the volume defined by the intersection of the laser beam and the viewing angle of the emitted light detector, as illustrated in Figure 2.1. Thus, LIF offers superior spatial resolution to that offered by passive spectroscopy.

2.2.1 Energy Level Transitions

In a standard LIF experiment, the probing laser beam is tuned to the resonant wavelength of a known energy level transition in the species under investigation. As shown in Figure 2.2, a target ion that is able to absorb laser light at a wavelength λ_{IE} will undergo a transition from an initial energy state to a second, intermediate state. The ground state of the species under investigation is typically not chosen for the initial state,

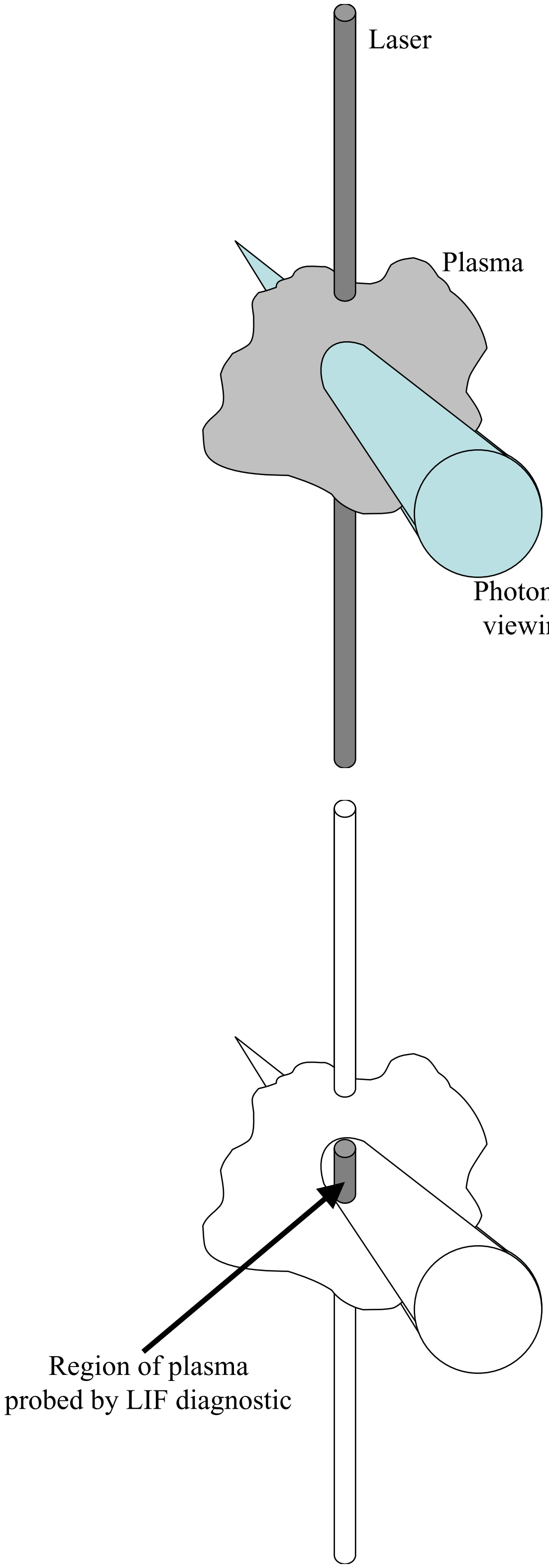

Figure 2.1. Schematic representation of an LIF experiment, illustrating the relationship between the plasma and the relative orientations of the laser beam and photomultiplier field of view. Only the shaded volume of plasma shown in the bottom figure will be probed by the LIF diagnostic.

as the input energy required for transitions from the ground state often lies outside the visible spectrum used in most commercial lasers. A metastable excited state is customarily chosen instead.

From the intermediate state, the ion will decay to one of a number of final states, including de-excitation back to the initial state. However, the ion may also transition to a new final state by emitting a photon of wavelength λ_{EF}. Consequently, measurement of fluorescent light emitted from the plasma at λ_{EF}, above that produced by spontaneous emission in the absence of the laser, will yield information regarding the absorption of laser radiation λ_{IE} by the initial state—more absorption at λ_{IE} will result in more fluorescence at λ_{EF}. Various parameters of the plasma under investigation, including ion temperature and density as well as the presence of external electromagnetic fields, can affect the distribution of ions that will experience induced fluorescence in response to a given laser wavelength. LIF can provide estimates for these plasma parameters via experimental measurement of this distribution.

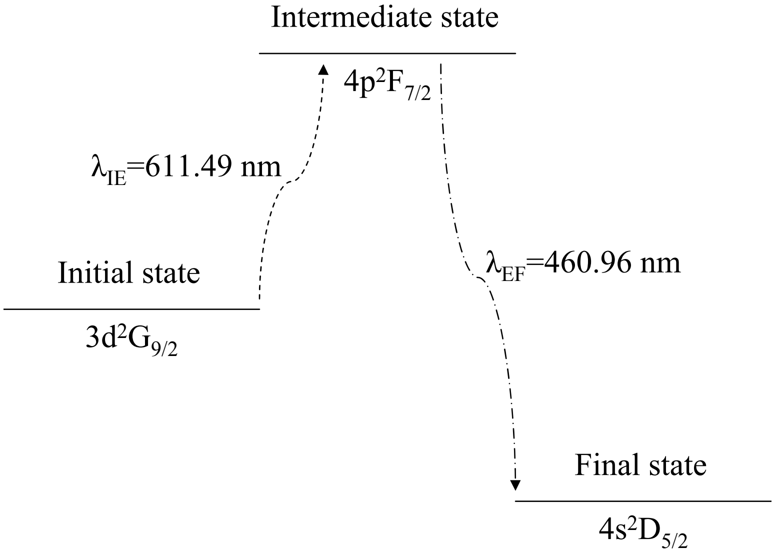

Figure 2.2. Representative LIF energy level transition scheme. The 611.49–460.96 nm transition is used in the work presented in this thesis.

2.2.2 Narrowband/Broadband Considerations

An important consideration in any LIF experiment is the bandwidth of the probing laser relative to the width of the ion distribution function. If the laser bandwidth is much broader than the distribution function, then nearly all of the ions in the initial energy state will transition to the intermediate state. In order to extract useful information regarding plasma parameters, a narrow bandwidth photodetection system must be employed to measure emitted fluorescent light—for example, a spectrometer with good spectral resolution. In this “broadband” configuration, the ion distribution function will be measured along the direction of viewing of the photodetector.

If the bandwidth of the scanning laser is narrower than the ion distribution function, then a second, “narrowband” mode of operation is possible. In this case the wavelength of the laser can be scanned across the transition resonance, exciting only a fraction of the total distribution function at a time. A narrow bandwidth emitted light collection apparatus may still be used; however, a collection apparatus with bandwidth wider than that of the distribution function can be employed as well. When using a broad bandwidth photodetector, it is assumed that any induced fluorescence above spontaneous emission results from only those ions excited by the narrow bandwidth laser; the precise wavelength of the fluorescent light is not measured, and the ion distribution will be computed as a function of input laser wavelength. Thus, the ion distribution function in “narrowband” operation is measured along the direction of laser propagation and not that of the photodetector. All LIF measurements described in this thesis have been performed using the combination of a narrow bandwidth laser and a broad bandwidth detector.

2.3 Line Broadening Mechanisms

This section introduces the principal mechanisms that can cause spectral broadening of a measured LIF distribution function.

2.3.1 Doppler Broadening

For ions with finite velocity **v** along the direction of laser propagation, the wavelength of laser light "seen" by the ions will be Doppler shifted according to the relation

$$\lambda = \left(1 + \frac{\boldsymbol{v} \cdot \hat{\boldsymbol{k}}}{c}\right)\lambda_0 \tag{2.1}$$

where λ_0 is the laser wavelength in the laboratory frame and **k** is the direction of laser propagation. This can also be expressed as

$$\frac{\lambda - \lambda_0}{\lambda_0} = \frac{v_{\parallel}}{c} \tag{2.2}$$

If it can be assumed that the plasma ion velocity distribution $f(v_{\parallel})$ is Maxwellian, then

$$f(v_{\parallel}) = \sqrt{\frac{m_i}{2\pi\kappa T_i}}\exp\left(\frac{-m_i(v_{\parallel} - u)^2}{2\kappa T_i}\right) \tag{2.3}$$

where u is the mean ion propagation velocity, T_i the ion temperature, and m_i the ion mass. To use Equation 2.3 to determine the ion temperature T_i via a measurement of the induced fluorescent emission from the plasma, a relationship between the distribution function $f(v_{\parallel})$ and the observed light intensity I(λ) is required. The wavelength of incident laser light seen by a plasma ion is dependent upon the parallel component of the ion's velocity; this argument can be extended to an assertion that the intensity of induced fluorescent emission in response to a given laser wavelength will be proportional to the number of ions moving with the necessary velocity to absorb the incident laser light at the wavelength necessary to undergo an energy level transition. In other words, the relationship between I(λ) and $f(v_{\parallel})$ is given by

$$I_{DOPPLER}(\lambda)\, d\lambda \sim f(v_{\parallel})\, dv_{\parallel} \tag{2.4}$$

Combing Equations 2.2, 2.3, and 2.4 yields

$$I_{DOPPLER}(\lambda) = \sqrt{\frac{m_i c^2}{2\pi\kappa T_i \lambda_0^2}}\exp\left[\frac{-m_i}{2\kappa T_i}\left(\frac{c(\lambda - \lambda_0)}{\lambda_0} - u\right)^2\right] \tag{2.5}$$

Thus, the observed intensity of induced fluorescence as a function of incident laser wavelength should have a Gaussian shape. Equation 2.5 is maximized when the argument of the exponential term is 0. This immediately provides an expression for u, the mean ion propagation velocity

$$u = \left(\frac{\lambda_{PEAK} - \lambda_0}{\lambda_0}\right) c \tag{2.6}$$

where λ_{PEAK} is the laser wavelength in the laboratory frame that induces the maximum fluorescent signal.

The half-width of the intensity distribution function in Equation 2.5 provides the desired relationship between the measured induced fluorescent emission from the plasma and the ion temperature

$$T_i = 1.7 \times 10^8 \mu \left(\frac{\Delta\lambda_{FWHM}}{\lambda_0}\right)^2 \tag{2.7}$$

where T_i is measured in eV and μ is the mass number of the ion.

It should be noted that the induced fluorescent light emitted from the plasma will itself be Doppler shifted as seen by the photodetector, as noted in the earlier discussion of broadband and narrowband LIF techniques. However, a detector possessing even a modestly broad input bandwidth centered on the emission wavelength of interest should be capable of collecting all emitted photons, given the small magnitude of these shifts. For example, for an Ar II plasma moving at 100 km/s, the expected Doppler shift of the λ_0=460.96 nm emission line is only 0.15 nm; most commercial interference filters have a bandwidth of 1 nm or more.

2.3.2 Stark Broadening

As plasma density increases, the collision rate between plasma particles also increases ($\nu_{ij} \sim n_i \sigma_{ij} v_j$, where n_i is the plasma density). In a highly ionized plasma, the majority of collisions will occur between charged particles. The combination of high density and high degree of ionization can result in the creation of strong localized electric fields in the plasma; interactions between these electric fields and the dipole moments of plasma ions will cause a perturbative splitting of the atomic energy levels of the ions, leading to a wavelength shift in both emitted and absorbed spectral lines. As these electric fields are created by collisions that are assumed to be random, field strength and orientation will vary throughout the plasma, leading to a broadening of observed spectral lines instead of the sharp bifurcation that would be expected in response to a uniform external field. This randomized line broadening can be expressed mathematically by a Lorentzian distribution

$$I(\lambda) \sim \left(1 + \frac{4(\lambda - \lambda_0)^2}{(\Delta\lambda_{FWHM})^2}\right)^{-1} \tag{2.8}$$

where λ_0 represents the central wavelength of the measured profile, which again may be shifted from the natural resonant wavelength of the transition in question.

Griem (1964) presents an expression that relates the $\Delta\lambda_{FWHM}$ of the above Lorentzian profile as a function of electron density and temperature, n_e and T_e.

$$\Delta\lambda_{FWHM} = 2 \times 10^{-17}\left[1 + 1.75 \times 10^{-4}\alpha\left(1 - 1.02 \times 10^{-3}\frac{n_e^{\frac{1}{6}}}{T_e^{\frac{1}{2}}}\right)\right]\omega n_e \tag{2.9}$$

where α and ω are constants for a given energy level transition. If the plasma under investigation is both singly ionized and nearly fully ionized, then the electron density n_e will be a good approximation for the plasma density n. As Equation 2.9 requires knowledge of the electron temperature before plasma density can be calculated, it is often necessary to implement an alternative means of calculating plasma density when the electron temperature is unknown. Aparicio and colleagues (1998) report that the Stark $\Delta\lambda_{FWHM}$ is an approximately linear function of the electron density for plasmas in the regime of $n_e \approx 0.2$–2×10^{23} m^{-3}. (The $\Delta\lambda_{FWHM}$ in Equation 2.9 is effectively linear in n if α is sufficiently small. Most α values reported by Griem are between 0.01–0.05.) For the Ar II transition at 611.49 nm, Aparicio identifies a Stark width of 34.7 pm at $n_e \approx 10^{23}$ m^{-3} for plasmas with an ion temperature of ~2 eV. Calculations of ion density that extrapolate from this result are presented in Chapters 3 and 4 of this thesis.

2.3.3 Zeeman Broadening

Zeeman broadening of spectral lines emitted from a plasma occurs when an external magnetic field interacts with the magnetic moment of ions, causing a splitting of atomic energy levels. This perturbation results in the separation of a resonant transition wavelength into multiple lines. Griem (1964) gives an expression for the magnitude of such splitting about an unperturbed spectral line of wavelength λ in a species subjected to a uniform magnetic field **B**

$$\Delta\lambda_{ZEEMAN} \approx 10^{-9}\lambda^2 B \tag{2.10}$$

where λ is given in Å and B in kilogauss. The applied external magnetic field used in the spheromak experiments described in this thesis does not exceed $B \approx 0.5$ kG; for the Ar II transition at $\lambda = 6114.9$ Å, Equation 2.10 suggests an expected Zeeman $\Delta\lambda_{FWHM}$ of approximately 0.02 Å (2 pm) in response to this field. As will be shown in later chapters, this width is small in comparison to the total measured line broadening. In addition, Zeeman splitting on the order of 1 pm approaches the limit of the scanning resolution of the laser system used in the experiments. For these reasons, potential Zeeman broadening effects are not deconvolved from the measured linewidths reported in this thesis.

2.3.4 Instrumental Broadening

The ideal tool for an LIF experiment is a tunable laser with a perfect δ-function output, emitting all of its radiation at precisely the desired wavelength. However, real lasers have finite bandwidths, and measured LIF signals are therefore the result of electron transitions induced by laser wavelengths within a certain range about the central wavelength of interest. The observed ion distribution function will be broadened as a result, as the measured fluorescent signal in response to a given incident laser wavelength λ will in fact be the aggregate signal induced by a range of wavelengths Δλ. Figure 2.3 depicts the effect that laser lineshape can have upon LIF signal measurement.

If the functional form of the laser lineshape is known, this factor can be decon-

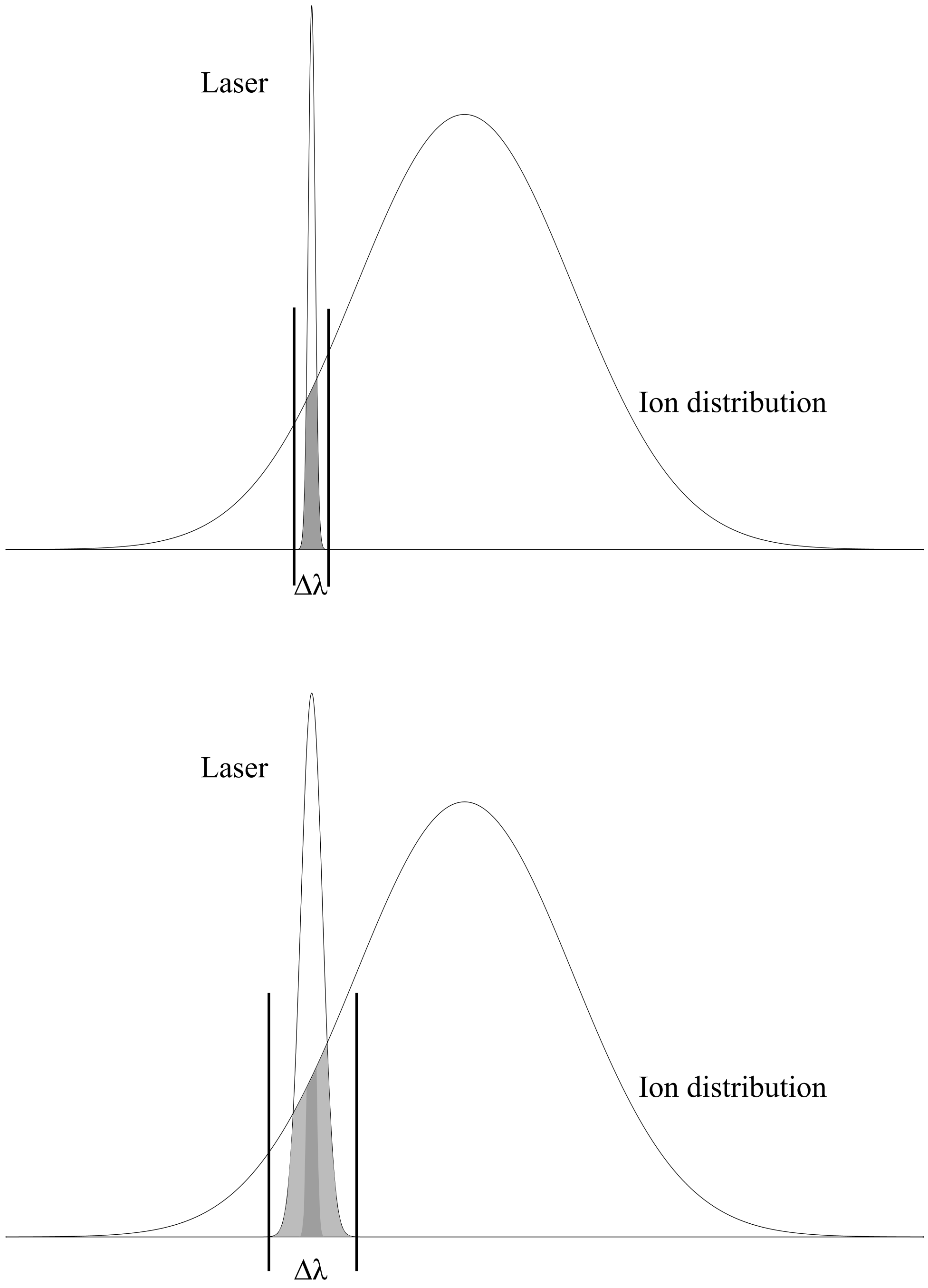

Figure 2.3. Instrumental broadening effect. As the bandwidth $\Delta\lambda$ of the probing laser increases, more fluorescence (shaded region) is induced from the same ion distribution by laser radiation away from the central wavelength. As this will artifically increase the LIF signal detected at the tails of the distribution, the measured lineshape will be broadened.

volved from other broadening effects. Even without such knowledge, reducing the bandwidth of the laser serves to minimize the influence of instrumental broadening upon LIF measurements. Section 3.3 of this thesis contains a discussion of the experimental apparatus that has been employed to mitigate laser instrumental broadening in the present investigation.

2.3.5 Power Broadening

The spectral intensity of the probing laser can also broaden measured ion distribution functions. The magnitude of the recorded LIF signal is linearly proportional to the intensity of the laser; doubling the laser power will double the measured signal strength. This relation holds until a saturation limit is reached, after which an increase in the number of laser photons at a given wavelength λ will not result in any additional electron energy level transitions. However, due to the finite bandwidth of the laser, an increase in power above the saturation limit will also increase the spectral intensity of radiation in the $\Delta\lambda$ range described in Section 2.3.4. If the ions susceptible to induced fluorescence at wavelengths in that range are not saturated, then an increase in laser power will result in increased signal by virtue of inducing more transitions away from the central λ, broadening the width of the observed distribution function.

A simple remedy to mitigate the effects of power broadening is to operate the laser system at a spectral intensity below the saturation limit, which can be determined by increasing laser power until the response in measured LIF signal is no longer observed to be linear. An additional check is to calculate ion temperatures (via the Doppler broadening mechanism) for increasing laser power levels. The temperature should not be affected so long as the system is in the non-saturated regime; once an increase in T_i is seen, it is likely that the increase in the width of the distribution is the result of the onset of power broadening.

For the investigations described in this thesis, the probing laser has been maintained at sufficiently low spectral intensity that the response of LIF signal intensity to a change in laser power is linear, and therefore power broadening is not believed to affect the accuracy of the reported measurements.

2.3.6 Combinations of Broadening Mechanisms

The observed width of the induced fluorescent emission distribution will be due to the cumulative effect of all broadening mechanisms present. If the mechanisms can be assumed to be acting independently, this combination can be represented mathematically by expressing the final observed spectrum as the convolution of the component broadened spectra. For example, two separate broadened spectra I_1 and I_2 will convolve to yield

$$I(\lambda) = \int I_1(\lambda - \xi) I_2(\xi)\, d\xi \tag{2.11}$$

2.3.7 The Voigt Lineshape

Some broadening mechanisms will dominate the observed emission spectrum more than others, depending upon the parameters of the plasma in question. Of particular interest to the present work is the distribution described by the convolution of a Doppler broadened spectrum (a Gaussian function) and a Stark broadened spectrum (a Lorentzian function.) The resultant line shape of this convolution is known as the Voigt profile.

$$I(\lambda) \sim \int \frac{\exp\left(\dfrac{-\xi^2}{\Delta\lambda^2_{FWHM,\,D}}\right)}{1 + \dfrac{(\lambda - \xi)^2}{\Delta\lambda^2_{FWHM,\,S}}}\, d\xi \tag{2.12}$$

In Chapters 3 and 4 of this thesis, measured ion distribution functions are analyzed using a Voigt model, including the application of a computational method described by Bruce and colleagues (2000) that allows for the Doppler and Stark components of Equation 2.12 to be calculated without the need for an explicit deconvolution. Estimates for ion temperature, ion velocity, and plasma density can thus all be derived from the same set of experimental observations.

2.4 Discussion

Chapters 3 and 4 of this thesis describe experiments in which laser induced fluorescence has been applied to the study of spheromaks, plasmas in a particular magnetic confinement configuration that will be described in greater detail in those chapters.

Before proceeding to the discussion of those experiments, however, the actual method by which the LIF diagnostic will be implemented will be reviewed here, for clarity. The wavelength of the probing laser is swept across the ion distribution for the particular energy level transition of interest, with the resultant induced fluorescent light detected at the photomultiplier. Emitted light intensity as a function of incident laser wavelength, $I(\lambda)$, is then fitted to the theoretical models predicted by the spectral line broadening mechanisms discussed earlier in this chapter. Finally, plasma parameters are estimated from the shape of these fitted curves.

Laser induced fluorescence is a powerful diagnostic tool, one that affords both good spatial and temporal resolution of measurements, as well as the ability to distinguish between species within a plasma via the excitation of an energy level transition unique to a particular ionization state. These traits are utilized in the investigations reported in the following chapters, which are among the first experiments to examine spheromak plasmas with LIF.

2.5 References

J.A. Aparicio, M.A. Gigosos, V.R. González, C. Pérez, M.I. de la Rosa, and S. Mar, "Measurement of Stark broadening and shift of singly ionized Ar lines," *J. Phys. B: At. Mol. Opt. Phys.*, **31**, 1029 (1998).

S.D. Bruce, J. Higinbotham, I. Marshall, and P. Beswick, "An analytical derivation of a popular approximation of the Voigt function for quantification of NMR spectra," *J. Mag. Res.*, **142**, 57 (2000).

H.R. Griem, *Plasma Spectroscopy* (McGraw-Hill, Inc., 1964).

Chapter 3
Coaxial Spheromak Device

3.1 Introduction

This chapter describes laser induced fluorescence experiments performed on plasmas produced in a spheromak confinement configuration. The objective of these experiments is to apply the LIF principles detailed in Chapter 2 toward the study of the formation and evolution of spheromak plasmas. Laser induced fluorescence is expected to provide information regarding such plasma parameters as ion density and temperature.

3.2 Spheromaks

Bellan (2000) defines the spheromak as “an axisymmetric magnetohydrodynamic equilibrium with (i) a simply connected bounding surface, (ii) both toroidal and poloidal magnetic fields, and (iii) at least some closed poloidal flux surfaces.” The toroidal direction in an axisymmetric system is taken to be the azimuthal direction about the axis of symmetry (φ direction), while the poloidal magnetic field consists of the field components orthogonal to this toroidal direction, as illustrated in Figure 3.1. One characteristic of the spheromak configuration is that the magnetic field confining plasma in a spheromak state is generated by electric currents within the plasma itself, rather than by external means such as field coils. This feature makes possible the simply connected topology of the spheromak, as there is no need for a physical linkage between the plasma and an external device.

The spheromak is a Taylor state, categorized as a system in which magnetic energy B^2 is minimized subject to the constraint that magnetic helicity is held constant. (Taylor, 1974). Magnetic helicity is defined as the volume integral of $\mathbf{A}\bullet\mathbf{B}$, where $\mathbf{A}$ is the vector magnetic potential. It is straightforward to show that the magnetic field which satisfies this condition is given by the equation

$$\nabla \times \boldsymbol{B} = \alpha \boldsymbol{B} \tag{3.1}$$

where α is uniform. Ampère's law allows the left hand side of this equation to be rewritten as $\mu_0\mathbf{J}$, and therefore a spheromak in a Taylor state also satisfies the condition that $\mu_0\mathbf{J}=\alpha\mathbf{B}$. Because **J** is parallel to **B** in such a configuration, the ideal MHD force **J**×**B** is identically 0 and the configuration is referred to as a force-free state. It is important to note that a Taylor state is a state toward which a system naturally evolves; plasma instabilities tend to decrease magnetic energy in such a manner that the final configuration of the system satisfies the Taylor force-free criteria.

3.2.1 The Importance of Spheromaks

What can be gained from the study of spheromaks? Some of the properties of the spheromak configuration, namely that it is self-organizing and represents an evolution toward a minimum energy state, make it likely that some naturally occurring plasmas should exhibit spheromak-like behavior. Recent investigations, including those conducted by Hsu and Bellan (2002), have found that the physics underlying the formation of spheromaks may bear some relation to that of astrophysical plasmas, including a magnetic topology dependence upon the parameter α, although such astrophysical plasmas are not necessarily believed to be true spheromaks. Nevertheless, the study of laboratory simulations may yield information pertinent to their astrophysical counterparts.

In addition, the spheromak configuration has also been studied as a possible means of achieving sustained nuclear fusion. Because confinement in such a system would be provided by the plasma itself, the design for a spheromak-based reactor would likely be simpler than one that utilizes large field coils to produce magnetic confinement in another configuration (a tokamak, for example). Plasma instabilities and non-ideal behavior may ultimately serve to limit the practicality of the spheromak as a fusion device; however, the field of investigation remains open.

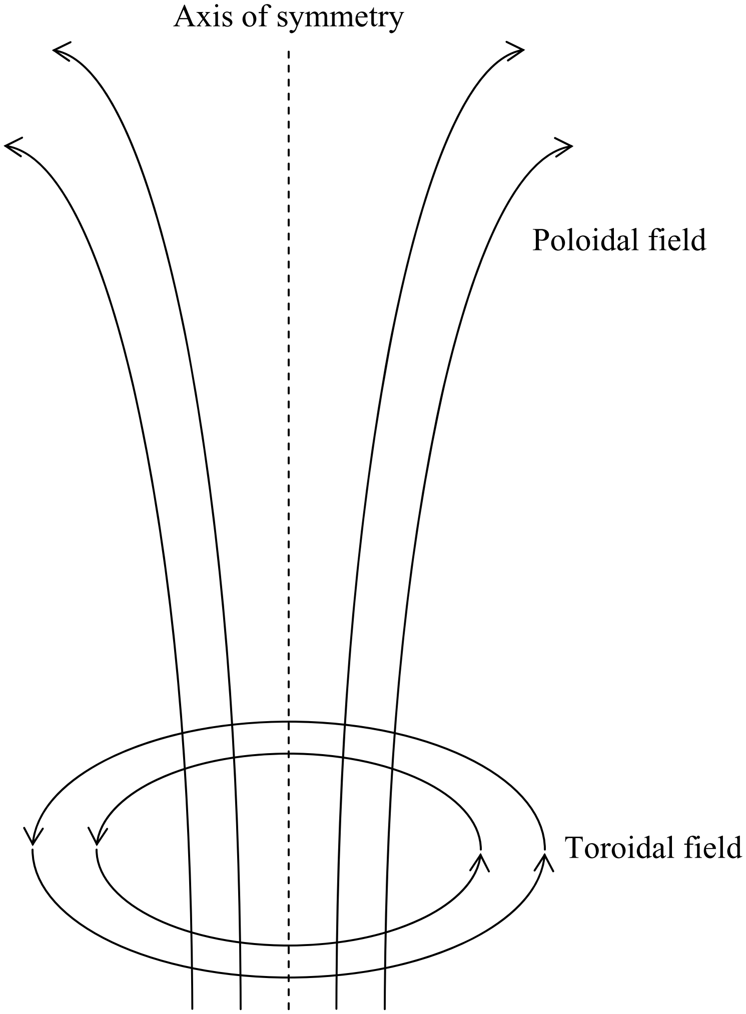

Figure 3.1. Relative orientations of the poloidal and toroidal directions in an axisymmetric field configuration.

3.2.2 Spheromaks and LIF

The appeal of using a laser induced fluorescence diagnostic to investigate plasmas in a spheromak configuration comes as a consequence of the physical systems (both natural and artificial) in which spheromak physics is expected to play a role. The spheromak is a plasma confinement configuration, one that may have applications in the field of nuclear fusion. Ion density and temperature are two key parameters used in assessing the quality of any proposed fusion scheme, and LIF is ideally suited to measuring both of these quantities, as discussed in Chapter 2. While LIF measurements cannot be made of ionized hydrogen plasmas, such as those that would be present in a fusion device, studies of other gases in the same configuration should still provide valuable information.

Following a similar line of reasoning, the use of LIF to study laboratory spheromaks that simulate certain astrophysical plasmas may lead to deeper understanding of the physics governing the naturally occurring phenomena. The spatial resolution of LIF allows for specific regions of these plasmas to be probed selectively. For example, the density at the head of a plasma jet can be compared to that found in the tail, or the temperature profile of a plasma can be measured from its bounding surface to the central core. Other diagnostics, including passive spectroscopy, cannot provide such information.

3.2.3 Coaxial Spheromak Formation

The remainder of this chapter describes an experiment designed to perform laser induced fluorescence measurements on singly ionized argon plasmas in a spheromak configuration generated by a device employing coaxial electrodes. A schematic representation of the device is shown in Figure 3.2. The common geometric axis of the electrodes provides the requisite axis of symmetry for spheromak formation; toroidal magnetic fields will therefore be those along the azimuthal direction encircling this geometric axis.

Electrostatic breakdown of gas in the interelectrode region (accomplished through the use of a switched capacitor bank) will drive a current **J** in the radial direction between

Side view

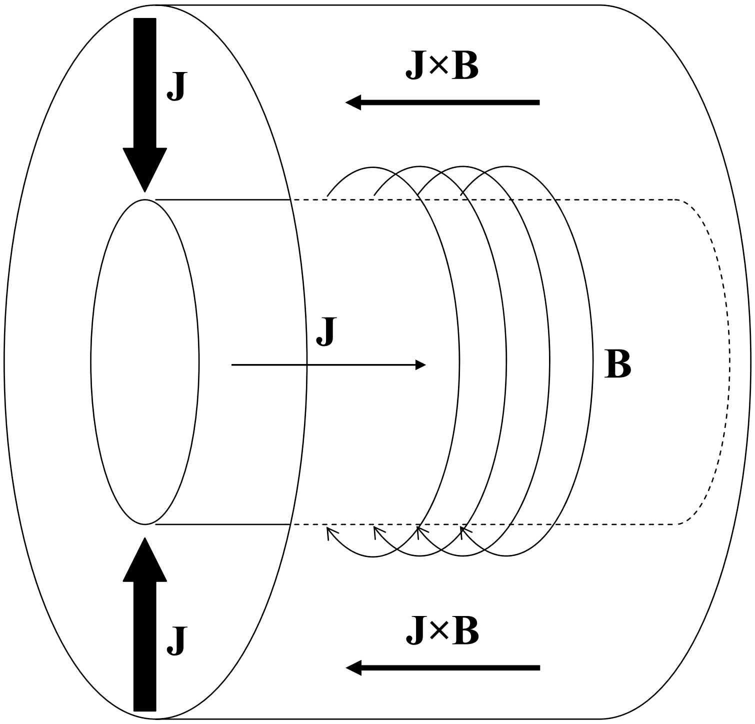

End view

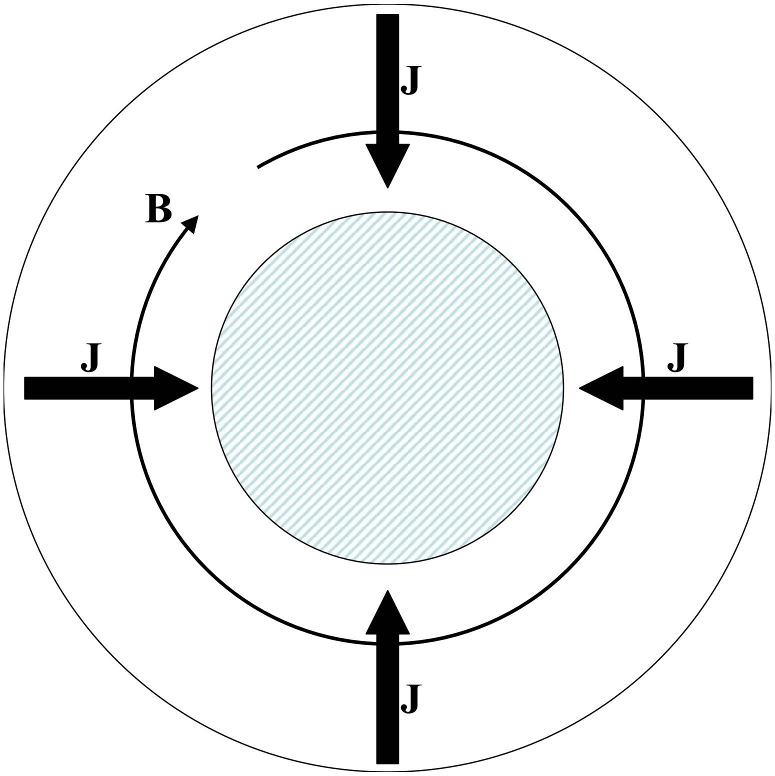

Figure 3.2. Coaxial spheromak generation. An external capacitor bank drives a current **J** in the radial direction between electrodes. As current flows through the inner electrode, an azimuthal **B** is created. **J×B** forces parallel to the spheromak axis then propel the plasma into the vacuum chamber.

electrodes. Once plasma is present, a complete electrical circuit will be formed and current will also flow through the inner electrode itself, parallel to the axis of symmetry, and thus generate a toroidal magnetic field within the plasma. As **J** in the interelectrode region lies in the radial direction and **B** is azimuthal, a **J**x**B** force parallel to the geometric axis will be present and will push the plasma out of the interelectrode region. Once the plasma enters the main body of the vacuum chamber, it may detach from the coaxial device and undergo self-organization toward a force-free Taylor state. The present experiment is intended to study these detached plasmas as they evolve.

3.3 Apparatus

3.3.1 Coaxial Spheromak Device

The coaxial spheromak device is shown in Figure 3.3. The device employs a Marshall gun configuration using two coaxial cylindrical electrodes. The outer electrode is a 16 cm diameter tungsten-coated copper tube, while the inner electrode consists of a 6.4 cm diameter copper tube encased in a tantalum sheath. The inner electrode serves as the cathode, while the outer electrode is connected to machine ground and acts as the anode, such that the interelectrode current **J** is directed inward.

A 120 μF capacitor bank is used to charge the inner electrode to voltages in the range of –4 to –6 kV; a setting of –6 kV has been used to produce the results presented in this chapter. The capacitor bank discharge is initiated by a krytron-fired ignitron switch that is triggered by a signal transmitted over fiber optic cable so as to prevent ground loops.

Custom-built gas puff valves inject argon gas into the volume between electrodes. These valves consist of an aluminum disc, held in place by a spring, that covers a 1/4” Swagelock tube attached to the vacuum chamber. Argon gas at 45 psi fills a small plenum behind the disc. To inject gas into the chamber, an electromagnetic coil inside the valve

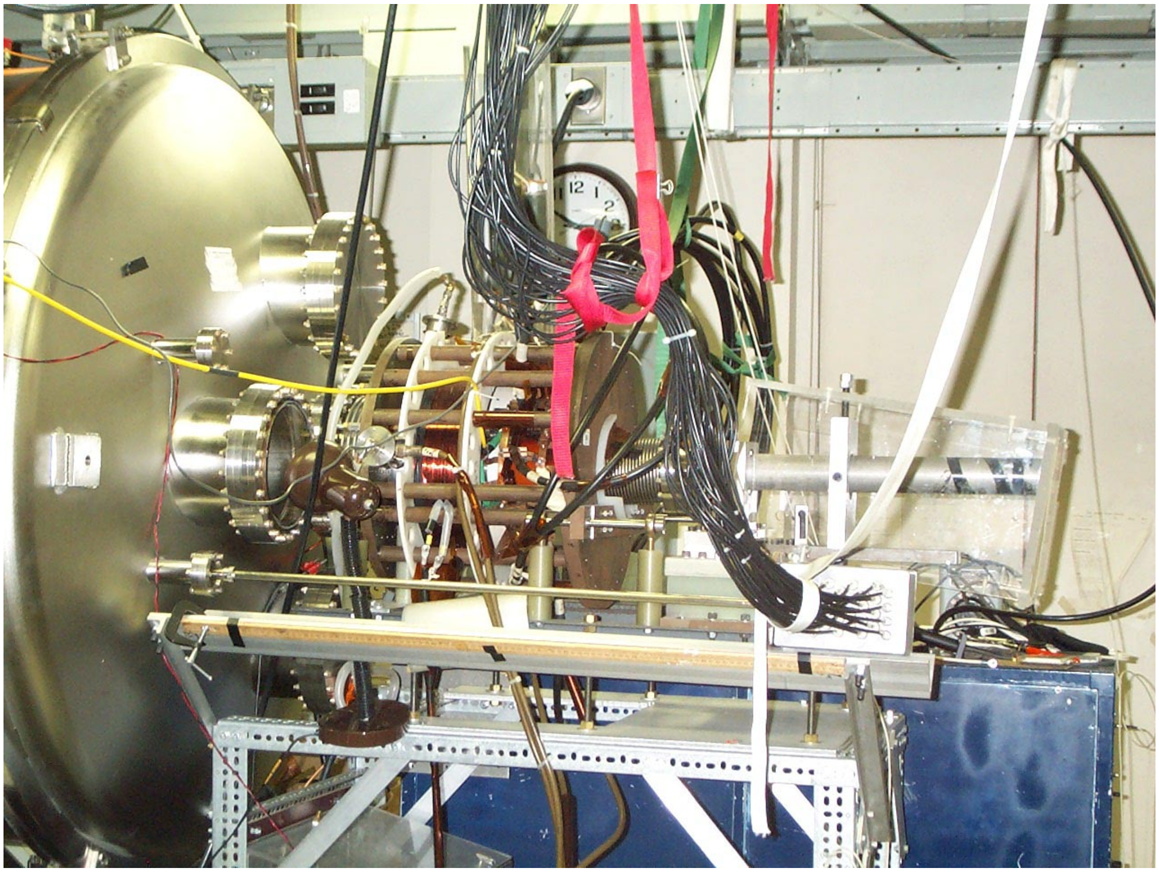

Figure 3.3. Coaxial spheromak device (exterior view).

is pulsed, repelling the aluminum disc away from the tube opening via the diamagnetic effect. The restoring force of the spring and the force exerted by the gas pressure differential quickly return the aluminum disc to its original position ($t<100$ μs), closing the valve. The amount of gas introduced into the vacuum chamber is therefore dependent upon the voltage used to pulse the electromagnetic coil and the static pressure of gas in the plenum prior to opening. Empirical observation demonstrates that a charge of ~620 V on the capacitor bank that pulses the gas valve coil provides sufficient gas for this experiment.

An electromagnetic coil mounted outside the coaxial electrodes, in atmosphere, provides a poloidal bias magnetic field. This coil is powered by a pulsed capacitor bank and is capable of generating up to 6 mWb of magnetic flux, although 2 mWb is the maximum flux that has been applied during the experiments described in this chapter.

The coaxial gun is mounted on the end dome of a large cylindrical vacuum chamber (1.5 m diameter, 2 m length). A Varian Megasorb roughing pump is used to bring the chamber from atmosphere down to ~10^{-3} Torr. High vacuum for the chamber is then established with an APD Cryogenics model APD-12S cryopump. Nominal base pressures in the chamber lie in the range of $1–2\bullet10^{-7}$ Torr.

3.3.2 Laser

The laser system used in this experiment consists of a Lambda Physik model LPD 3001 tunable dye laser pumped by a Laser Photonics model MY-32 ND:YAG laser. The nominal output wavelength of the YAG laser is 1064 nm; frequency-doubling optics inside the YAG chassis reduce the wavelength to 532 nm prior to the beam entering the dye laser. The YAG pulse duration is fixed at 15 ns, and the YAG is triggered at a repetition rate of 15 Hz by means of an external timing circuit.

The output wavelength of the dye laser is adjustable by means of angle tuning, in which the laser grating is tilted via stepper motor such that the desired emission wavelength is at normal incidence to the end mirror. The wavelength range over which the dye

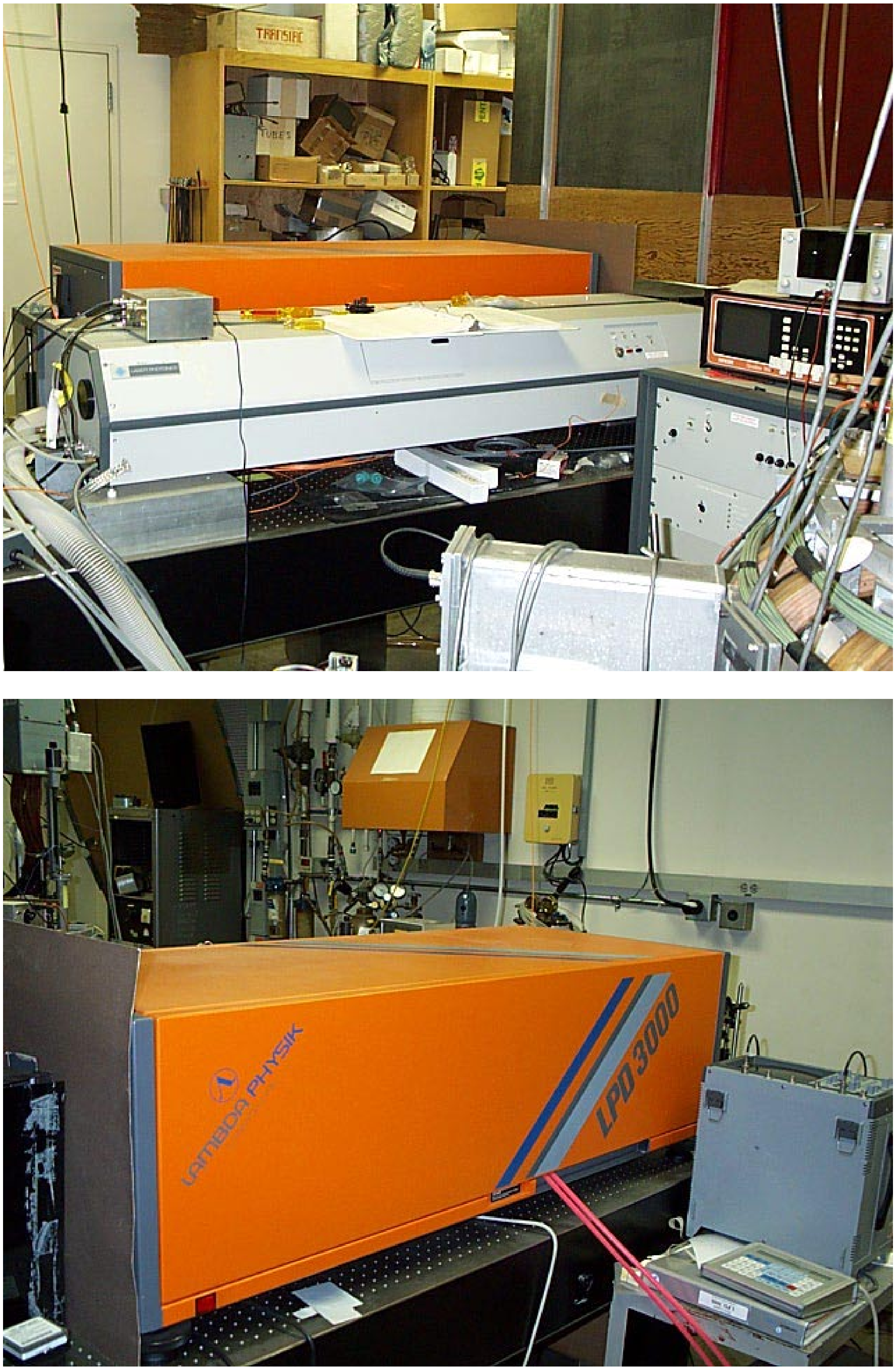

Figure 3.4. Laser system. Photons at 532 nm produced by the YAG laser (top) excite the Rhoadmine 640 dye used in the dye laser (bottom), causing emission near 612 nm. The output wavelength of the dye laser is controlled via angle tuning.

laser may be tuned depends upon the dye solution present in the laser. A 0.3 g/mol solution of Rhodamine 640 has been used in this experiment; the manufacturer claims maximum output power for this solution is achieved at a wavelength of ~612 nm, close to the expected 611.49 nm wavelength of the Ar II transition probed in this experiment. Manual control of the grating stepper motor allows for the laser wavelength to be changed in 1 nm increments, and the output wavelength has been calibrated via spectrometer.

3.2.3 Optical Fiber

The lasers used in this experiment are located in a different room than that containing the coaxial spheromak device. The use of mirrors to direct the laser beam into the vacuum chamber is impractical from a design perspective, so optical fiber is used instead. An achromatic doublet (f=5.08 cm, φ=2.54 cm, Newport PAC040) focuses the laser into the entrance aperture of the optical fiber assembly, as shown in Figure 3.5.

The exit ferrule of the optical fiber is mounted on a 2.75” diameter port of the spheromak vacuum chamber by means of a Lucite block. Lucite is used as it is electrically insulating, thus protecting the fiber from possible transient high voltages associated with the surface of the vacuum chamber. An achromatic doublet (f=5.08 cm, φ=1.27 cm, Newport PAC528) for collimating the laser beam after it exits the fiber is placed in a cavity inside the Lucite. After final in situ adjustments to the separation between the end of the optical fiber ferrule and the lens to obtain optimum collimation, the fiber ferrule is fixed in place with a set screw.

3.2.4 Experimental Timing

Control over experimental timing is achieved with custom CAMAC time delay sequencer modules. An eight-channel module with 50 ns time resolution triggers the YAG laser flashlamps and Q-switch (768.4 μs separation) in response to a 15 Hz timing signal phase-locked to the 60 Hz AC line power.

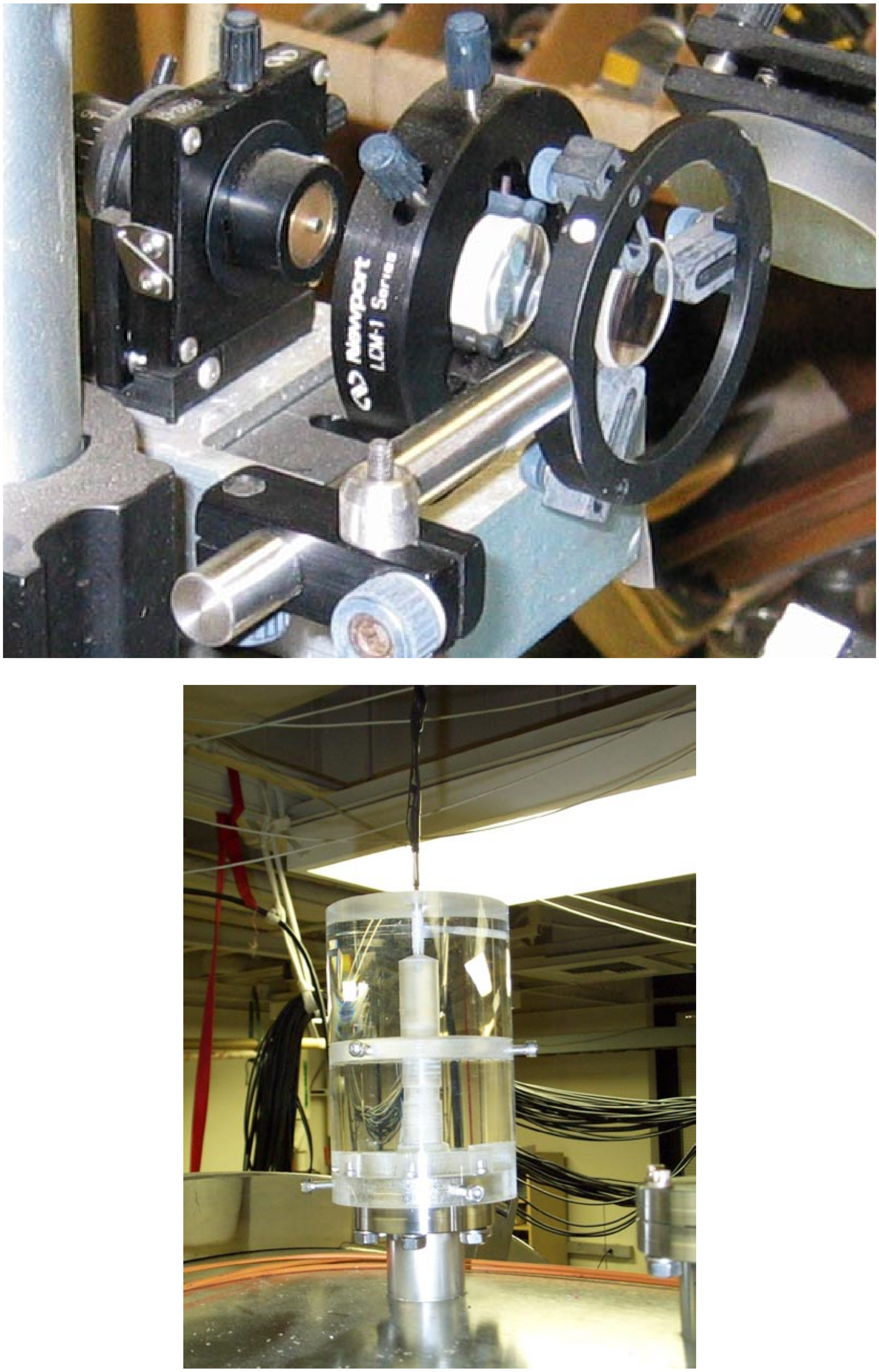

Figure 3.5. Optical fiber assembly. (Top) An achromatic doublet focuses the laser into the entrance of the fiber assembly. (Bottom) The output ferrule of the fiber is mounted to the spheromak vacuum chamber with a Lucite block that also contains a collimating lens.

A twelve-channel CAMAC module provides the discharge triggers for all capacitor banks involved in spheromak formation, as well as the trigger to the oscilloscope that digitizes the photomultipler signal. Fiber optics are used to transmit the timing signals from the CAMAC modules to prevent ground loops and other electrical feedback. Table 3.1 details the various time delay settings used in this experiment.

An important concern in the design of the experiment is the synchronization of the single-shot spheromak discharge with the 15 Hz pulsed laser system. Two approaches are possible: to have a signal associated with the spheromak discharge trigger the laser timing sequencer, or to have the laser timing sequencer initiate spheromak formation.

In the present experiment it is impossible to use a signal generated after the spheromak has formed to trigger the laser and produce a successful LIF measurement, due to the operating requirements of the YAG laser. A delay of 768.4 μs is needed between the excitation of the YAG's flashlamps and the subsequent triggering of the Q-switch that permits the beam to exit the YAG. The duration of a typical argon spheromak in the experiment is 20–30 μs. Thus, no diagnostic (for example, a probe monitoring coaxial gun voltage) can send a signal to the laser after plasma has formed and have the resulting beam intercept the spheromak before the plasma dissipates.

It would be possible to have a pair of timing signals from the twelve-channel module trigger the laser (one signal for the flashlamps and one for the Q-switch). However, this would result in only a single laser pulse every several minutes; while the laser can operate in such a single-shot mode, it is more likely to generate a consistent output profile when running at its nominal high repetition rate. Therefore, it is desirable to implement a means of having the laser's eight-channel timing sequencer module generate output pulses at 15 Hz and yet also trigger a single spheromak discharge. This can be achieved via the use of a flip-flop circuit.

In the present experiment the eight-channel delay module sends trigger signals to the flashlamp and Q-switch circuits as usual, while an additional channel sends a signal

Laser System Time Delays	
Event	Time
Synchronization signal sent to spheromak time delay generator	---
YAG flashlamps	22.7958 ms
YAG Q-switch	23.5642 ms

Spheromak Time Delays	
Event	Time
Stuffing flux coil trigger	---
Gas valves trigger	21.8 ms
Main capacitor bank discharge	23 ms
Oscilloscope trigger	23 ms (variable)

Table 3.1. Timing delays used in the coaxial spheromak LIF experiment.

over optical fiber to the input of a flip-flop circuit located near the twelve-channel module. The spheromak formation sequence is normally initiated by means of a handheld push-button that sends a signal over fiber optic cable to the twelve-channel module. Now, the output of the push-button is instead routed to the D input of the flip-flop. When this input detects the push-button signal, it goes to a logical high state, and the flip-flop will generate one output pulse upon receiving the next clock pulse from the fiber carrying the signal from the eight-channel module. The maximum delay between depressing the push-button and the ensuing output pulse from the flip-flop will be no more than 66.7 ms, over which time the spheromak capacitor banks will discharge only a negligible amount. Therefore, this flip-flop configuration satisfies the requirements for a system that will synchronize the spheromak and the laser. Figure 3.6 illustrates the chronological order of events associated with the laser and spheromak generation systems.

3.2.5 First Photomultipler Configuration

Figure 3.7 shows the first experimental configuration used for the collection of emitted fluorescent light from the plasma. The assembly views the plasma through a 6” circular window on the side of the vacuum chamber, looking in a direction perpendicular

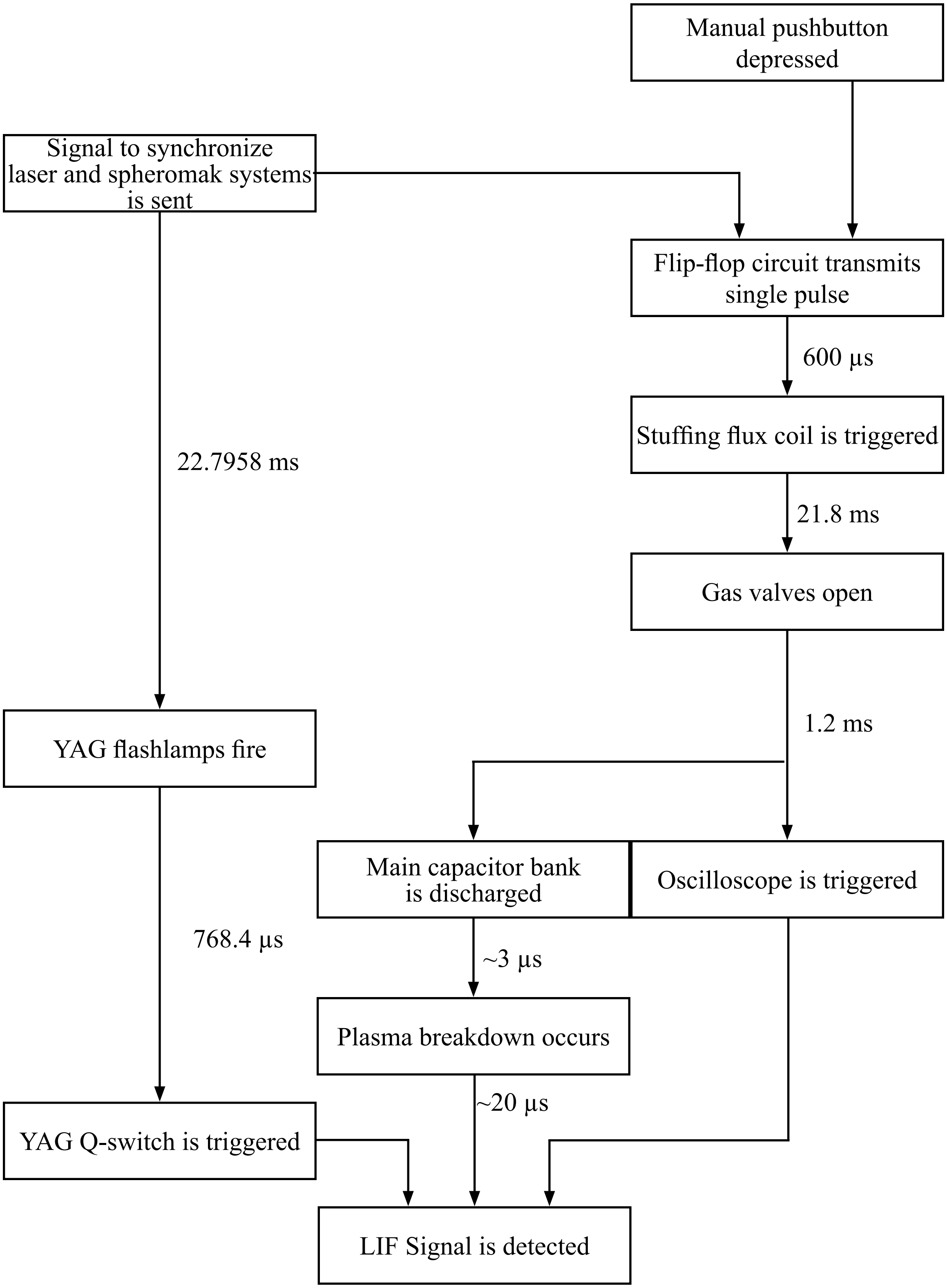

Figure 3.6. Chronology of the LIF spheromak experiment.

to the spheromak's axis of symmetry. A Thorn EMI QL30F/RFI electron tube is used as the photomultiplier element; the QL30F is battery-powered, an important design consideration as a photomultipler connected to AC power would be more susceptible to ground loops and electrical interference caused by the multiple high voltage switches used in the experiment. A 2" diameter narrow bandwidth interference filter (1 nm $\Delta\lambda_{FWHM}$) centered on the 460.96 Ar II emission line is mounted in front of the photomultiplier.

Due to the large physical size of the QL30F assembly and the available space in the laboratory, it is necessary to mount the photomultiplier at a 90° angle to the intended viewing direction and to use a mirror to reflect emitted light from the plasma onto the photomultiplier head. A biconvex lens (f=20.0 cm, φ=5.08 cm, Newport KBX166) is placed between the plasma and the mirror to focus light from the region of plasma illuminated by the laser onto the photomultiplier head. To prevent saturation of the photomultiplier, an ND 1.0 neutral density filter is also incorporated into the optical path.

Multiple attempts at detecting an LIF signal using this photomultiplier configuration have been made, but none has proven successful. Spontaneously emitted background light emission at the 460.96 nm wavelength is readily observed but without any induced transitions caused by the probing laser. The QL30F has a 15 ns rise time, which may be too slow for the present experiment in which the induced fluorescence signal is expected to have a duration of <30 ns.

3.2.6 Second Photomultiplier Configuration

As a result of the failure of the first light collection apparatus to detect an induced fluorescence signal, a different experimental configuration is needed. As the slow rise time of the QL30F electron tube is suspected to be the most serious design flaw, a 0.78 ns rise time Hamamatsu H6779 has been selected as the new photomultiplier element. The Hamamatsu is also a much smaller device than the Thorn EMI, eliminating the need for the 90° turn and accompanying mirror in the optical path.

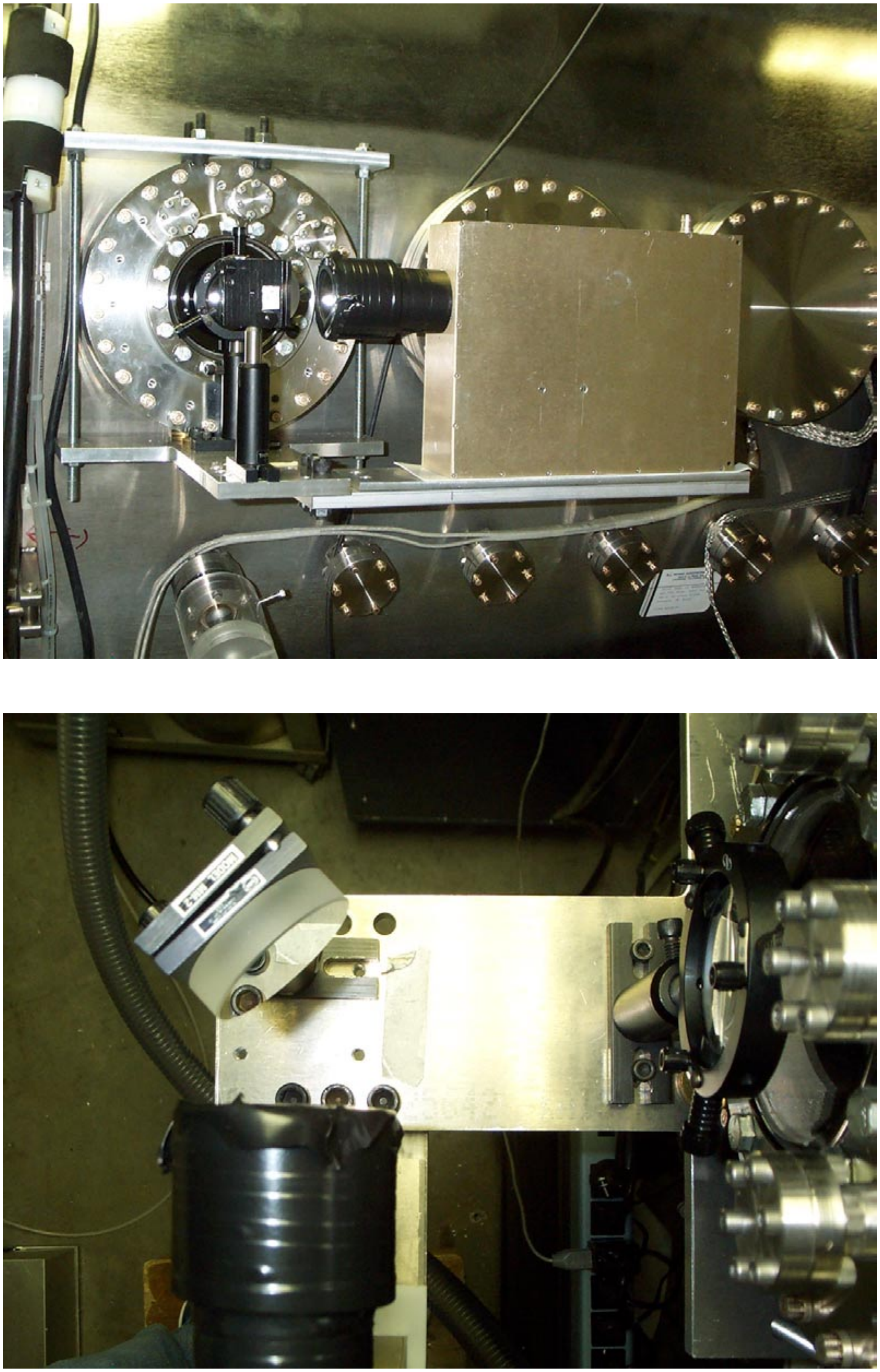

Figure 3.7. First photomultiplier configuration. The ND filter, normally located between the lens and mirror, has been removed for clarity.

A LeCroy VV100BTB 10× amplifier has been integrated into the photomultiplier circuit to boost the output signal amplitude. Twelve 1.5 V rechargeable lithium ion batteries provide electrical power for the photomultiplier and amplifier. The photomultiplier, amplifier, batteries, and ancillary circuitry are enclosed in a metal box to shield against electromagnetic interference, as shown in Figure 3.7. The photomultiplier assembly has been designed and constructed by F. Cosso.

The f=20.0 cm biconvex lens is again used to focus light onto the photomultiplier. A 1” diameter 1 nm bandwidth interference filter centered on the 460.96 nm Ar II line is placed in front of the photomultiplier head.

An opaque mask has been placed on the 6” window of the vacuum chamber to further reduce the amount of extraneous light reaching the photomultiplier. This mask consists of a 6” diameter disk of thick black paper with a central rectangular aperture to allow light from the region of plasma illuminated by the laser to pass through. This mask effectively prevents light from reaching the photomultiplier from regions of the plasma other than that illuminated by the laser (and those areas of the plasma directly in front of and behind this region along the line of sight of the photomultiplier).

3.2.7 Data Acquisition

A LeCroy 9314 oscilloscope (4 channels, 100 Ms/s sampling rate) is used to measure the output signal of the photomultiplier and to store this data for subsequent analysis. Aeon CAMAC digitizers are used with other diagnostic equipment on the coaxial experiment; however, their maximum digitization rate of 10 MHz (100 ns between memory addresses) is insufficient to record the induced fluorescence signal properly, as the signal is expected to last on the order of <30 ns.

3.2.8 Photodiode

To aid in fine tuning the synchronization between the laser system and the sphero-

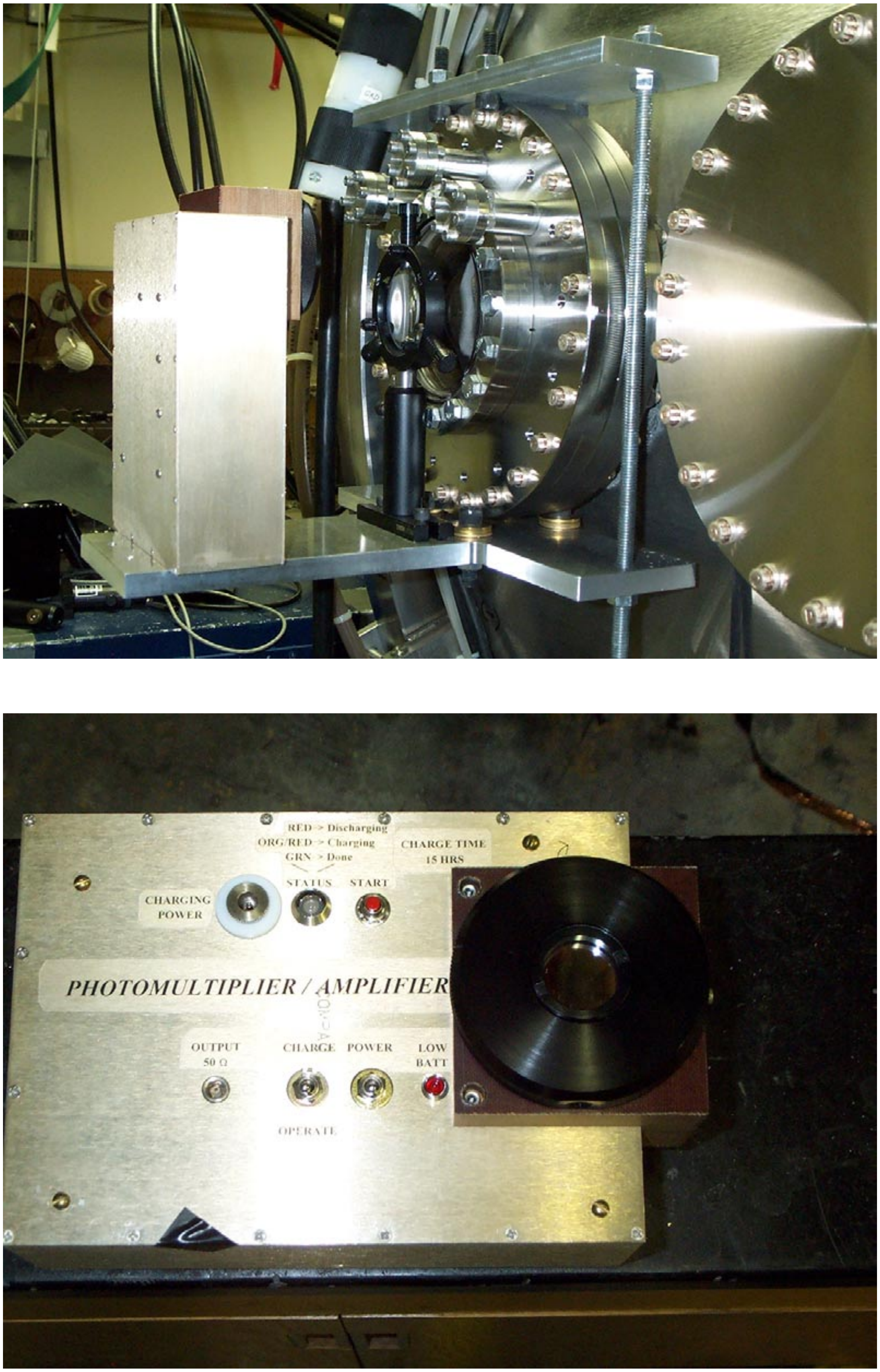

Figure 3.8. Second photomultiplier assembly.

Figure 3.9. Opaque mask to prevent extraneous light from reaching the photomultiplier.

mak formation apparatus, a photodiode is placed in the beam path of the laser after it has exited the vacuum chamber. The diode is located approximately 1 m from the intersection of the central axis of the spheromak and the laser; therefore, the laser may be expected to pass through the plasma ~3 ns prior to detection of the beam by the photodiode. Use of this technique proves useful in selecting a precise time relative to the formation of the spheromak plasma to perform LIF measurements. Calibration of the signal level of the photodiode is unnecessary, as the only information needed for synchronization is the time at which the laser first strikes the diode.

3.4 Observations

3.4.1 Measured LIF Signal

Fluorescent light from the argon plasma is collected by the photomultiplier, and the photomultiplier's output voltage is then recorded by the LeCroy 9314 oscilloscope. This model oscilloscope possesses an RS-232 interface; however, the software used for data transfer to a computer is prone to failure, so output to an X-Y plotter has been used for hard copy recording of oscilloscope traces. A sample output page from the plotter, displaying four representative LIF signals detected by the photomultiplier, is shown in Figure 3.10. The induced fluorescence signals caused by the probing laser can be seen in the highlighted box. The oscilloscope's built-in signal measurement functions are used to record the voltage levels corresponding to both the LIF peak maxima and the background emission, such that the magnitude of the induced fluorescence signals are accurately recorded. A plot of measured LIF signal peaks as a function of incident laser wavelength is provided in Figure 3.11.

3.4.2 Fitting to Theoretical Model

A dataset consisting of measured induced fluorescent light intensity as a function

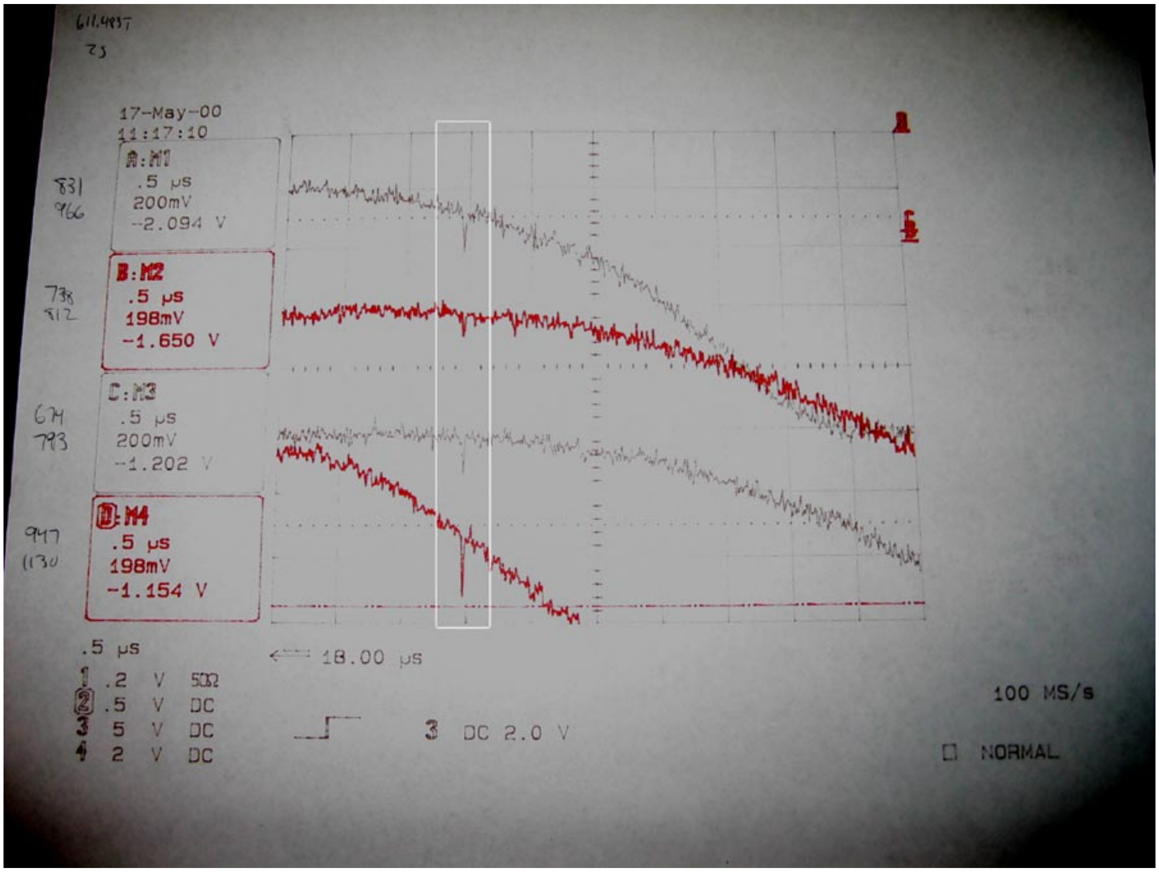

Figure 3.10. Photomultiplier signal traces as recorded by the LeCroy 9314 oscilloscope. The sharp peaks inside the highlighted box represent induced fluorescence caused by the probing laser.

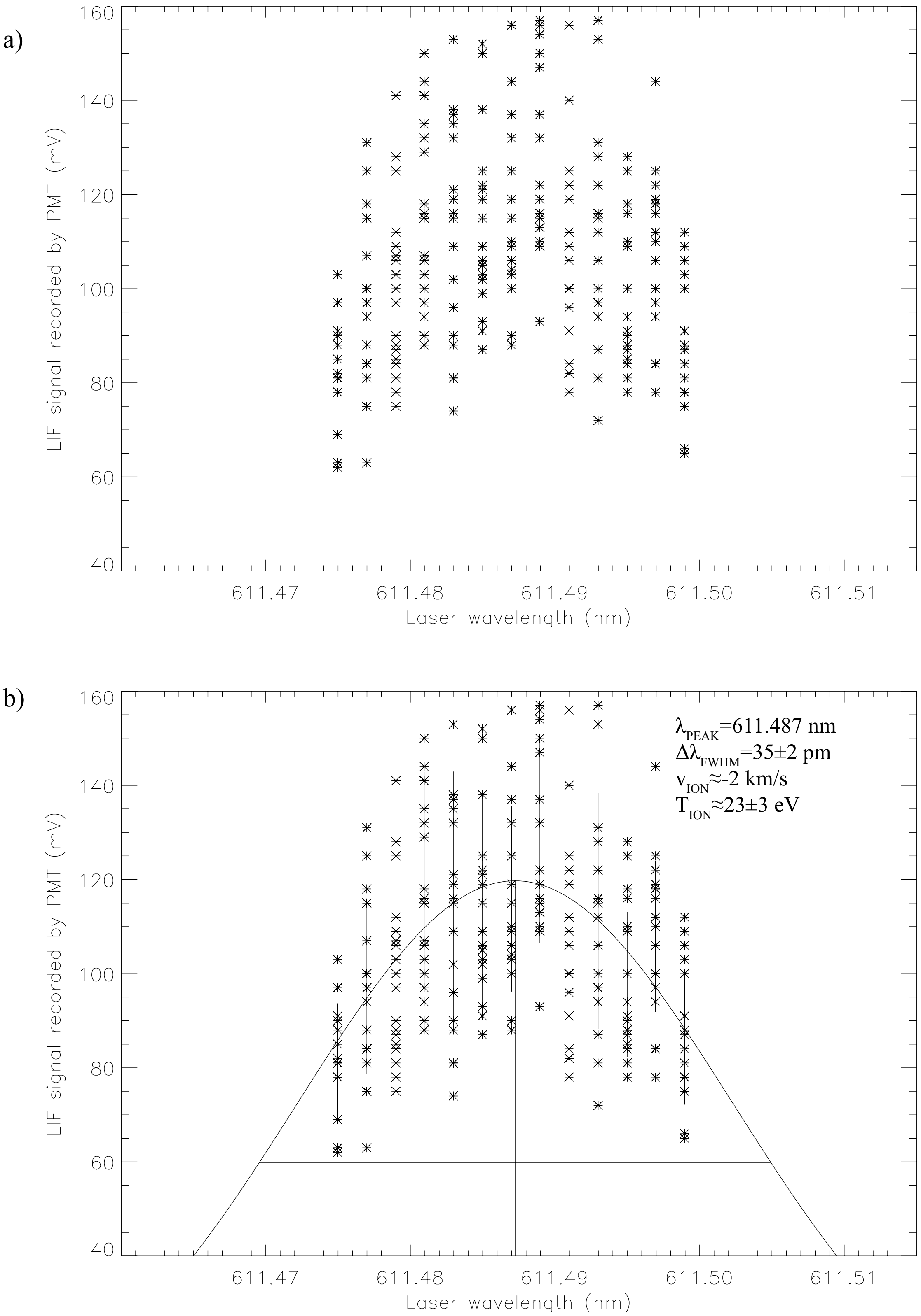

Figure 3.11. a) Photomultiplier signal of laser induced fluorescence at 460.96 nm as a function of incident laser wavelength for λ_{LASER}=611.475–611.499 nm. Twenty (20) plasma shots are made at each wavelength shown. Best-fit curves are shown for b) Doppler, c) Stark, and d) Voigt line broadening models.

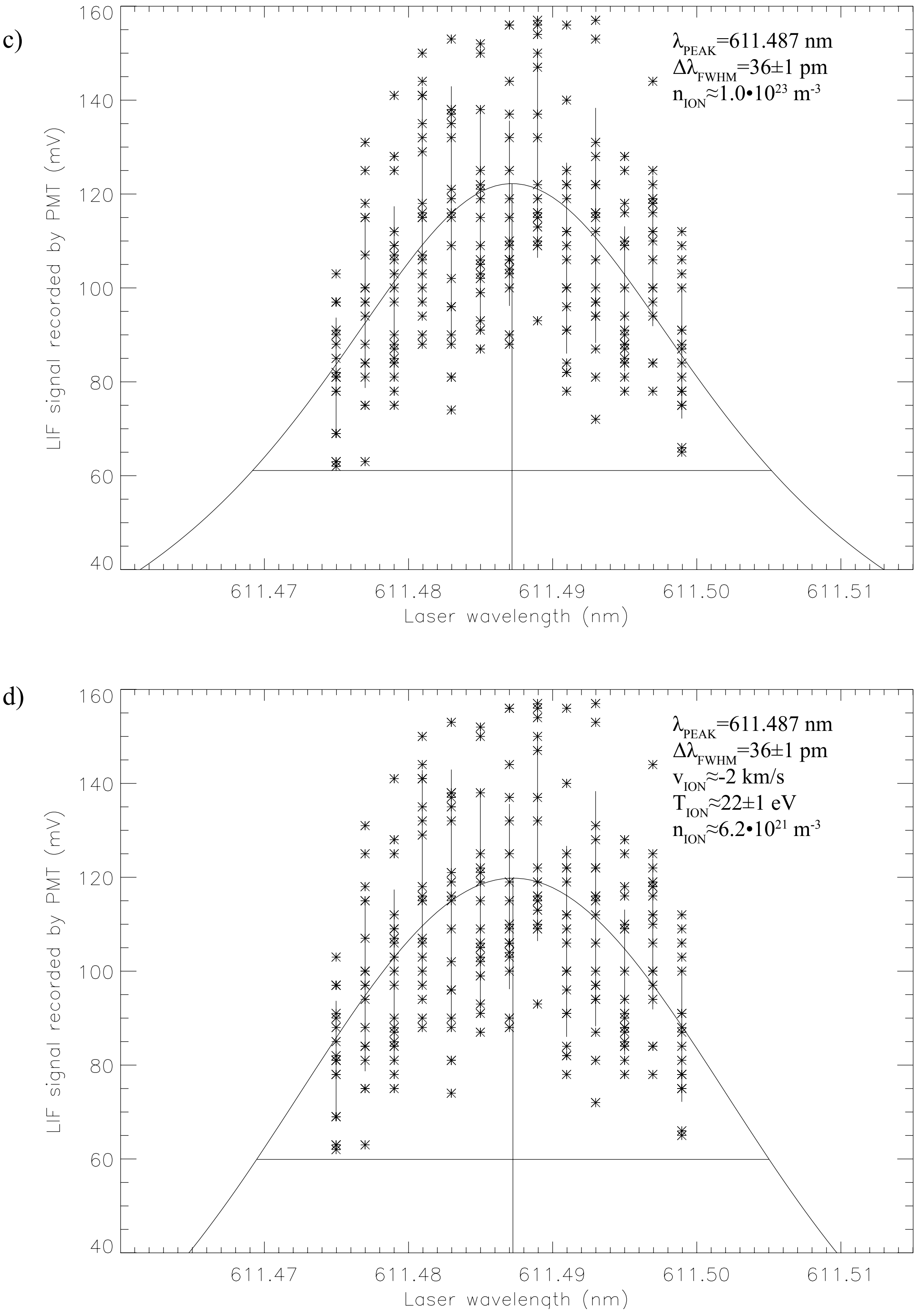

Figure 3.11. a) Photomultiplier signal of laser induced fluorescence at 460.96 nm as a function of incident laser wavelength for λ_{LASER}=611.475–611.499 nm. Twenty (20) plasma shots are made at each wavelength shown. Best-fit curves are shown for b) Doppler, c) Stark, and d) Voigt line broadening models.

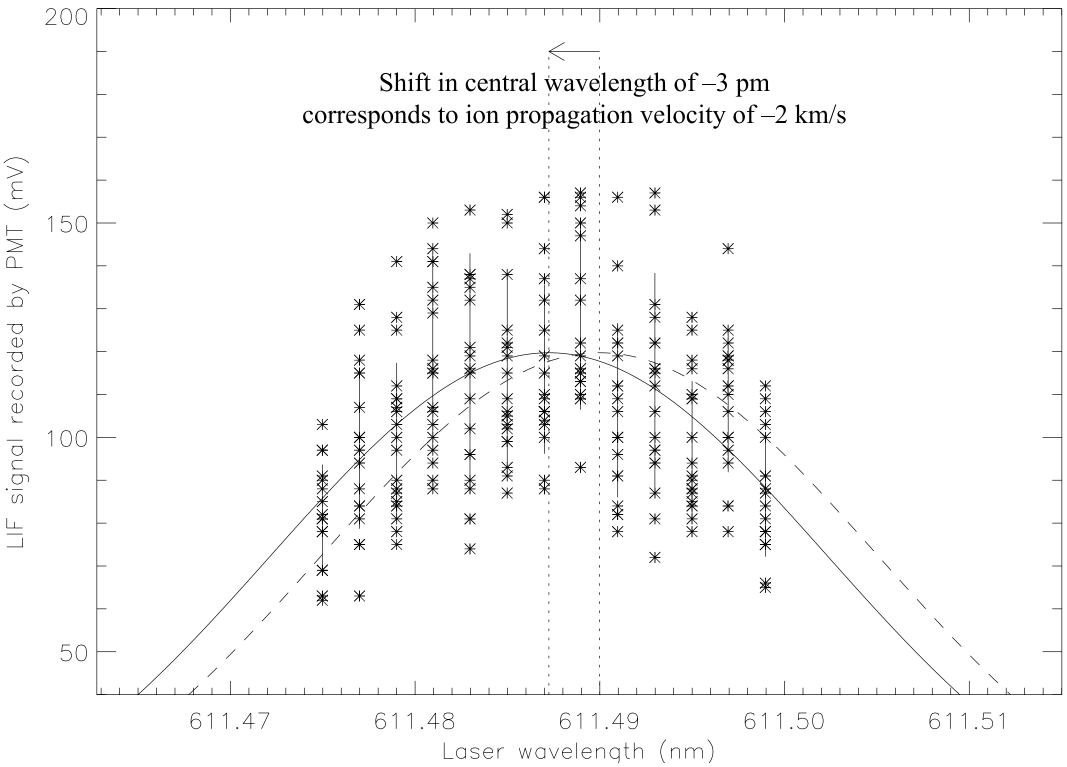

Figure 3.12. Ion propagation velocity corresponding to the shift in observed central wavelength of the ion distribution function for the data shown in Figure 3.11. The solid curve represents the measured distribution, while the dashed curve illustrates the same data centered about the non-shifted wavelength of 611.49 nm.

of incident laser wavelength can be analyzed with respect to the spectral line broadening mechanisms discussed in Chapter 2 to yield estimated values of the plasma parameters associated with those mechanisms. The Interactive Data Language (IDL) software package has been used for all computations presented in the following sections.

3.4.2.1 Doppler Broadening

If the dominant spectral line broadening mechanism responsible for the width of the distribution shown in Figure 3.11 is Doppler broadening due to thermal motion of the ions, the relationship between emitted fluorescent light intensity and incident laser wavelength should take the form of a Gaussian function. The built-in IDL routine GAUSSFIT performs a least-squares fit of a user-supplied dataset to a Gaussian; this routine has been used to fit the coaxial spheromak data to a function of the form

$$I(\lambda) = A_0 \exp\left(-\frac{x^2}{2}\right) \tag{3.2}$$

$$x = \frac{2\,(\lambda - A_1)}{A_2} \tag{3.3}$$

where the fitted parameters A_0, A_1, and A_2 correspond to the function's peak amplitude, wavelength at this maximum amplitude, and $\Delta\lambda_{FWHM}$ of the function, respectively. Due to the Gaussian form utilized by GAUSSFIT, the $\Delta\lambda_{FWHM}$ of the distribution returned by the routine is actually given by $2\bullet(2\ln 2)^{1/2}\bullet A_2 \approx 2.35\bullet A_2$. For the LIF signal data collected from the coaxial gun experiment, the best-fit parameters for the data shown in Figure 3.11 are found to be A_0=120±2 mV, A_1=611.487 nm, and A_2=15±1 pm.

The value for the A_1 parameter can be used to calculate an estimate for the ion propagation velocity, as described by Equation 2.2. Using λ_0=611.49 nm as the expected resonant wavelength corresponding to the energy level transition from the initial state to the intermediate state of the Ar II fluorescence under investigation, the computed value of A_1 suggests an ion velocity of –2 km/s. (A velocity less than 0 represents motion away from the incident laser beam; motion toward the laser would be represented by a positive velocity.) With the present experimental configuration, this means that the vertical component of the velocity of the diagnosed volume of plasma is directed downward at the time the measurement is made. In experiments on hydrogen plasmas formed by the same coaxial apparatus, Yee and Bellan (2000) use magnetic field measurements to calculate a plasma propagation rate of 86 km/s in the axial direction. Differences in experimental conditions (gas species, capacitor bank voltages, time delay settings) will tend to limit the validity of comparisons between these two experiments.

As discussed in Chapter 2, ion temperature is related to the $\Delta\lambda_{FWHM}$ of the Gaussian distribution when Doppler broadening dominates. The best-fit model to the experimental data collected from the coaxial spheromak experiment yields a $\Delta\lambda_{FWHM}$ of 35±2 pm. Inserting this value into Equation 2.7 results in a calculated ion temperature of 23±2 eV.

3.4.2.2 Stark Broadening

If the plasma produced by the coaxial spheromak device is of high ion density and low ion temperature (to the extent that line broadening due to thermal motion can be ignored), the observed lineshape of the fluorescent light distribution should be caused primarily by the Stark effect. In this case, the function to which the experimental data should be fit is a Lorentzian distribution.

IDL does not contain a predefined routine for fitting data to a Lorentzian distribution; however, the IDL CURVEFIT routine allows for fitting to any user-supplied non-linear function for which the partial derivatives with respect to the unknown parameters are known. CURVEFIT has been used to fit the experimental data set to the function

$$I(\lambda) = A_0 \frac{1}{\pi} \frac{1}{1 + x^2} \tag{3.4}$$

where x has the same definition as in Equation 3.3, and A_0, A_1, and A_2 again correspond to the fitted function’s peak amplitude, wavelength at maximum amplitude, and $\Delta\lambda_{FWHM}$, respectively. Defining the function in this form allows for A_2 to represent the $\Delta\lambda_{FWHM}$ of the distribution without a correction factor. The best-fit parameters to this Stark model are found to be A_0=384±1 mV, A_1=611.487 nm, and A_2=36±1 pm.

Based upon the discussion presented in Section 2.3.2 on the Stark fitting calculations of Aparicio and colleagues, a Stark $\Delta\lambda_{FWHM}$ of 36 pm corresponds to a plasma ion density of ~$1.0 \cdot 10^{23}$ m^{-3}.

3.4.3 Voigt Profile

The previous two sections have analyzed the collected LIF data by assuming that the observed line broadening is caused entirely by one broadening mechanism, either Doppler or Stark. These exercises have merit, as they serve to place upper limits on the calculated values that should be expected for ion temperature and density; however, the observed lineshape results from the presence of both mechanisms. As discussed in Section 2.3.7, the combined effect of Doppler and Stark broadening is known as the Voigt profile and is represented mathematically as the convolution of the two functions.

$$I(\lambda) \sim \int \frac{\exp\left(\frac{-\xi^2}{\Delta\lambda^2_{FWHM,D}}\right)}{1 + \frac{(\lambda - \xi)^2}{\Delta\lambda^2_{FWHM,S}}} d\xi \tag{3.5}$$

Instead of directly fitting experimental data to the function defined by Equation 3.5, a less computationally intensive alternative is frequently used that approximates the convolution as a linear combination of a Gaussian function and a Lorentzian function, where the $\Delta\lambda_{FWHM}$ of these two functions are set equal to each other, such that this value is also the $\Delta\lambda_{FWHM}$ of the fitted lineshape. The true linewidths of the convolved Gaussian and Lorentzian in Equation 3.5 are subsequently computed using the fitted $\Delta\lambda_{FWHM}$ and the fractional contribution of each function to the linear combination. Bruce (2000) presents an extensive discussion of this approximation and of the error it introduces and claims the error in linewidth of the calculated Voigt shape is on the order of 1–3%. The area under the function is expected to deviate from the true value by no more than 0.72%.

To make use of this linear combination approximation, the experimental data is fitted to the function

$$I(\lambda) = A_0\left[A_3\frac{1}{\pi}\frac{1}{1+x^2} + (1-A_3)\sqrt{\frac{\ln 2}{\pi}}\exp\left(-\ln 2\cdot x^2\right)\right] \tag{3.6}$$

x, A_0, A_1, and A_2 have the same meaning as in the separate Doppler and Stark models presented in the last two sections. The constant coefficients involving π and ln 2 stem from the use of normalized expressions for the Lorentzian and Gaussian functions (an additional factor of 2 common to both functions has been incorporated into A_0).

The A_3 parameter denotes the fractional contribution of the Stark function to the overall lineshape, such that $1-A_3$ represents the Doppler contribution; it is expected that $0\leq A_3\leq 1$. Wertheim (1974) asserts that lineshapes in which the best-fit A_3 lies outside this range are possible and indicate the presence of significant line broadening from a mechanism other than Doppler or Stark considerations. For the LIF data collected from the coaxial gun and shown in Figure 3.11, the best-fit parameters to this model are A_0=263±1 mV, A_1=611.487 nm, A_2=36±1 pm, and A_3=0.1.

To obtain ion temperature and density information from this model, it is necessary to determine the linewidths of the original Doppler and Stark components which convolve to give the Voigt lineshape in Equation 3.5. Bruce provides an empirically calculated relationship between the $\Delta\lambda_{FWHM}$ of the fitted lineshape in Equation 3.6 and the $\Delta\lambda_{FWHM}$ of the Doppler component of Equation 3.5 as a function of the Doppler fraction $1-A_3$.

$$\Delta\lambda_{FWHM,\,Doppler} = \Delta\lambda_{FWHM,\,Voigt}\left(\frac{1-A_3}{0.97}\right)^{0.43} \tag{3.7}$$

The $\Delta\lambda_{FWHM}$ of the fitted Voigt function is, by construction, the parameter A_2. Using the computed value for A_3, we calculate an expected Doppler $\Delta\lambda_{FWHM}$=34±1 pm, which corresponds to an estimated ion temperature of 22±1 eV by Equation 2.7.

A relationship between the $\Delta\lambda_{FWHM}$ of the fitted Voigt function in Equation 3.6 and those of the convolved Gaussian and Poisson functions in Equation 3.5 is given in Whiting (1968), based on fitting to data originally obtained by Van de Hulst and Reesinck

(1947). The relationship has the form

$$\Delta\lambda_{FWHM,\,Stark} = \frac{\Delta\lambda^2_{FWHM,\,Voigt} - \Delta\lambda^2_{FWHM,\,Doppler}}{\Delta\lambda_{FWHM,\,Voigt}} \tag{3.8}$$

As the $\Delta\lambda_{\mathrm{FWHM}}$ of the fitted Voigt function and the calculated $\Delta\lambda_{\mathrm{FWHM}}$ of the Doppler component are now known quantities, the $\Delta\lambda_{\mathrm{FWHM}}$ of the Stark contribution follows directly and is computed to be ~2 pm. This value corresponds to a plasma ion density of $\sim 6.2 \bullet 10^{21}$ m^{-3}. As the Voigt model assumes broadening due to both ion temperature and density effects, the values returned by this analysis are more likely to represent the actual parameters of the plasma under investigation than those values given by the models that assume the presence of only one broadening effect. It should be noted that the goodness-of-fit statistic returned by the IDL fitting routines is virtually identical for all three models.

3.4.4 Sources of Experimental Error

It is important to identify potential sources of error that may adversely affect the reliability of the data collected in this experiment and the subsequent interpretation of that data. The data plotted in Figure 3.11 exhibits considerable shot-to-shot variation in the signal level of fluorescent light measured by the photomultiplier. While some natural variation is to be expected, such large uncertainties warrant further consideration.

The measured LIF signal depends upon the spectral intensity of the laser used to probe the plasma; more laser power can yield more induced fluorescence transitions and hence a larger signal at the photomultipler. In the present experiment, the laser system is operated in a configuration in which shot-to-shot variation in dye laser power is no worse than 5–10%, as monitored by a Molectron J4-09 pyrocell detector. It is therefore unlikely that the laser system is the primary cause for the observed data variations.

A change in the plasma itself can cause a change in the observed signal; in particular, if the number of target ions varies between plasma shots. The coils in the gas valves used in the present experiment are energized by a capacitor bank that employs electrolytic capacitors. Bellan (2002) has studied the behavior of similar capacitors driving current through the coil of an identically constructed gas valve, as well as through a dummy load for comparison, and concluded that as the temperature of the electrolytic capacitors increases, the amount of current output by the capacitors increases despite the charging voltage being held constant. Greater current supplied to the coil of a gas valve results in a longer opening time and more gas being allowed to pass through the valve and into the vacuum chamber. It is reasonable to postulate that this could result in higher density plasmas. The impact of this heating effect can be considerable; Bellan reports a temperature increase of 10 ºC (from ~25 ºC to ~35 ºC) can result in a 250% increase of He gas flow through the gas valve. Such a temperature change can easily take place over the course of a day's experiments, during which the capacitors begin at room temperature and are then subjected to several hundred cycles of charging and discharging. The thermal dependence of the capacitor bank was not fully appreciated at the time of the experiments described in this chapter, and therefore capacitor temperature/gas throughput data is not available. However, this effect is likely to be the cause for a considerable portion of the variation seen in Figure 3.11.

3.4 Discussion

The use of laser induced fluorescence to study the behavior of plasma in a spheromak confinement configuration is a relatively novel application of the diagnostic technique; among the reasons for the limited number of such investigations may be the fact that spheromak experiments studying the use of the configuration for fusion purposes predominantly run in hydrogen gas, where LIF cannot provide data.

Whatever the cause for the small number of non-hydrogen experiments, this experiment has served as proof of principle that LIF measurements can be performed on plasmas formed by spheromak devices. Despite initial difficulties in developing an experimental apparatus capable of producing a signal, these problems have been resolved and it is now possible to generate such signals across the range of resonant laser wavelengths for a desired energy level transition. Such data has been fitted to LIF theoretical models to yield calculated values for ion temperature, density, and propagation velocity. The inclusion of additional diagnostics, such that these values may be corroborated and the ion parameters correlated with other plasma parameters to assist in forming a more complete picture of spheromak evolution, should be made a high priority in further refinements to the experiment.

Shortly after the completion of the measurements described in this chapter, the coaxial spheromak device was removed from the vacuum chamber in a scheduled transition to a new experiment that employs a spheromak formation apparatus based on coplanar geometry, as contrasted with the more traditional coaxial Marshall arrangement. As a result, it has not been possible to perform additional LIF experimental runs on the coaxial device to probe other locations in the plasma or to measure ion parameters as a function of time. Nevertheless, it is expected that the techniques developed for experiments on the coaxial device can be applied to this new coplanar gun. These investigations will be described in Chapter 4.

3.5 References

J.A. Aparicio, M.A. Gigosos, V.R. González, C. Pérez, M.I. de la Rosa, and S. Mar, “Measurement of Stark broadening and shift of singly ionized Ar lines,” *J. Phys. B: At. Mol. Opt. Phys.*, **31**, 1029 (1998).

P.M. Bellan, *Spheromaks* (Imperial College Press, 2000).

P.M. Bellan, “Thermal instability of electrolytic capacitor bank used for gas puff valve,” *Rev. Sci. Instrum.*, **73(8)**, 2900 (2002).

S.D. Bruce, J. Higinbotham, I. Marshall, and P. Beswick, “An analytical derivation of a popular approximation of the Voigt function for quantification of NMR spectra,” *J. Mag. Res.*, **142**, 57 (2000).

S.C. Hsu and P.M. Bellan, “A laboratory plasma experiment for studying magnetic dynamics of accretion discs and jets,” *Mon. Not. R. Astron. Soc.*, **334**, 257 (2002).

J.F. Kielkopf, “New approximation to the Voigt function with applications to spectral-line profile analysis,” *J. Opt. Soc. Amer.*, **63(8)**, 987 (1973).

J.B. Taylor, “Relaxation of toroidal plasma and generation of reverse magnetic fields,” *Phys. Rev. Let.*, **33(19)**, 1139 (1974).

G.K. Wertheim, M.A. Butler, K.W. West, and D.N.E. Buchanan, “Determination of the Gaussian and Lorentzian content of experimental line shapes,” *Rev. Sci. Instrum.*, **45(11)**, 1369 (1974).

E.E. Whiting, “An empirical approximation to the Voigt profile,” *J. Quant. Spectrosc. Radiat. Trans.*, **8**, 1379 (1968).

J. Yee, “Experimental investigations in spheromaks: injection into a tokamak and formation in an unbounded environment,” (Ph.D. dissertation, California Institute of Technology, 2000).

J. Yee and P.M. Bellan, “Taylor relaxation and λ decay of unbounded, freely expanding spheromaks,” *Phys. Plas.*, **7(9)**, 3625 (2000).

Chapter 4
Planar Spheromak Experiments

4.1 Introduction

The experiment to measure laser induced fluorescence signals in Ar II plasmas generated by the coaxial spheromak device, as described in Chapter 3, resulted in the successful calculation of values for the key parameters of ion density, temperature, and propagation velocity for plasmas produced by one set of experimental control settings. While the inclusion of data from additional experimental runs would have been required to provide meaningful insight into the physics of spheromak evolution in that experiment, the identification of a laboratory technique that can excite a reproducible LIF signal in spheromak plasmas should prove useful when attempting to make similar measurements on plasmas produced by other experimental devices. This chapter describes an investigation aimed at applying the techniques learned in the coaxial spheromak experiment to an experiment involving a new plasma generation device, one with electrodes configured in a geometry that is not only coaxial but also coplanar.

4.2 Spheromaks Revisited

4.2.1 Coplanar Generation of Spheromaks

Possessing an axis of symmetry is a required characteristic for a spheromak configuration. One approach to implementing this symmetry in the design of a spheromak experiment is to utilize axisymmetric electrodes, as did the device used in the experiment described in Chapter 3. However, that configuration—two nested coaxial cylinders—is not the only possible implementation of a coaxial electrode design. Hsu and Bellan (2002) have designed and constructed a plasma generating device with coaxial electrodes whose principal surfaces lie in a common plane, rather than in two nested cylinders. So as to avoid confusion with the coaxial device described in Chapter 3, this new configuration will henceforth be identified as the coplanar device, or coplanar gun. The geometry of the coplanar device is illustrated in Figure 4.1.

Spheromak formation in the coplanar device follows a sequence of events similar to that seen in the earlier coaxial device. The gas to be ionized is injected through a set of apertures in the gun electrodes, and electrostatic breakdown of the gas is again achieved via the use of a switched capacitor bank. Eight separate breakdown pathways form, one for each pair of gas injection apertures (gas breaks down between each aperture on the cathode and the closest aperture on the anode). These eight plasma flux tubes, equally distributed in the azimuthal direction and roughly identical in size, are informally referred to as “spider legs” due to their visual appearance.

After breakdown of the gas, current flows through the plasma, and a toroidal magnetic field forms in the region under the arch of the spider legs. At the inner electrode, the eight spider legs can be thought of as eight parallel current paths; these parallel currents will attract each other and eventually merge into one central column of plasma. Figure 4.2 displays a sequence of three photographs that depict the formation of the spider legs and their subsequent merger to form the central column.

Evolution of the coplanar spheromak has been discussed extensively at the theoretical level by Bellan (2003) and investigated experimentally by You, Yun, and Bellan (2005). $\mathbf{J}\times\mathbf{B}$ forces near the footpoints of the spider legs (or central column) act to accelerate plasma into the flux tube, after which the ingested plasma travels along the length of the tube. Toroidal magnetic flux is carried along with this plasma, increasing the flux density in regions of the tube far from the footpoints. This leads to an increased magnetic pinch force acting on the tube that reduces its radius; this process continues until the tube has become axially uniform, at which time the $\mathbf{J}\times\mathbf{B}$ force disappears. The now axially uniform tube can continue self-organizing toward the final expected Taylor state.

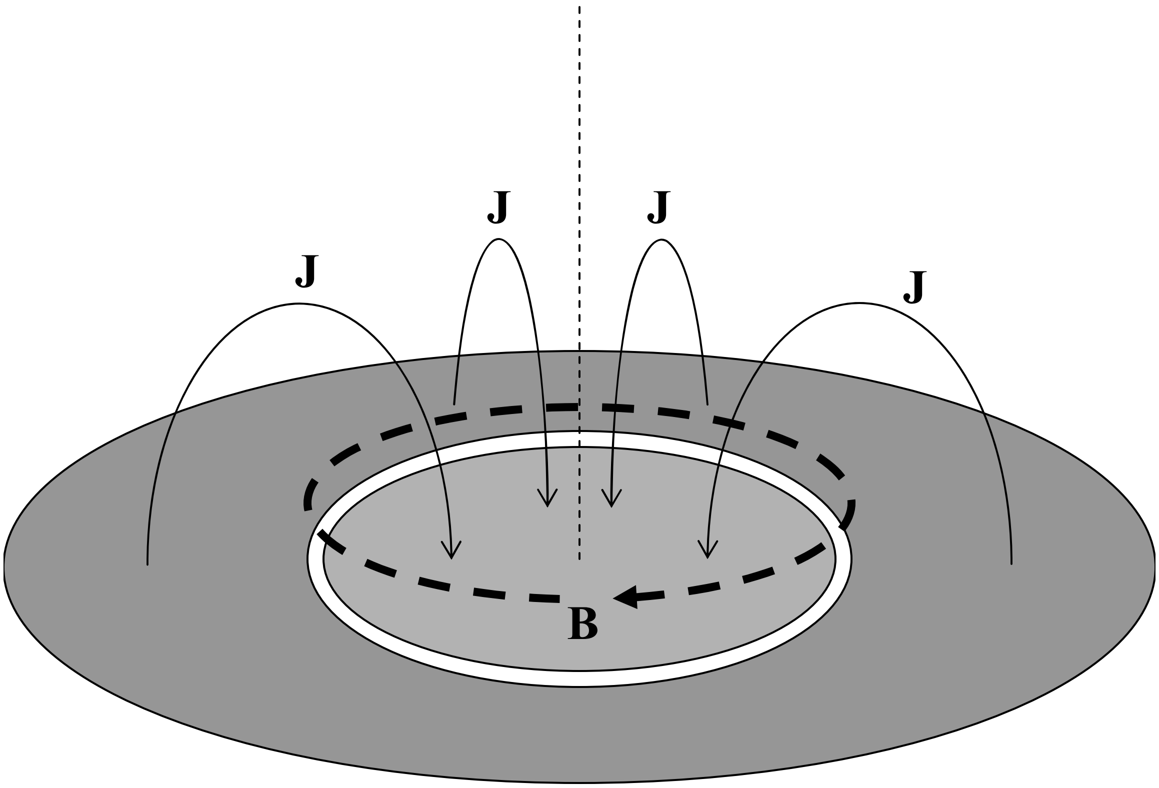

Figure 4.1. Coplanar spheromak device geometry. An external capacitor bank (not shown) drives current **J** from the anode (outer electrode) to the cathode. Eight current pathways are formed between the eight pairs of gas injection apertures on the electrodes; for clarity, only four pathways are depicted above. These poloidal currents will generate a toroidal magnetic field **B**, as shown.

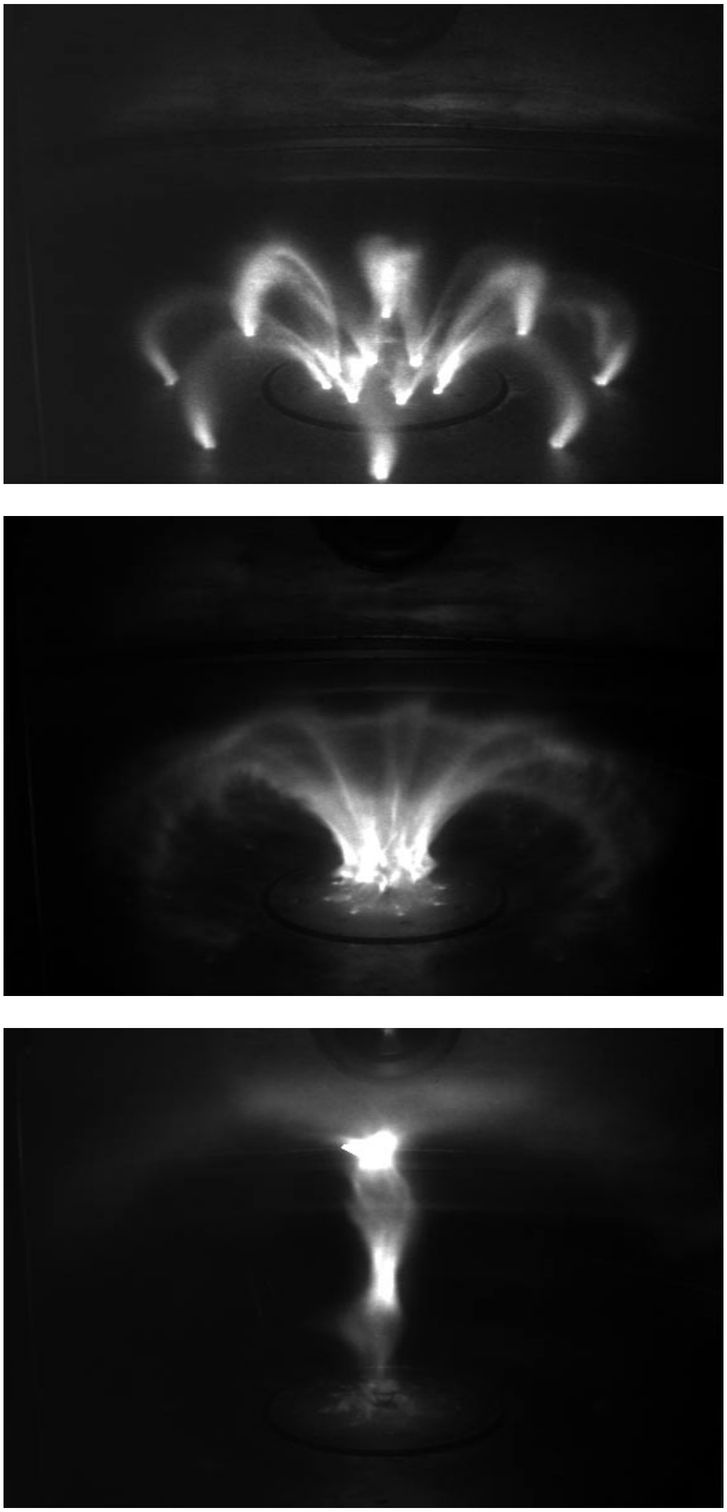

Figure 4.2. The eight spider legs formed at plasma breakdown in the coplanar device quickly merge into one central column. The column narrows in diameter as it ingests more plasma, in accordance with the theory proposed by Bellan (2003). From top to bottom, the photographs are taken at 3 μs, 6 μs, and 11 μs after the breakdown capacitor has discharged. These images were produced by a Princeton Instruments 576-G/RB-E ICCD camera.

4.2.2 The Role of α

Chapter 3 presented a brief description of the fundamental magnetic field topology common to all spheromak configurations. One of the key points is that the spheromak tends to relax to a force-free state (**J**×**B**=0) while maintaining constant magnetic helicity K=∫(**A•B**)d**S**. As noted in Section 3.2, the magnetic field that satisfies this condition is described by

$$\nabla \times \boldsymbol{B} = \alpha \boldsymbol{B} \tag{4.1}$$

To give physical significance to the parameter α in the context of the coplanar spheromak experiment, Equation 4.1 is integrated over the surface of the inner electrode.

$$\int_{GUN} (\nabla \times \boldsymbol{B}) \bullet d\boldsymbol{S} = \int_{GUN} \alpha \boldsymbol{B} \bullet d\boldsymbol{S} \tag{4.2}$$

$$\int_{GUN} \mu_0 \boldsymbol{J} \bullet d\boldsymbol{S} = \int_{GUN} \alpha \boldsymbol{B} \bullet d\boldsymbol{S} \tag{4.3}$$

$$\mu_0 I_{GUN} = \alpha \psi_{GUN} \tag{4.4}$$

$$\alpha = \frac{\mu_0 I_{GUN}}{\psi_{GUN}} \tag{4.5}$$

where I_{GUN} is the current at the inner electrode and ψ_{GUN} is the flux of poloidal magnetic field passing through the inner electrode. Thus α can be interpreted as the ratio of current flowing through the electrode to the poloidal magnetic flux. From Ampère’s law, a current I_{GUN} flowing in the poloidal direction generates a magnetic field in the toroidal direction. Hence, α is also proportional to the ratio of the toroidal field to the poloidal field (modulo a factor of r, the radius of the inner electrode). The total magnetic field **B** will be the vector sum of the toroidal and poloidal components; the relative strengths of the two components will determine the pitch angle of the overall field, which will have a helical shape as illustrated in Figure 4.3. A large α is indicative of a strong toroidal field relative to that in the poloidal direction, and the corresponding **B** will be highly twisted. Conversely, a spheromak with small α will exhibit very little twisting of the magnetic field.

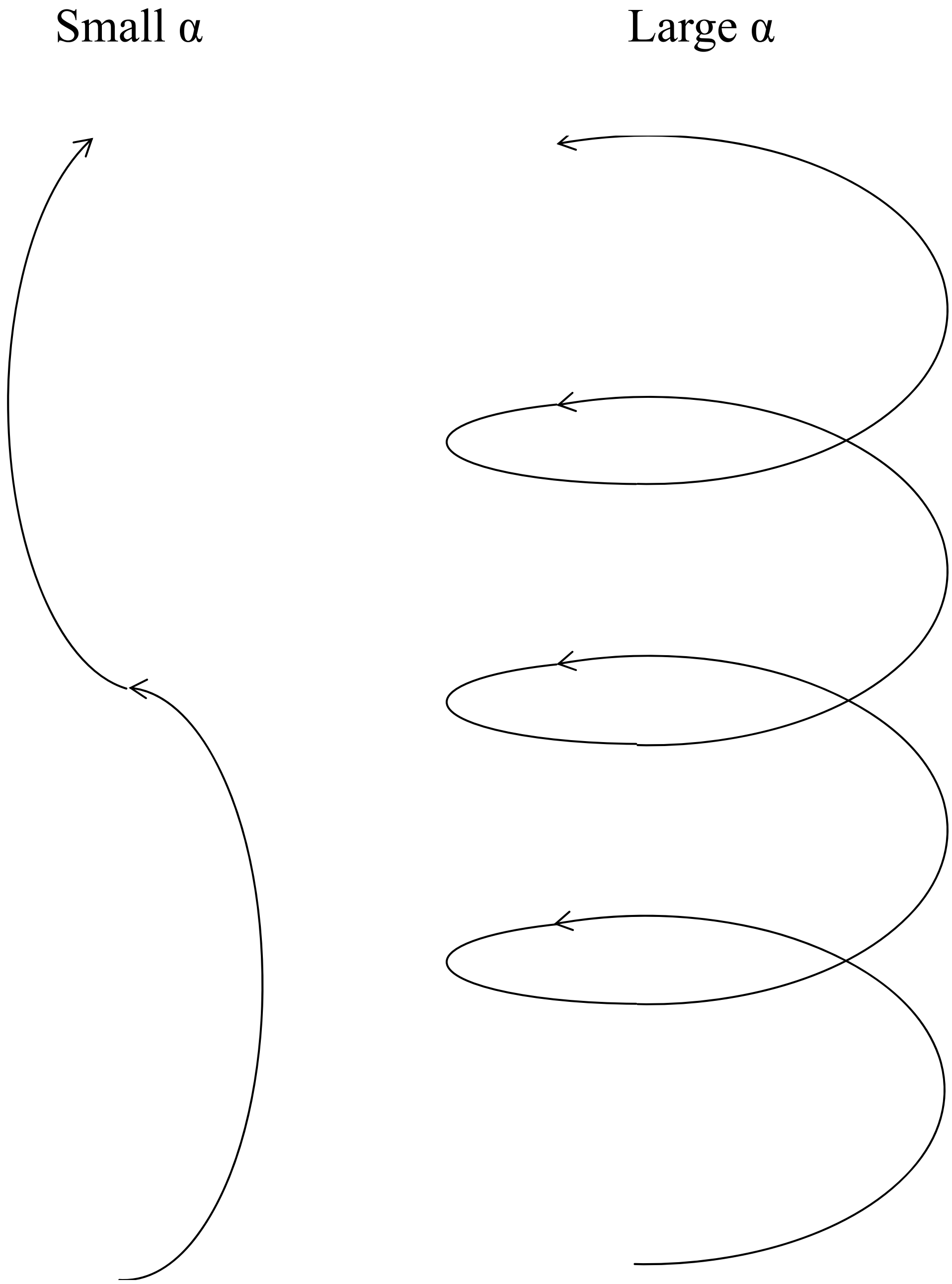

Figure 4.3. The relation of α to plasma twisting. As the value of α increases, the ratio of the toroidal magnetic field to the polodial field grows, leading to a more helical structure.

The preceding argument suggests that it should be possible to control the value of α experimentally by varying the applied stuffing flux ψ_{GUN} and/or the current I_{GUN} driven through the spheromak gun, which in practice is determined by the charging voltage used in the capacitor bank connected to the gun. The use of a laser induced fluorescence diagnostic to study plasmas of varying α may yield information regarding the extent to which plasma twistedness affects such parameters as ion temperature, density, and propagation velocity.

4.2.3 Free Expansion

Many experiments that generate plasmas in a spheromak configuration make use of a flux conserver—a conducting wall that surrounds the volume where plasma is present. Because the wall is composed of a material that is a strong conductor, the normal component of magnetic field lines must vanish at the surface, and as a result field lines form closed flux surfaces within the region bounded by the flux conserver.

By design, no flux conserver is used for the investigations described in this thesis. Instead, the vacuum vessel has been made sufficiently large in comparison to the size of the plasma that the plasma is able to expand into an effectively infinite half-space. The vacuum vessel has a diameter of ~1.5 m, while the cross-sectional diameter of the plasma at formation is on the order of 10 cm. While the magnetic field at the surface of the (conducting) chamber wall will experience the same flux conserving effect as described above, this should be occurring sufficiently far from the plasma that the plasma is able to expand freely on the time scale of the experiment. One means of testing this hypothesis is to perform orientation-sensitive measurements on the plasma to observe if there are any changes in plasma behavior after it expands to a certain size. The available laser induced fluorescence diagnostic is ideally suited for this purpose. In addition to being able to probe a specific region of plasma via selection of the volume intersected by the plasma, laser beam, and viewing angle of the photomultiplier, LIF can also selectively measure ion parameters along a chosen direction. In particular, the Doppler broadening mechanism is sensitive to the orientation of the laser as it passes through the plasma, as noted in Section 2.3.1. If a substantial difference is noted between the values found for the ion propagation rate and ion temperature along different directions, this may indicate that interactions with the wall are affecting spheromak evolution even without a dedicated flux conserver present.

4.2.4 Course of Experimental Investigation

The experiments described in the remainder of this chapter have been designed to continue the use of laser induced fluorescence to measure ion parameters in Ar II plasmas generated in a spheromak configuration, a configuration now produced by the coplanar device. Two possible courses of experimental investigation present themselves. For a given configuration of LIF-associated apparatus (specifically the orientation of the laser beam and photomultiplier viewing direction), the spheromak control settings can be manipulated to produce plasmas of different α values, and the ion parameters of the resulting plasmas can be measured and analyzed to note similarities and differences. Alternatively, for a fixed set of spheromak control settings, the orientation of the laser beam can be changed to probe the plasma along a direction of interest; two obvious candidates are observations with the laser either parallel to or perpendicular to the axis of symmetry of the spheromak.

Certain useful modifications to the experimental apparatus, suggested by practical experience acquired during the investigations performed on the previous coaxial device, have been made prior to proceeding with attempts to produce and record laser induced fluorescence signals from coplanar spheromak plasmas. Also, additional diagnostics have been incorporated into the experiment to assess the validity of the plasma parameters calculated from LIF measurements. These equipment modifications are detailed in Section 4.3.

4.3 Apparatus

4.3.1 Planar Spheromak Device

The coaxial spheromak device described in Chapter 3 was dismantled shortly after the laser induced fluorescence experiments that produced the data presented in that chapter. S. Hsu has installed a new spheromak gun, one utilizing coplanar electrodes, at the location on the vacuum chamber previously occupied by the coaxial device. The cathode of this coplanar gun consists of an 8” (20.3 cm) diameter copper disc; the anode is a copper annulus, concentric with the cathode, with a 20” (50.8 cm) outer diameter and an 8.5” (21.6 cm) inner diameter; the two electrodes are thus separated by a 1/4” annular gap. The coplanar electrodes are shown in Figure 4.4.

Many of the electrical and gas injection subsystems used for spheromak formation in the coplanar gun are the same as those used in the coaxial gun experiment. The specifications of this equipment are repeated here for convenience, with any substantial modifications noted.

A 120 μF capacitor bank charges the inner electrode, which is connected as the cathode, to voltages in the range of –4 to –6 kV. The capacitor bank discharge is initiated by a krytron/ignitron switch that is triggered by a signal transmitted over fiber optic cable. Optical isolation of the trigger circuit is used to prevent ground loops from adversely affecting the capacitor bank.

Improved versions of the custom-built gas puff valves inject argon gas into the vacuum chamber through a set of apertures in the coplanar gun electrodes. Each gas valve consists of an aluminum disc, held in place by a spring, which covers the entrance to a 1/4” Teflon tube that leads to the electrode apertures through additional stainless steel and copper tubing. Argon gas at 45 psi fills a small plenum behind the disc. To inject gas into the chamber, an electromagnetic coil on the valve is pulsed, repelling the aluminum disc away from the tube opening via the diamagnetic effect. The restoring force of the

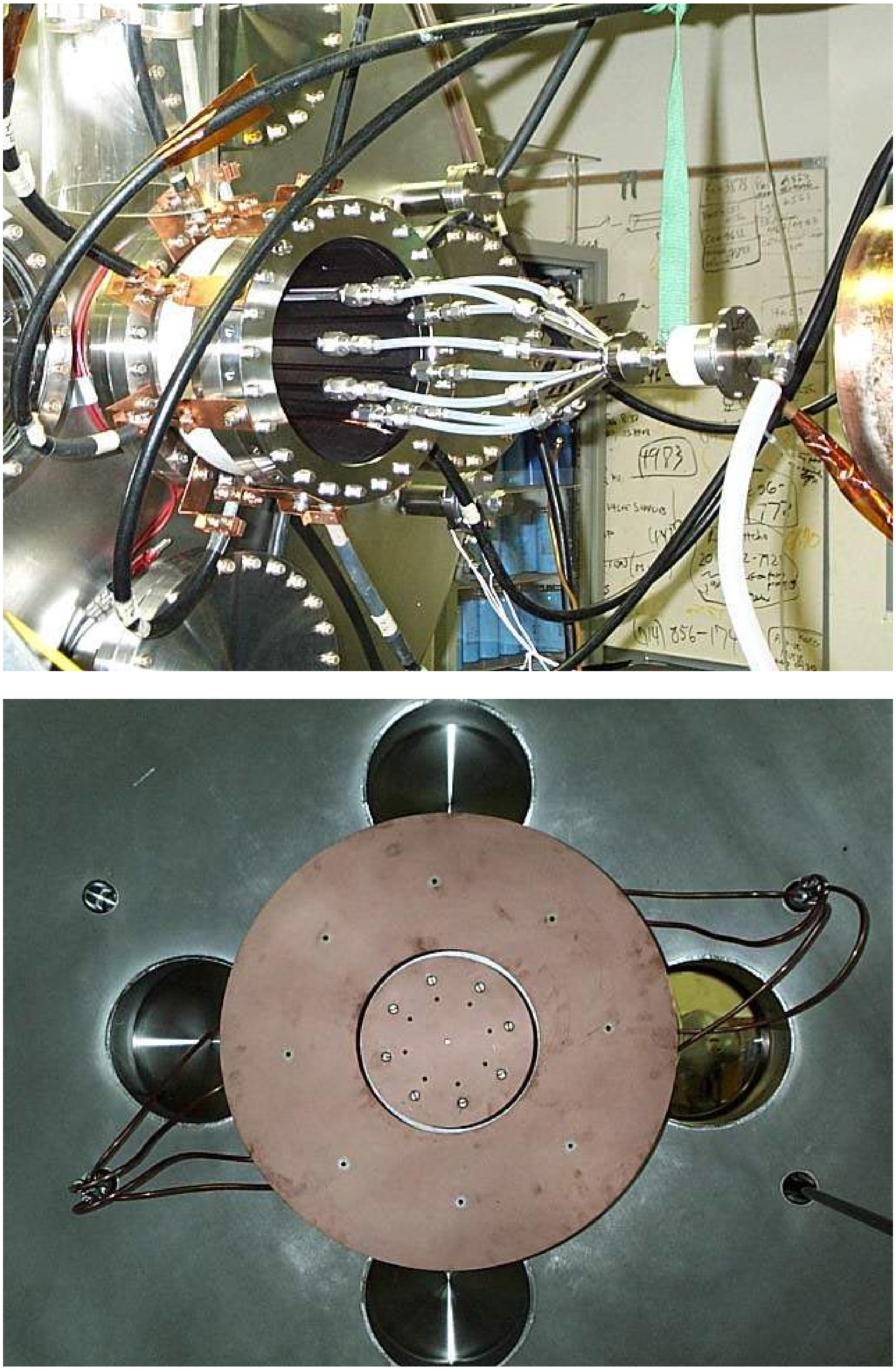

Figure 4.4. Coplanar spheromak device. (Top) Exterior view. (Bottom) Interior view.

spring and the force exerted by the gas pressure differential quickly return the aluminum disc to its original position, closing the valve. The amount of gas introduced into the vacuum chamber is therefore dependent upon the voltage used to pulse the electromagnetic coil and upon the static pressure of gas in the plenum prior to opening. The new gas valves contain stronger springs than those used in the valves in the coaxial spheromak experiment—an enhancement intended to give more consistent performance in terms of the quantity of gas injected during each opening.

The inner and outer electrodes of the coplanar gun each contain eight 1/4” diameter apertures, with the eight openings on each electrode uniformly spaced 45° apart, as seen in Figure 4.5. The holes on the inner electrode lie along a circle of radius of 4.8 cm, while those on the outer electrode are 17.8 cm from the center of the annulus. All eight apertures on the inner electrode are connected to a single gas valve, while the eight on the outer electrode are fed by two valves (four apertures per valve).

A new stuffing flux coil has been mounted within the body of the inner electrode reentry port to provide a poloidal bias magnetic field. This coil is powered by a pulsed capacitor bank and can generate up to 6 mWb of magnetic flux at the surface of the inner electrode. The coil is shown in Figure 4.6.

The coplanar gun is attached to the center reentry port at one end of the large cylindrical vacuum chamber (1.5 m diameter, 2 m length) previously described in Chapter 3. The inner electrode is affixed to the reentry port proper, while the outer electrode is held in place by two supports bolted to the wall of the vacuum chamber, with some additional support provided by the 1/4” copper tubing that connects the electrode to the gas injection vacuum feedthroughs. A Varian Megasorb roughing pump brings the chamber from atmospheric pressure down to ~10^{-3} Torr. High vacuum for the chamber is then established with an APD Cryogenics model APD-12S cryopump. Nominal base pressures inside the chamber lie in the range of $1–2\times10^{-7}$ Torr.

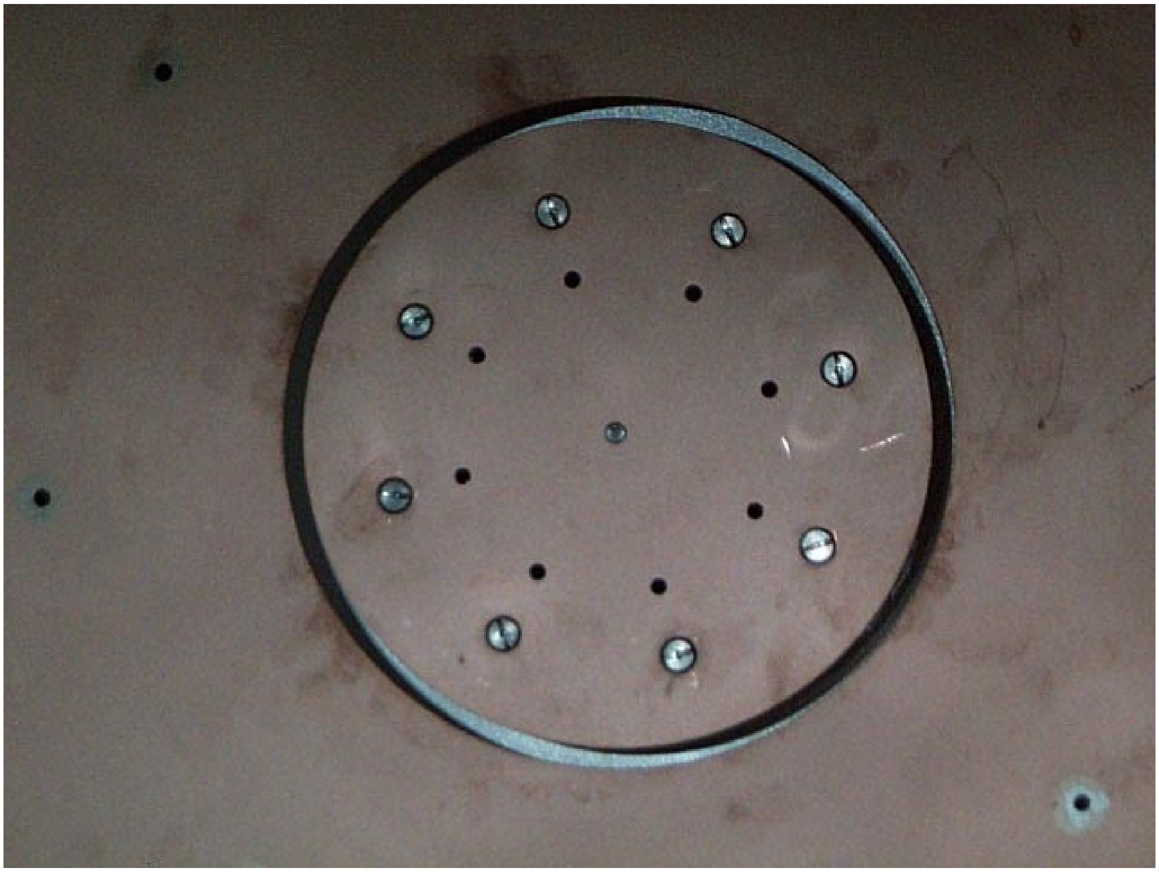

Figure 4.5. Gas injection points on the coplanar gun electrodes. The inner and outer electrodes each contain eight 1/4” apertures, connected by copper tubing to gas puff valves outside the vacuum chamber. An additional aperture located at the center of the inner electrode is not used in the present experiment.

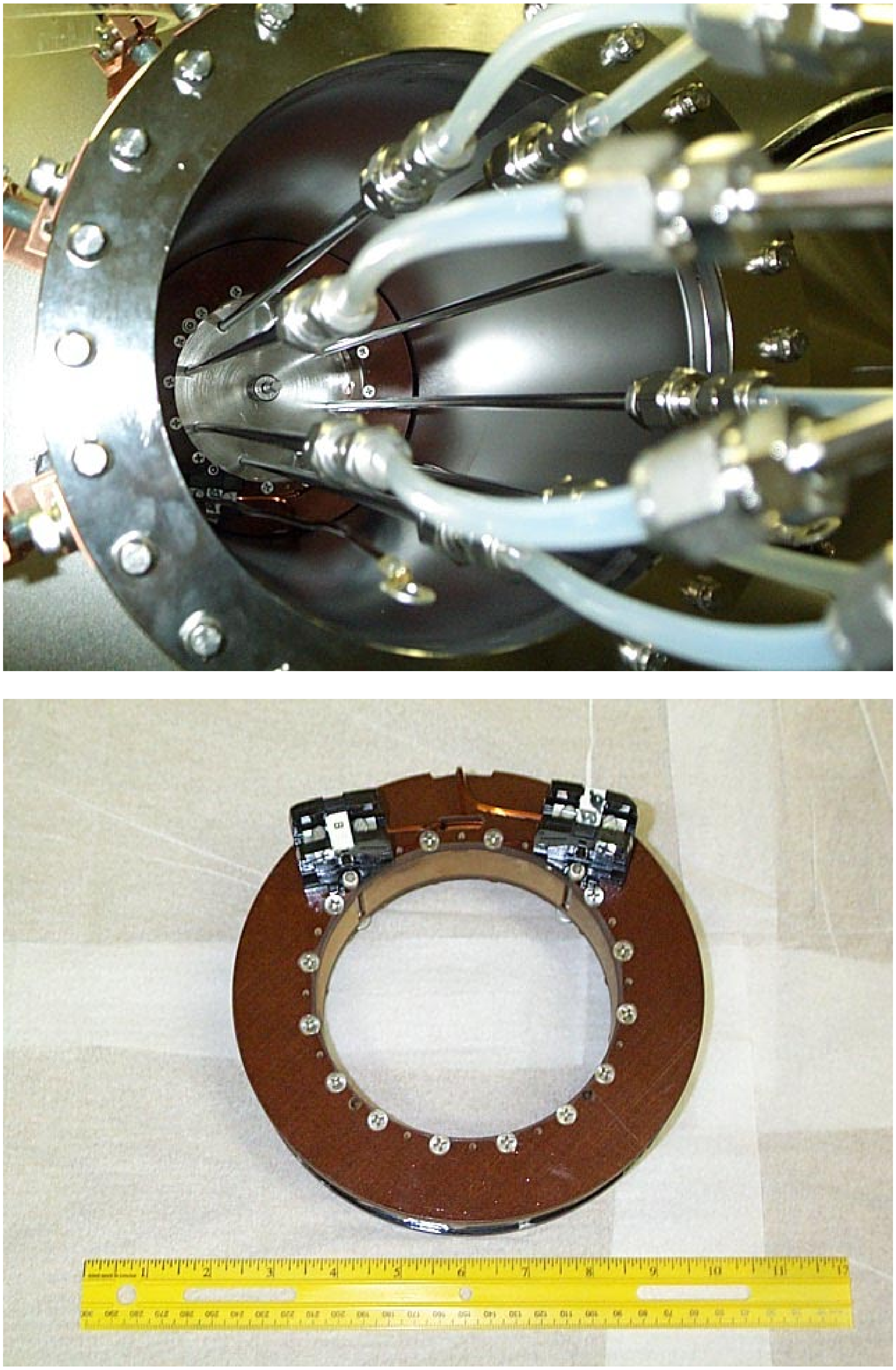

Figure 4.6. Stuffing flux coil. (Top) The coil located within the body of the inner electrode reentry port during normal operation. (Bottom) The coil prior to installation.

4.3.2 Second Gas Valve Power Supply

During early testing of the coplanar gun, electrical breakdown of argon gas frequently occurred in the Teflon tubing connecting the gas valves to the coplanar electrodes, instead of in the interelectrode region as desired. This left a dark residue (most likely burned Teflon) in the gas lines, as shown in Figure 4.7. This phenomenon was not observed in similar tests using hydrogen gas.

One possible explanation for this behavior is that the body of the gas valve floats at an electrical potential for which the Paschen criterion for breakdown, which will be discussed in another context and in greater detail in Chapter 5, is satisfied for argon but not for hydrogen. The capacitor bank that energizes the gas valve coils is connected to AC power through an isolation transformer, such that the ground potential of the capacitor bank is floating. The gas valves connected to the outer electrode of the coplanar gun will tend to float at a potential near that of the body of the vacuum chamber, which is connected to universal ground. However, the gas valve connected to the inner electrode will tend to float near the charging potential of the inner electrode, typically –4 to –6 kV. The gas valves are connected through their shared power supply, so their final potential must lie somewhere between these two limits. The resulting combination of distance between gas valves and coplanar electrodes, potential difference between the gas valves and electrodes, and gas pressure can lead to breakdown in the Teflon tubing.

Assuming this effect to be the cause of the breakdown in the gas lines, a second capacitor bank has been assembled to separate the charging systems of the inner and outer gas valves. With the outer electrode gas valves free to float near ground potential and the inner electrode valve able to float near the potential of the inner electrode, breakdown is no longer observed in the Teflon tubing.

4.3.3 Experimental Time Delays

The CAMAC time delay sequencers described in Chapter 3 are used once again

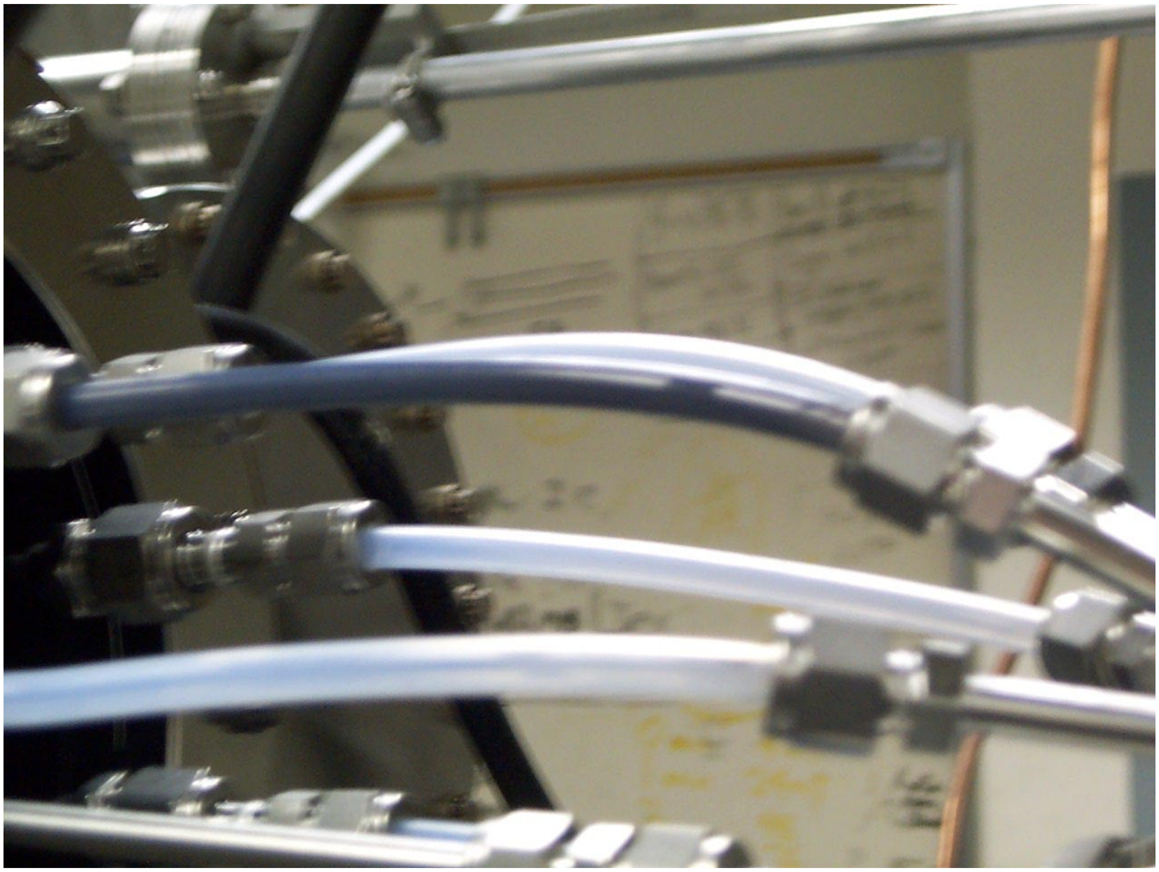

Figure 4.7. Gas injection line to the inner electrode after plasma breakdown has occurred in the Teflon tube, leaving a dark residue. A second power supply for the gas valve system has been added to the experiment to eliminate this problem.

in the coplanar experiment. The new stuffing flux coil achieves its peak magnetic field in 10 ms, as contrasted with the 23 ms required for the coil used in the coaxial experiment; the relative time delays between trigger signals used in spheromak formation have been adjusted accordingly. Also, the distance that gas must travel between the outer gas valves and the apertures on the surface of the outer electrode is longer than the corresponding distance for gas travelling from the inner gas valve to the inner electrode apertures; the two trigger signals are staggered such that gas will reach both electrodes simultaneously. Empirical observation shows that optimal performance for experiments using argon gas is achieved when the outer gas valves are triggered ~1 ms before the inner gas valve. Table 4.1 contains a list of experimental timings used in the present experiment. The spheromak time delays are shown relative to the stuffing flux coil trigger, the first event in the spheromak formation sequence. It should be noted that this trigger is sent 756 μs after the signal from the flip-flop synchronization circuit is received at the twelve-channel CAMAC module. With these time settings, the laser intercepts the plasma approximately 14 μs after the main capacitor bank has discharged, when the leading edge of the plasma passes in front of the field of view of the emitted light collection apparatus.

Laser System Time Delays	
Event	Time
Synchronization signal sent to spheromak time delay generator	---
YAG flashlamps	10 ms
YAG Q-switch	10.7684 ms

Spheromak Time Delays	
Event	Time
Stuffing flux coil trigger	---
Outer gas valves trigger	1.5 ms
Inner gas valve trigger	2.5 ms
Main capacitor bank discharge	10 ms
Imacon camera trigger	10.01 ms (variable)
LeCroy fast digitizer trigger	10.014 ms (variable)

Table 4.1. Experimental time delays used in the coplanar spheromak experiment.

4.3.4 Laser Collimating Lens

The collimating lens located at the exit ferrule of the optical fiber transmitting the laser beam has been replaced with a Newport PAC022 achromatic doublet prior to the experiments described in this chapter. This lens has a focal length of 25.4 mm; the distance between the lens and the ferrule tip is reduced accordingly to maintain proper collimation of the laser beam. The diameter of the new collimating lens is 12.7 mm, equal to that of the previous lens. This modification has been motivated by the observation that a 50.8 mm separation between ferrule and lens results in the diverging laser beam nearly extending outside the radius of the lens; at 25.4 mm, the entire beam is captured and collimated.

4.3.5 Target Probe

Proper alignment of the light collection optical components is crucial for an induced fluorescence signal to be detected. With the photomultipler outside the vacuum chamber and located approximately 1 m from the intersection of the plasma and the laser ($\varphi_{\text{intersection}} \approx 2$ cm), even a small misalignment can result in the photomultipler observing the incorrect region of the plasma and missing some portion of any LIF signal that may be present.

Following a suggestion by R. Stern, a target probe has been constructed to aid in alignment of the optical path. The target consists of a sandblasted Pyrex glass sphere ($\varphi_{\text{sphere}} \approx 3$ mm) attached to the end of a 44 cm aluminum rod that is mounted at a 90º angle to a stainless steel rod that can be translated through a vacuum flange to provide motion parallel to the axis of the spheromak. Aluminum has been used as it is more easily machinable than stainless steel, but the choice of material is not a critical design element. Figure 4.8 shows the target probe assembly as seen from inside the vacuum chamber.

When the target is at the same axial distance from the planar gun as the laser beam, the probe assembly is rotated to place the glass sphere on the spheromak axis proper. When the laser strikes the glass sphere, a specular reflection is created that can be

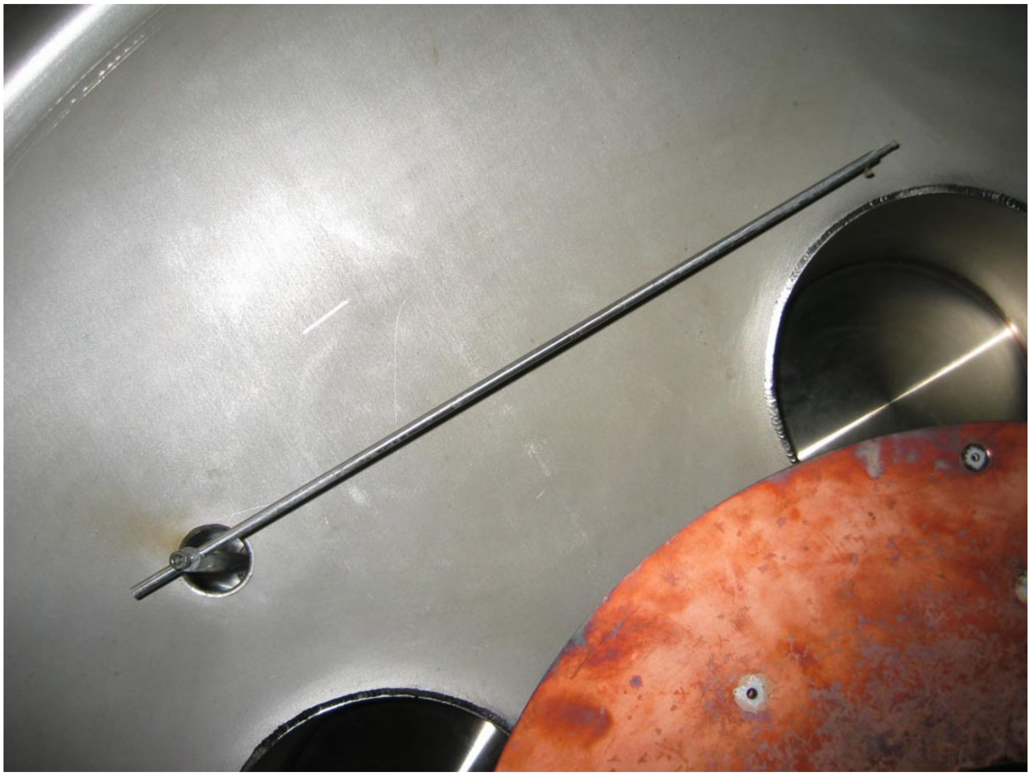

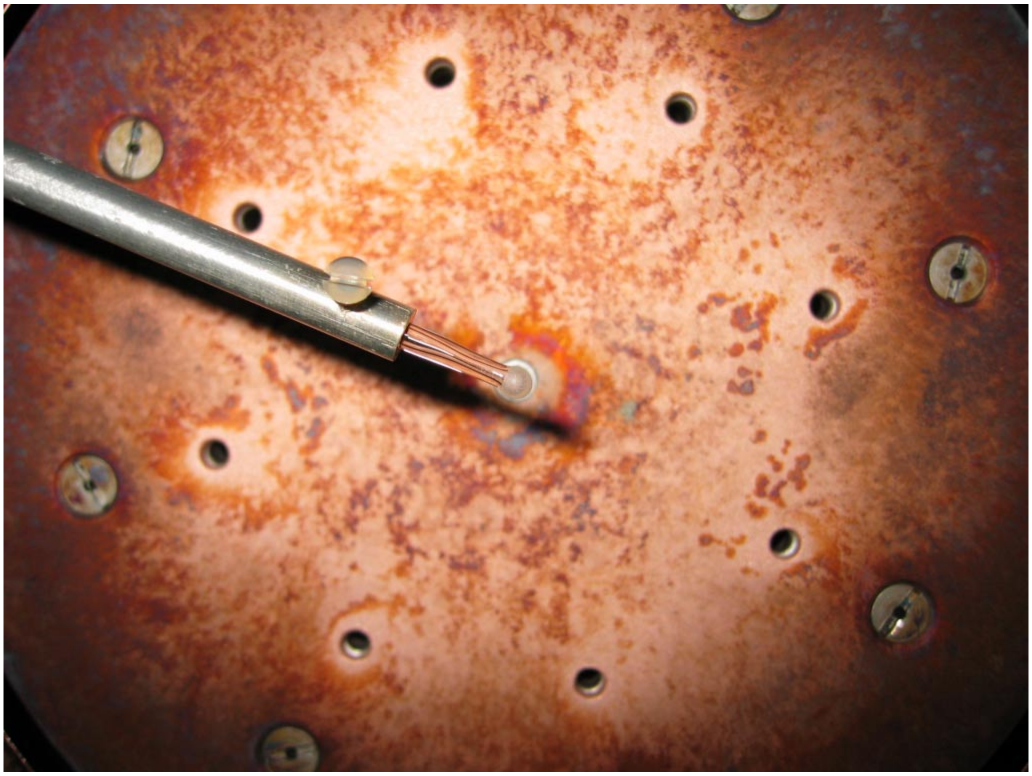

Figure 4.8. (Top) Target probe in neutral position and (bottom) rotated to place the glass sphere target at the intersection of the spheromak axis and the laser beam.

viewed from all directions. Sufficient laser power is available to produce a small output signal (5–10 mV) from the photomultiplier in response to this light, even with the 460.96 nm narrow bandwidth filter present. Thus, by illuminating the target with the laser and adjusting the orientation of the photomultiplier to maximize the detected signal, it is possible to align the PMT such that one is assured of imaging the region along the central axis of the spheromak that will be intersected by the laser. Once the optimal photomultiplier orientation has been determined, the target may be moved to a neutral position.

4.3.6 LIF Reentry Port

The fluorescent light collection design used in the previous coaxial gun experiment was vulnerable to a number of problems. Spontaneous light emission from regions of the plasma not illuminated by the laser could reach the photomultipler either via reflections off the interior walls of the vacuum chamber or by refraction through the convex lens located in front of the photomultiplier. The use of the opaque mask on the vacuum chamber window does appreciably reduce the amount of stray light collected, but a more effective solution is desirable.

A more serious concern with the light collection design is the potential for misalignment of the optical path, leading to the photomultiplier not detecting an LIF signal, as discussed in the previous section. One modification to the experiment that addresses both issues is the installation of a dedicated LIF reentry port that mounts the photomultiplier at one end of a tube that points directly at the intersection of the plasma and laser beam. Such a reentry port has been assembled and is shown in Figure 4.9. The port consists of a stainless steel tube (outer diameter=3/4”, length 4’) that is open at one end and has a 1.33” window flange mounted at the other end. The usable viewing surface of the window has a diameter of ~0.6”. A non-conducting Lucite block has been machined to secure the photomultiplier to the open end of the tube, such that the axis of the tube is centered on the photomultiplier head located behind the 460.96 nm interference filter.

The reentry port solves the alignment problem by virtue of the rigidity of the stainless steel tube, effectively connecting the photomultiplier and expected LIF signal region with a straight line. The level of extraneous light reaching the photomultiplier head is greatly reduced, as only that emitted light which goes through the reentry port window can reach the photomultiplier. To avoid oblique reflections within the body of the tube, the interior surface is lined with the same non-reflective paper used in the earlier opaque mask. The reentry port can be moved to situate the viewing window at a desired radial distance from the spheromak axis; a distance of 15–20 cm is typically used during experiments.

4.3.7 High Sampling Rate Digitizer

The LIF signals observed in the coaxial gun experiment described in Chapter 3 had a duration of ~30 ns, as was shown in Figure 3.10. It is therefore desirable to incorporate into the coplanar experiment a data acquisition system that possesses sufficient time resolution to sample such signals. The LeCroy model 6880 waveform digitizer contains a biphase clock operating at a frequency of 674 MHz, corresponding to a time resolution of 0.742 ns, adequate to yield approximately 40 data points per 30 ns LIF signal. The 6800 can store up to 10,000 memory locations per trace, resulting in a maximum total acquisition time of 7.42 μs.

One drawback of the LeCroy 6880 is its limited input voltage range. The 6880 accepts a fixed 0.5 V p-p input centered about a DC offset that can be programmed from –0.25 V to +0.25 V. As the output signal from the photomultiplier used in the experiment is negative, the offset for the 6800 is nominally set at –0.25 V to establish a window for measuring LIF signals between –0.75 V and –0.25 V. The gain of the photomultipler is typically set to produce a signal of approximately –5 V in response to the brightest region of plasma viewed, as any higher gain setting results in saturation of the detector, which affects its performance. To reduce the photomultiplier signal to a level that can be mea-

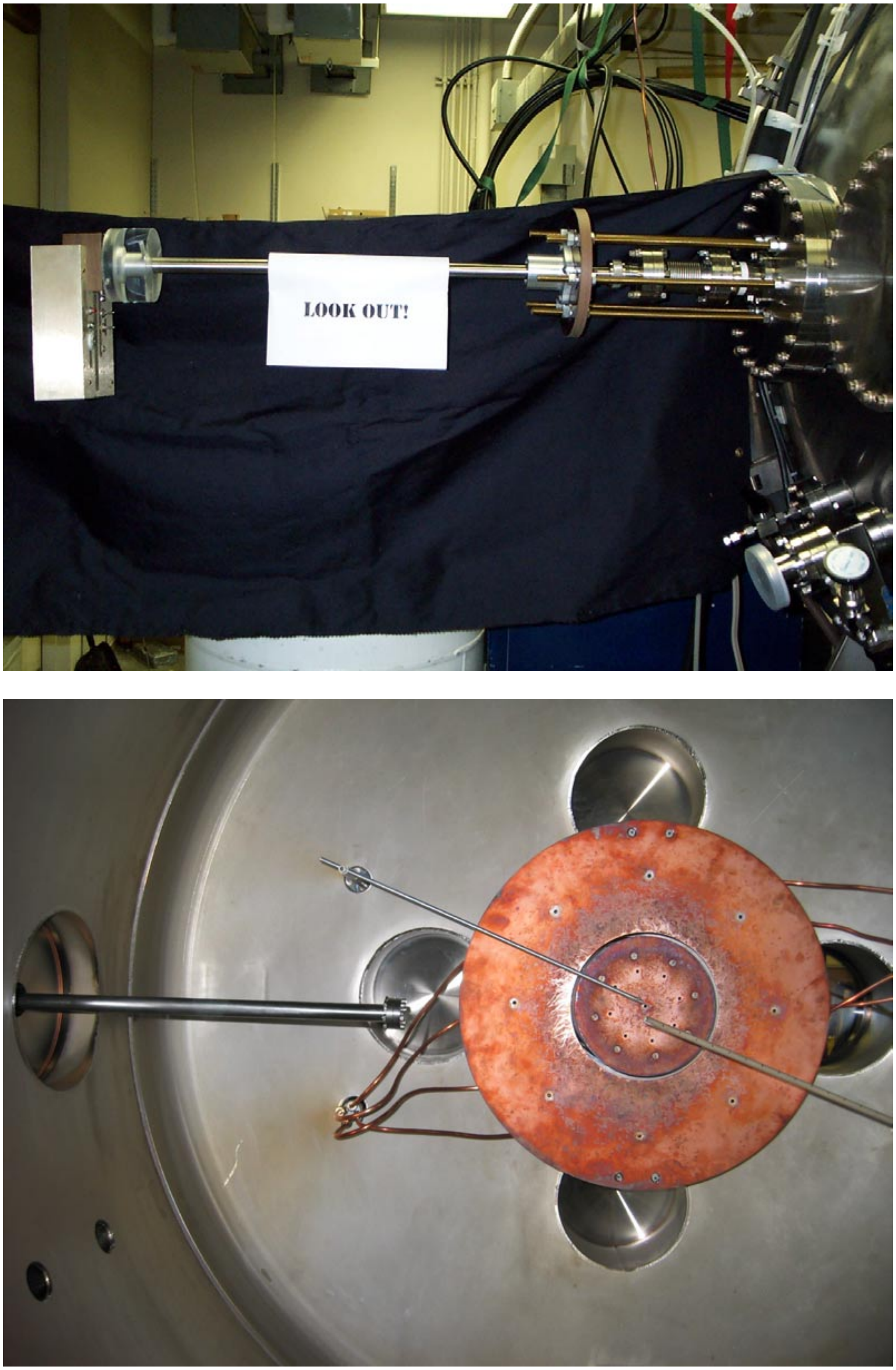

Figure 4.9. LIF reentry port. (Top) External view, with the photomultiplier mounted on the stainless steel tube. (Bottom) Reentry port, at left, as seen inside the vacuum chamber.

sured by the digitizer, 15 dB of coaxial attenuation is used at the input of the 6800.

Programming of the LeCroy 6800 and storage of the digitized photomultiplier data are performed by personal computer via GPIB interface.

4.3.8 High Speed Framing Camera

High speed photography has proven to be a valuable diagnostic tool in many plasma experiments, providing information on plasma position and morphology by means of imaging the visible light emitted by plasma ions and/or neutrals. Previous Caltech plasma experiments (Yee and Bellan 2000, among others) made use of Princeton Instruments model 576-G/RB-E ICCD cameras, which provide high quality 16-bit resolution images at shutter speeds of as little as 5 ns. One drawback of the Princeton camera is that it is a single exposure device. To study plasma evolution, a series of plasma shots must be made, with one photograph per discharge and each photograph taken at a different time relative to plasma breakdown. The still images can then be combined for viewing as a motion picture, but shot-to-shot variation between plasma discharges negatively impacts the usefulness of such data.

A DRS Hadland Imacon 200 ICCD camera was acquired during the course of the investigations described in this chapter. The Imacon employs an eight-way prism and computer-controlled time delays to take up to 16 photographs in response to a single trigger, with interframe intervals down to 100 ns. While Imacon pictures lack the resolution of those produced by the Princeton camera (the Imacon has only 10-bit resolution), the ability to image an individual plasma discharge from breakdown through the course of its evolution represents a considerable advantage over the single exposure device.

Imacon images have contributed to the work described in this thesis by providing visual information regarding plasma position, such that laser timing can be properly synchronized with spheromak formation to have the beam intersect the plasma at a desired stage. Also, a rough approximation of the ion propagation velocity can be estimated from

Imacon images of the plasma by tracking the location of distinguishable features in the plasma as a function of time, as will be described in Section 4.5.

4.4 Observations Perpendicular to the Spheromak Axis

This section presents results obtained in LIF experiments on plasmas produced by the coplanar gun in which the probing laser has been oriented perpendicular to the axis of the spheromak. Experimental controls have been set to produce plasmas that exhibit peak plasma currents of $I_{GUN}\approx120$ kA with an applied $\psi_{GUN}\approx2$ mWb, for an expected α value of $\alpha\approx75\ \mathrm{m}^{-1}$.

4.4.1 LIF Signal Measurement

Light from the argon plasma is again collected by the photomultiplier, whose output voltage is now recorded by a LeCroy 6880 digitizer and stored to computer hard drive for later analysis. A representative signal trace is shown in Figure 4.10; the induced fluorescence is seen as the sharp peak dipping below background level at t=470 ns. The photomultiplier signal recorded from 25–30 ns prior to the LIF maximum and the signal recorded from 25–30 ns after the maximum are averaged to provide a mean value for the amount of background light emission; this value is subtracted from the LIF signal prior to fitting data to the line broadening models. The shaded regions in Figure 4.10 represent those portions of the recorded photomultiplier signal that have been used to estimate the background emission level.

4.4.2 Fitting to Theoretical Model

The fitting of experimental data to the LIF spectral line broadening mechanisms is performed with IDL software routines in the same manner as described in Section 3.4. For the convenience of the reader, the models are once again explained in the following sections.

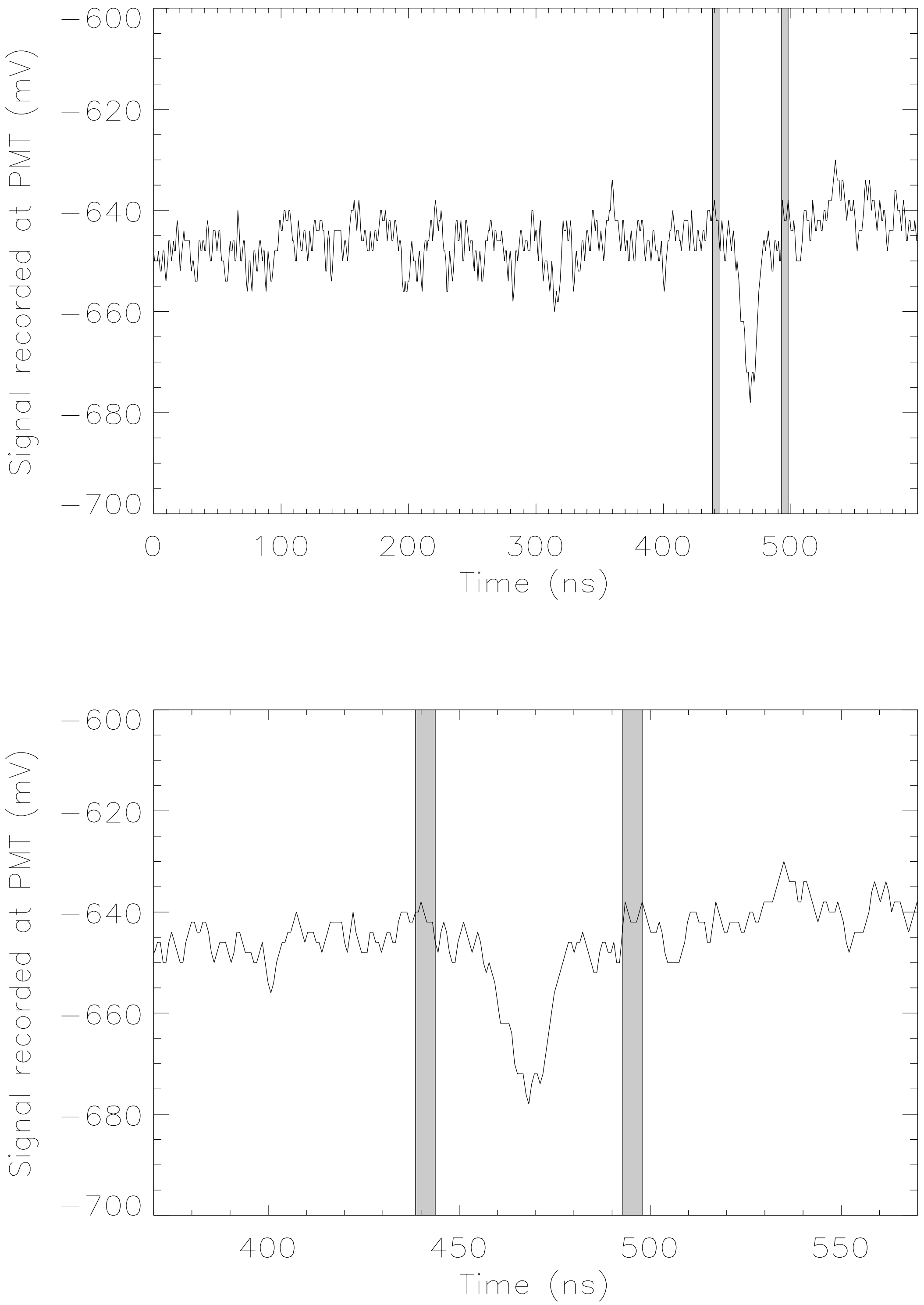

Figure 4.10. Photomultiplier signal recorded in the coplanar spheromak experiment. An LIF signal is clearly visible at t=470 ns. The average signal recorded in the shaded regions is taken as the level of background emission and is subtracted from the LIF signal prior to fitting theoretical line broadening models to the data.

4.4.2.1 Doppler Broadening

If the dominant spectral line broadening mechanism responsible for the width of the observed distribution in Figure 4.11 is Doppler broadening due to thermal motion of the ions, the functional form of the relationship between fluorescent light intensity and laser wavelength should be Gaussian. The IDL GAUSSFIT routine has been used to fit the collected LIF data to a function of the form

$$I(\lambda) = A_0 \exp\left(-\frac{x^2}{2}\right) \tag{4.6}$$

$$x = \frac{2\,(\lambda - A_1)}{A_2} \tag{4.7}$$

where the fitted parameter A_0 is the fitted function's peak amplitude, A_1 the wavelength at this peak amplitude, and $2\bullet(2\ln 2)^{1/2}\bullet A_2$ the $\Delta\lambda_{FWHM}$ of the Gaussian. For the data shown in Figure 4.11b, the best-fit parameters are A_0=27±1 mV, A_1=611.556 nm, and A_2=16±1 pm.

The A_1 parameter provides an estimate for the ion propagation rate, as defined by Equation 2.2. Taking λ_0=611.49 nm as the rest wavelength corresponding to the energy difference between the initial state and intermediate state of the Ar II fluorescence transition under investigation, the computed value of A_1 suggests an ion velocity of ~32 km/s. (A velocity greater than 0 represents motion toward the incident laser beam; motion away from the laser would be represented by a negative velocity.) In the present experimental configuration, this means that the vertical component of the velocity of the diagnosed volume of plasma is directed upward at the time the measurement is made.

Ion temperature in the Doppler broadening model is related to the $\Delta\lambda_{FWHM}$ of the fitted Gaussian distribution by Equation 2.7. The best-fit model to the experimental data collected in the present experiment suggests a $\Delta\lambda_{FWHM}$ of 38±2 pm. Inserting this value into Equation 2.7 results in a calculated ion temperature of 26±5 eV.

4.4.2.2 Stark Broadening

If the plasma produced by the coplanar spheromak device is of high ion density and low ion temperature (such that line broadening due to thermal motion may be ignored), the observed broadening of the fluorescent light distribution should be due to the Stark effect. Here, the function to which the experimental data should be fit is a Lorentzian distribution. The IDL CURVEFIT routine is used to fit the data to the function

$$I(\lambda) = A_0 \frac{1}{\pi} \frac{1}{1 + x^2} \tag{4.8}$$

where x, A_0, A_1, and A_2 have the same definitions as in the previous section. The best-fit parameters to the Stark model are found to be A_0=87±1 mV, A_1=611.556 nm, and A_2=37±1 pm.

According to the linear Stark fitting procedure of Aparicio and colleagues (1998), a Stark $\Delta\lambda_{FWHM}$ of 37 pm corresponds to a plasma ion density of $\sim 1.1 \cdot 10^{23}$ m^{-3}.

4.4.2.3 Voigt Profile

Assuming that the observed lineshape is due to the presence of both Doppler and Stark broadening mechanisms, the Voigt profile, the function to be fitted to the data is the convolution of each mechanism's individual broadening profile.

$$I(\lambda) \sim \int \frac{\exp\left(\dfrac{-\xi^2}{\Delta\lambda^2_{FWHM,D}}\right)}{1 + \dfrac{(\lambda - \xi)^2}{\Delta\lambda^2_{FWHM,S}}} d\xi \tag{4.9}$$

Instead of directly fitting experimental data to the function defined by Equation 4.9, a less computationally intensive alternative is often used that approximates the convolution as a linear combination of a Gaussian function and a Lorentzian function, where the $\Delta\lambda_{FWHM}$ of these two functions are set equal to each other, such that this value will also be the $\Delta\lambda_{FWHM}$ of the fitted lineshape. The true linewidths of the convolved Gaussian and Lorentzian in Equation 4.9 are subsequently computed using the fitted $\Delta\lambda_{FWHM}$ of the approximation and the fractional contribution of each function to the linear combination. Bruce (2000) presents an extensive discussion of this approximation and of the error it introduces and claims the error in linewidth of the calculated Voigt shape is on the order of

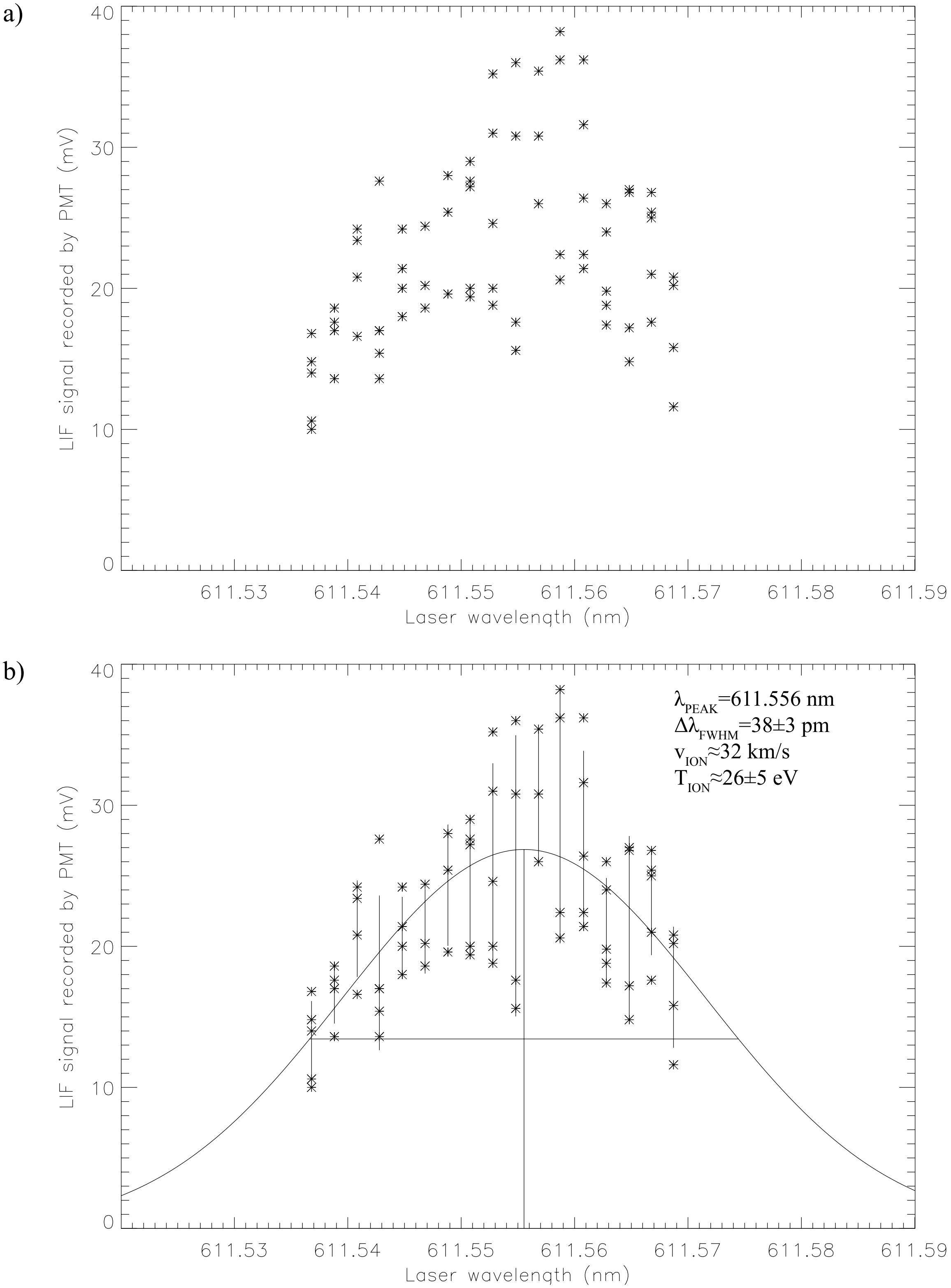

Figure 4.11. a) Photomultiplier signal of laser induced fluorescence at 460.96 nm as a function of incident laser wavelength for λ_{LASER}=611.537–611.569 nm. Five (5) plasma shots are made at each wavelength shown. Best-fit curves are shown for b) Doppler, c) Stark, and d) Voigt line broadening models.

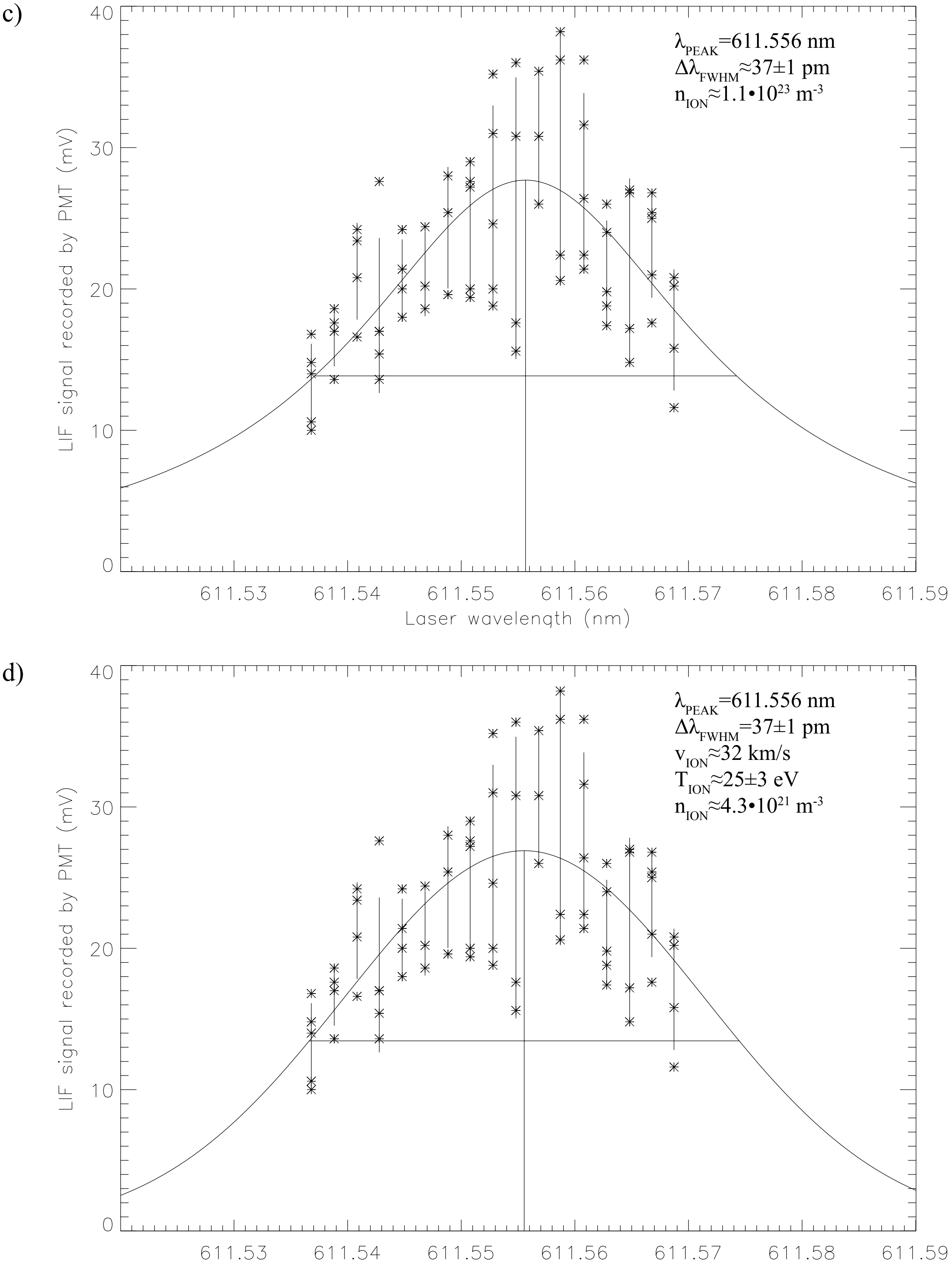

Figure 4.11. a) Photomultiplier signal of laser induced fluorescence at 460.96 nm as a function of incident laser wavelength for λ_{LASER}=611.537–611.569 nm. Five (5) plasma shots are made at each wavelength shown. Best-fit curves are shown for b) Doppler, c) Stark, and d) Voigt line broadening models.

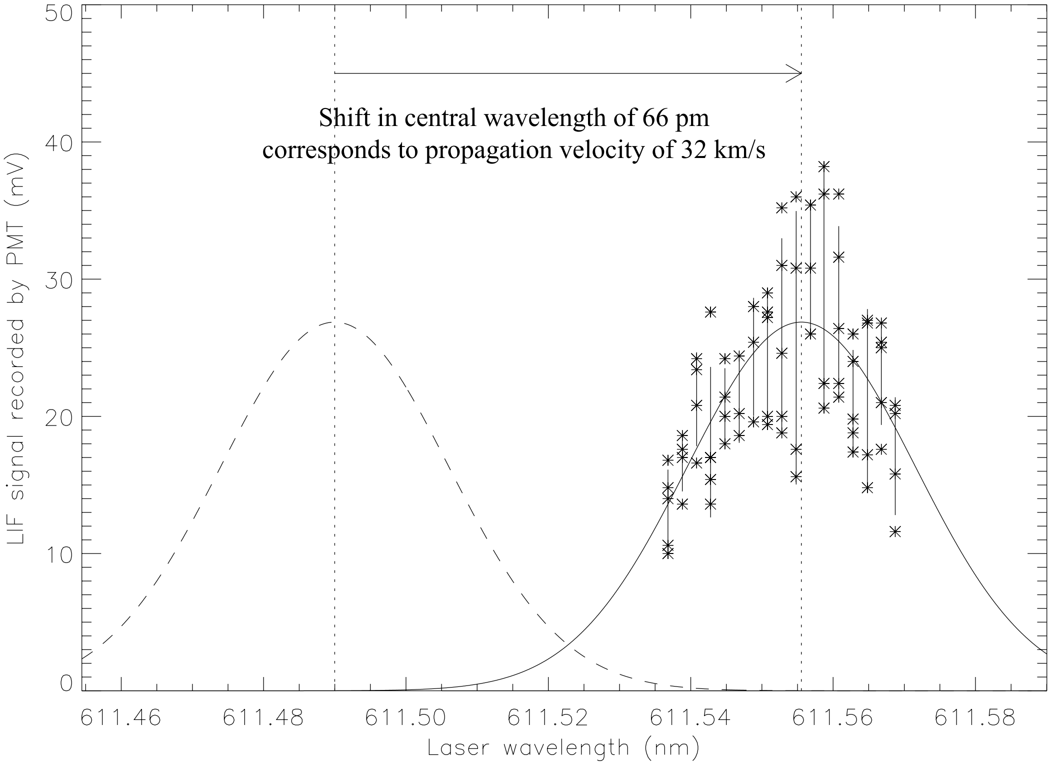

Figure 4.12. Propagation velocity corresponding to the shift in observed central wavelength of the ion distribution function for the data shown in Figure 4.11.

1–3%. The area under the function is expected to deviate from the true value by no more than 0.72%.

The experimental data is fitted with the function

$$I(\lambda) = A_0\left[A_3 \frac{1}{\pi}\frac{1}{1+x^2} + (1 - A_3)\sqrt{\frac{\ln 2}{\pi}}\exp\left(-\ln 2 \cdot x^2\right)\right] \tag{4.10}$$

x, A_0, A_1, and A_2 have the same meaning as in the separate Doppler and Stark models presented earlier. The constant coefficients involving π and ln 2 stem from the use of normalized expressions for the Lorentzian and Gaussian functions (an additional factor of 2 common to both functions has been incorporated into A_0). The A_3 parameter denotes the fractional contribution of the Stark function to the overall lineshape, such that $1–A_3$ represents the Doppler contribution. It is expected that A_3 will lie in the range $0 \le A_3 \le 1$. Wertheim (1974) asserts that lineshapes in which the best-fit A_3 lies outside this range are possible and indicate the presence of significant line broadening from a mechanism other than Doppler or Stark considerations.

For the coplanar gun data shown in Figure 4.11d, the best-fit Voigt parameters are A_0=59±3 mV, A_1=611.556 nm, A_2=38±1 pm, and A_3=0.07. To obtain ion temperature and density information, it is necessary to calculate the linewidths of the original Doppler and Stark components that convolve to give the Voigt lineshape in Equation 4.9. Bruce provides an empirically derived relationship between the $\Delta\lambda_{FWHM}$ of the fitted lineshape in Equation 4.10 and the $\Delta\lambda_{FWHM}$ of the Doppler component of Equation 4.9 as a function of the Doppler fraction $1–A_3$.

$$\Delta\lambda_{FWHM,\,Doppler} = \Delta\lambda_{FWHM,\,Voigt}\left(\frac{1 - A_3}{0.97}\right)^{0.43} \tag{4.11}$$

By construction, the $\Delta\lambda_{FWHM}$ of the fitted Voigt function is the parameter A_2. Using the computed value for $1–A_3$, we calculate an expected Doppler $\Delta\lambda_{FWHM}$=37±2 pm, which corresponds to an estimated ion temperature of 25±3 eV.

A relationship between the $\Delta\lambda_{FWHM}$ of the fitted Voigt function in Equation 4.10 and those of the convolved Gaussian and Poisson functions in Equation 4.9 is given in

Whiting (1968), based on fitting to data originally obtained by Van de Hulst and Reesinck (1947). This relationship has the form

$$\Delta\lambda_{FWHM,\,Stark}=\frac{\Delta\lambda^2_{FWHM,\,Voigt}-\Delta\lambda^2_{FWHM,\,Doppler}}{\Delta\lambda_{FWHM,\,Voigt}} \tag{4.12}$$

As the $\Delta\lambda_{\mathrm{FWHM}}$ of the fitted Voigt function in Equation 4.10 and the calculated $\Delta\lambda_{\mathrm{FWHM}}$ of the Doppler component in Equation 4.9 are now known quantities, the $\Delta\lambda_{\mathrm{FWHM}}$ of the Stark contribution follows directly and is computed to be ~1 pm. This value corresponds to a plasma ion density of $\sim 4.3 \bullet 10^{21}$ m^{-3}. As noted in Chapter 3, ion parameter estimates returned by the Voigt profile analysis, which assumes line broadening due to both ion temperature and density, are believed to approximate plasma parameters more accurately than estimates provided by the individual Doppler or Stark analyses.

Using line-integrated spectroscopic measurements, You, Yun, and Bellan (2005) report plasma densities between 10^{20}–10^{22} m^{-3} for both hydrogen and nitrogen plasmas generated by the coplanar spheromak device under experimental conditions comparable to those used in the present work. (The highest densities are found within the central column of plasma, with density decreasing as one moves away from the spheromak axis.) G. Yun reports in private communication that argon plasmas produced by the coplanar device have also been observed to exhibit similar densities. The LIF-calculated ion density given by the Voigt profile analysis thus falls within the range that would be expected based upon these passive spectroscopic measurements.

4.4.3 Additional Perpendicular Measurements

The LIF measurements detailed in the previous sections yielded one set of calculated ion parameters. To investigate the reproducibility of these results, a second experimental run has been performed using the same experimental control settings (capacitor bank charging voltages, timing sequencer delays, etc.) A qualitative assessment of the data obtained in the first run suggests that more plasma shots should be taken at each laser wavelength to reduce statistical variation, but that the laser wavelength may

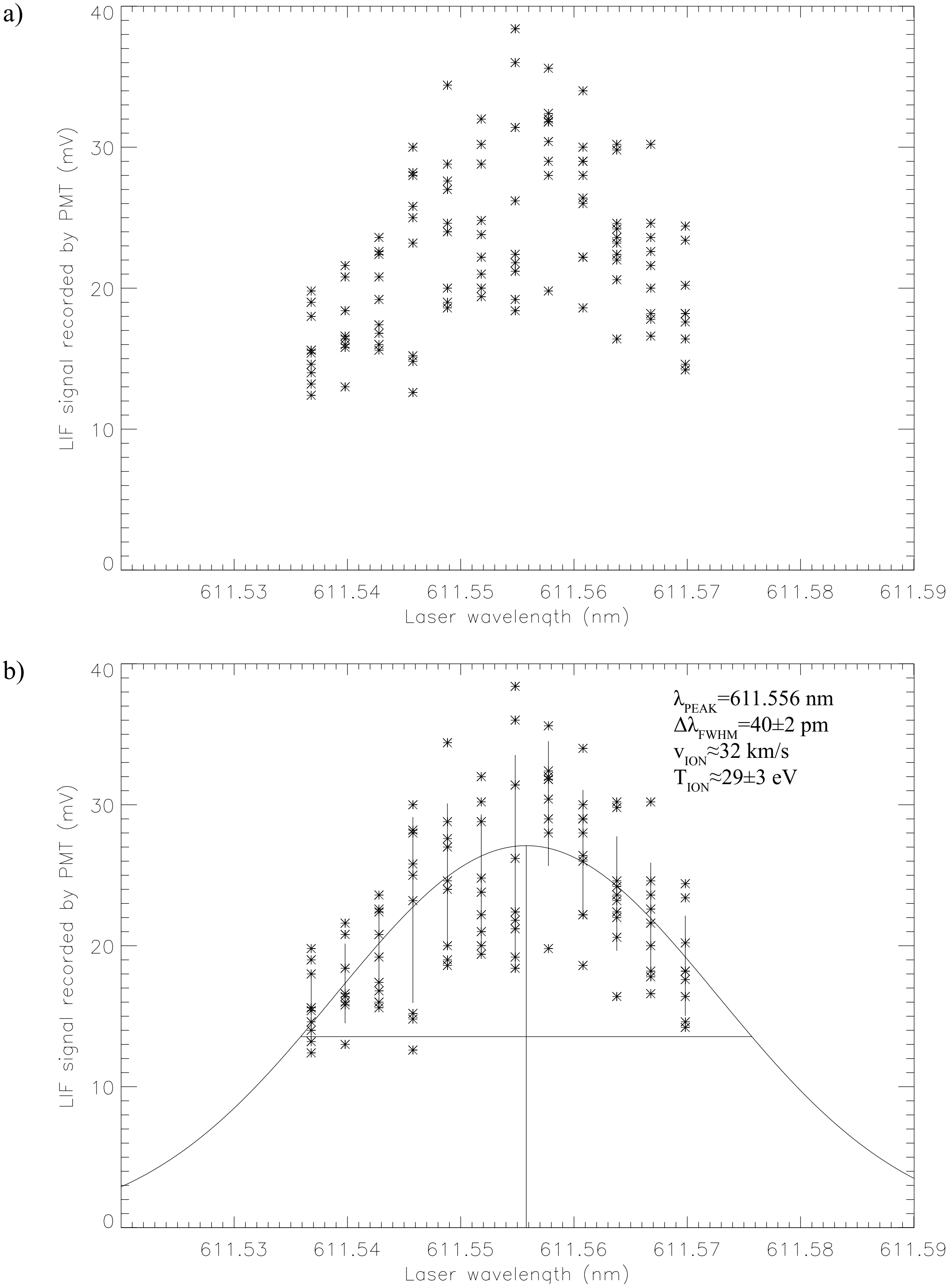

Figure 4.13. a) Photomultiplier signal of laser induced fluorescence at 460.96 nm as a function of incident laser wavelength for λ_{LASER}=611.537–611.570 nm. Ten (10) plasma shots are made at each wavelength shown. Best-fit curves are shown for b) Doppler, c) Stark, and d) Voigt line broadening models.

c)

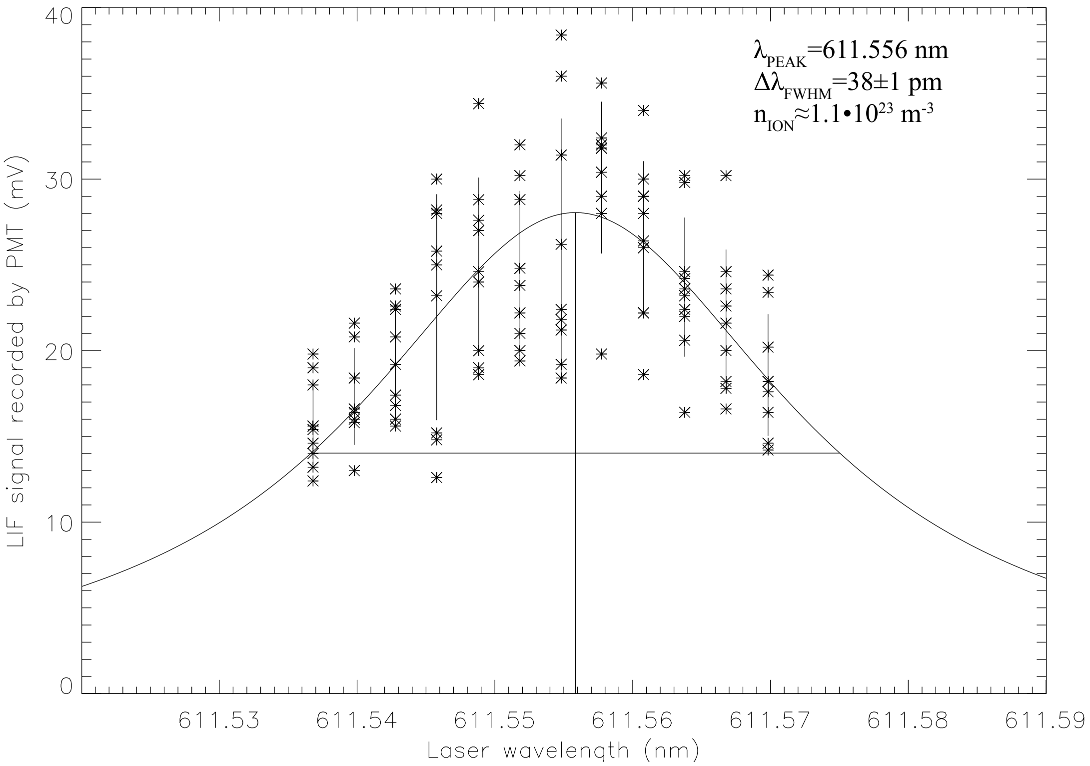

d)

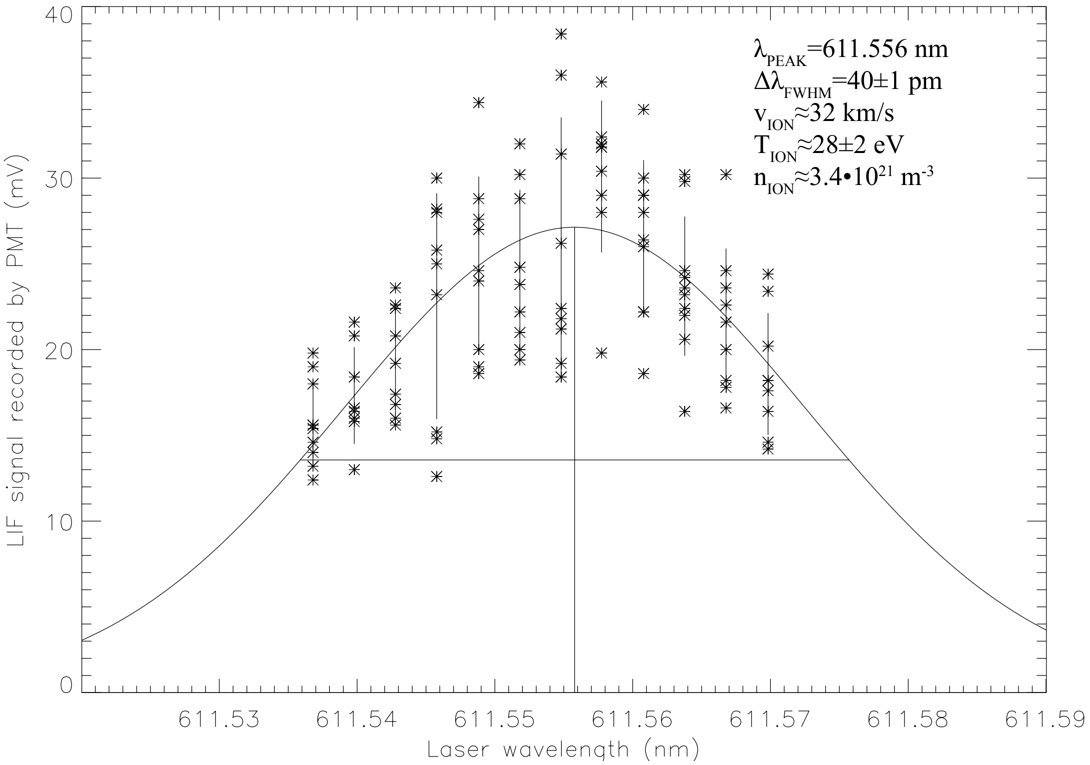

Figure 4.13. a) Photomultiplier signal of laser induced fluorescence at 460.96 nm as a function of incident laser wavelength for λ_{LASER}=611.537–611.570 nm. Ten (10) plasma shots are made at each wavelength shown. Best-fit curves are shown for b) Doppler, c) Stark, and d) Voigt line broadening models.

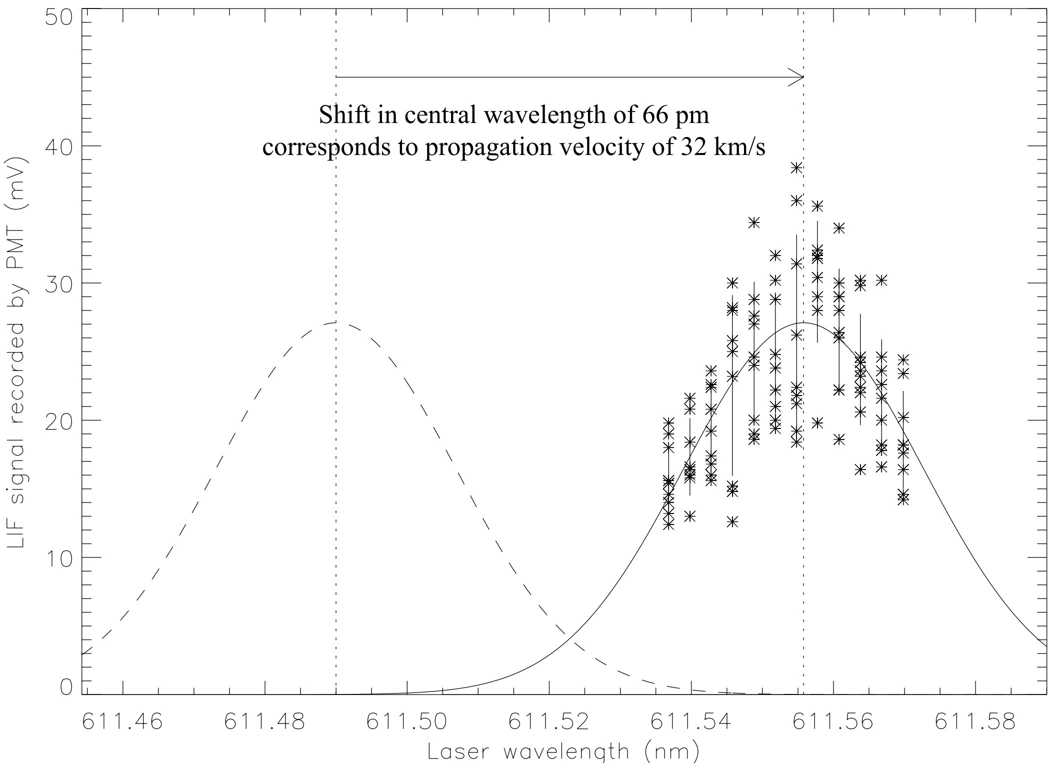

Figure 4.14. Propagation velocity corresponding to the shift in observed central wavelength of the ion distribution function for the data shown in Figure 4.13.

be changed in larger increments. Therefore, in this second experimental run, ten plasma shots are taken at each laser wavelength instead of five, and the laser wavelength is changed in 3 pm steps instead of the 2 pm used in the first run.

The LIF data collected in this experiment is shown in Figure 4.13. Fitting this data to the Doppler broadening model returns an estimated ion propagation rate of ~32 km/s and an ion temperature of 29±3 eV. The pure Stark broadening model suggests an ion density of $\sim 1.1 \cdot 10^{23}$ m^{-3}. Finally, the Voigt model returns ion parameter estimates of ~32 km/s propagation velocity, 28±2 eV ion temperature, and $\sim 3.4 \cdot 10^{21}$ m^{-3} ion density.

These values are in reasonable agreement with those calculated in the earlier experimental run. This suggests that the plasmas produced by the coplanar gun are repeatable, at least with regard to those ion parameters measured by the laser induced fluorescence diagnostic.

4.5 Observations Parallel to the Spheromak Axis

The spheromak LIF experiments described thus far have all been made with the probing laser directed perpendicular to the axis of symmetry of the spheromak. The following section describes the results of an experiment in which the optical fiber transmitting the laser has been moved to orient the beam in a direction nearly parallel to the spheromak axis.

4.5.1 On-axis Measurement Limitation

The laser beam cannot be oriented exactly along the axis of the spheromak, as the center port on the end dome of the vacuum chamber opposite the coplanar gun is occupied by equipment used in other plasma experiments. Therefore, the optical fiber is mounted on an adjacent port, and the laser enters the vacuum chamber off-axis by ~30 cm in the radial direction. The beam must be directed at an angle in order to intercept the plasma on the spheromak axis in the field of view of the LIF reentry port, which lies ap-

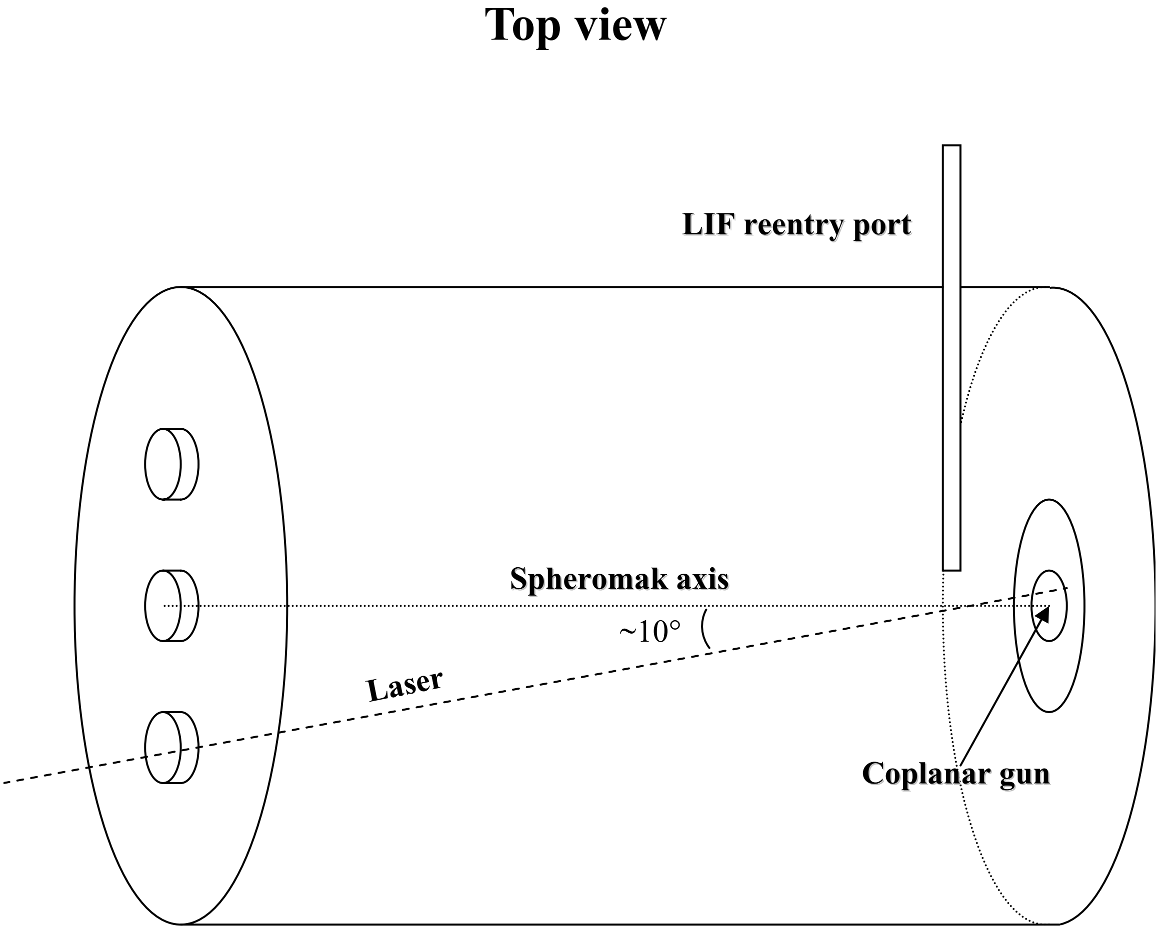

Figure 4.15. Geometry of LIF measurements made with the probing laser nearly parallel to the axis of the spheromak. The center port on the opposite end dome of the vacuum chamber is unavailable, so an off-axis port must be used instead. This requires the laser beam to form an angle of ~10° with the spheromak axis in order to intercept the plasma in front of the LIF reentry port.

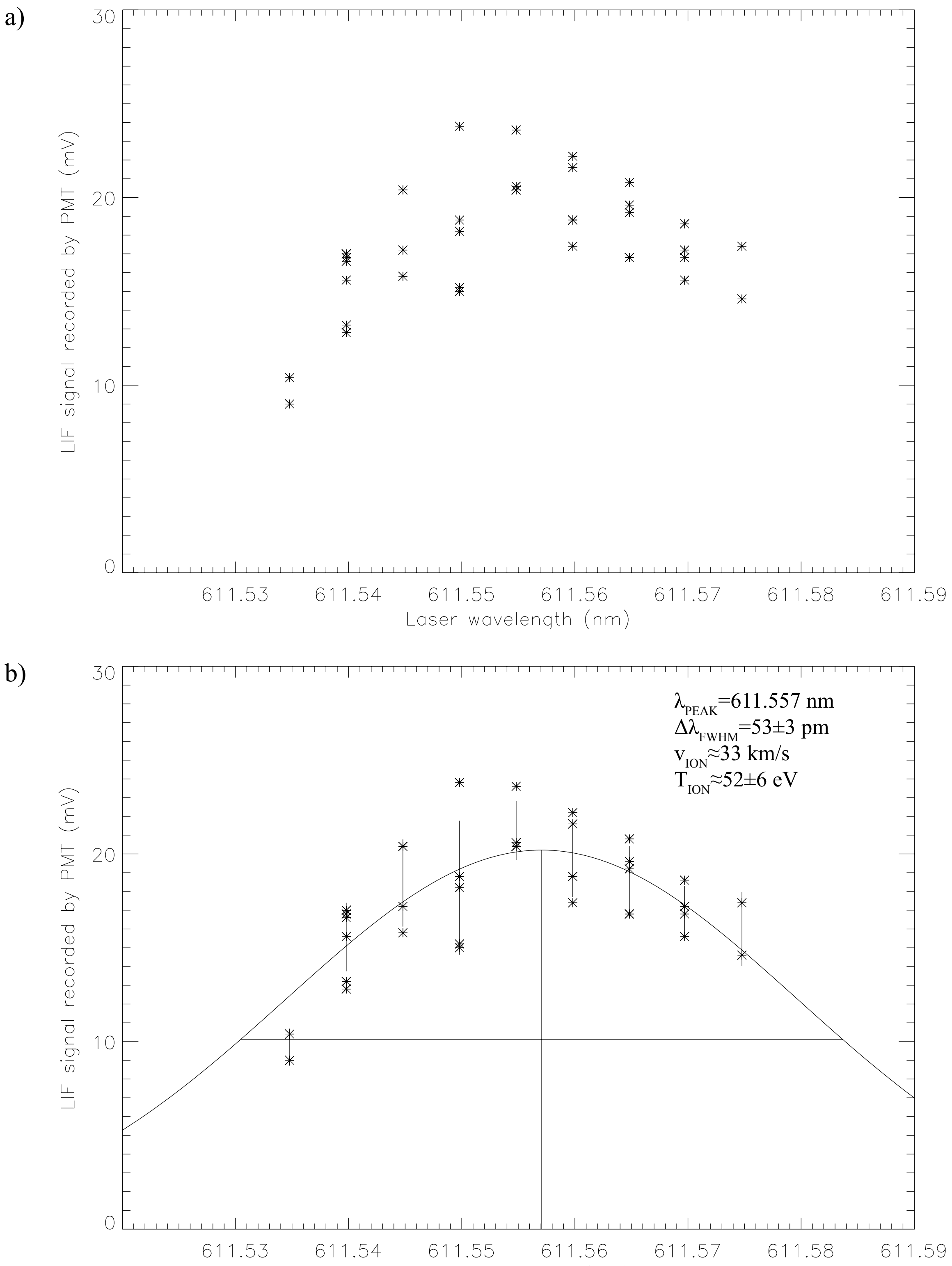

Figure 4.16. a) Photomultiplier signal of laser induced fluorescence at 460.96 nm as a function of incident laser wavelength for λ_{LASER}=611.535–611.570 nm. Best-fit curves are shown for b) Doppler, c) Stark, and d) Voigt line broadening models.

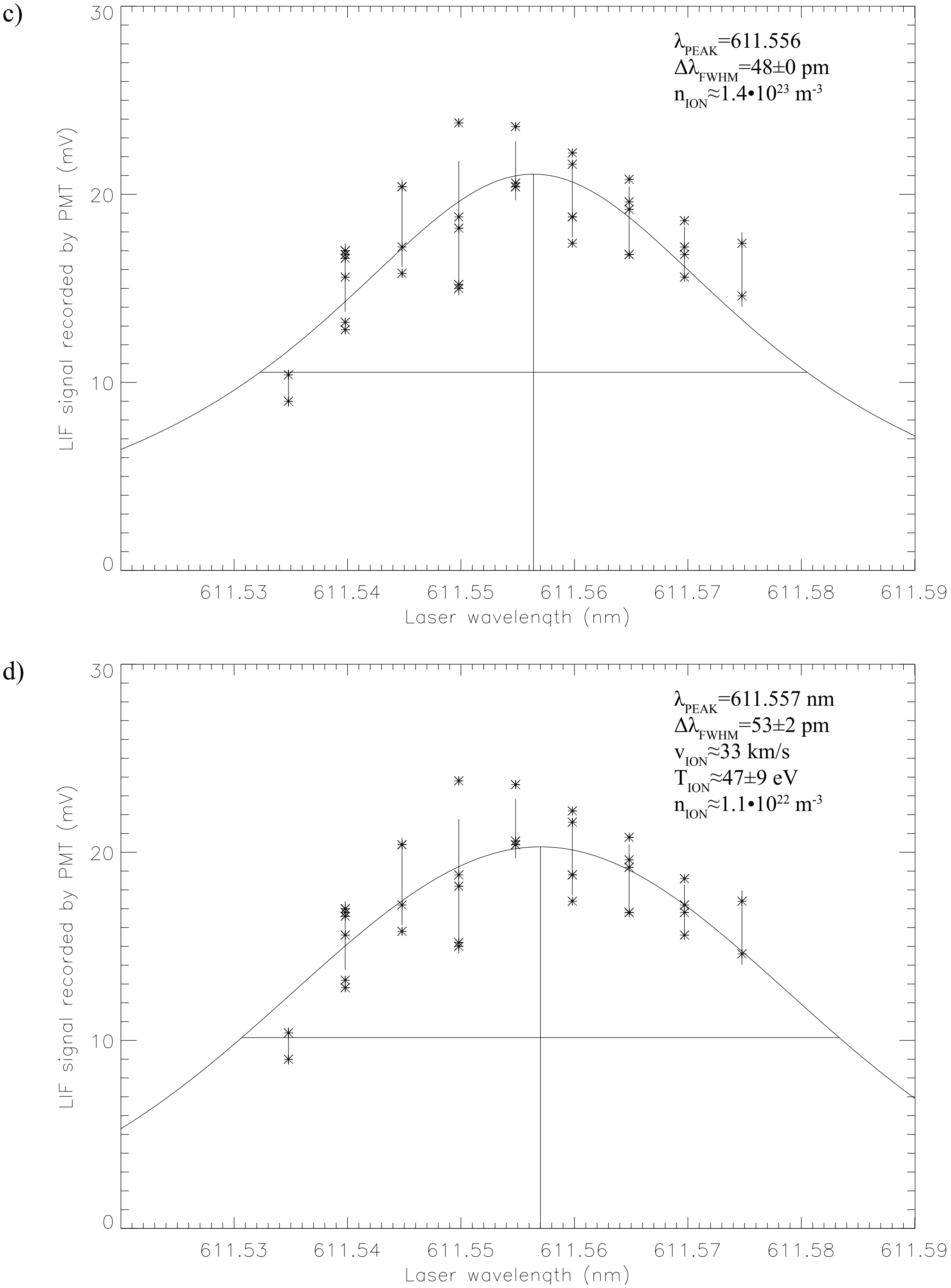

Figure 4.16. a) Photomultiplier signal of laser induced fluorescence at 460.96 nm as a function of incident laser wavelength for λ_{LASER}=611.535–611.570 nm. Best-fit curves are shown for b) Doppler, c) Stark, and d) Voigt line broadening models.

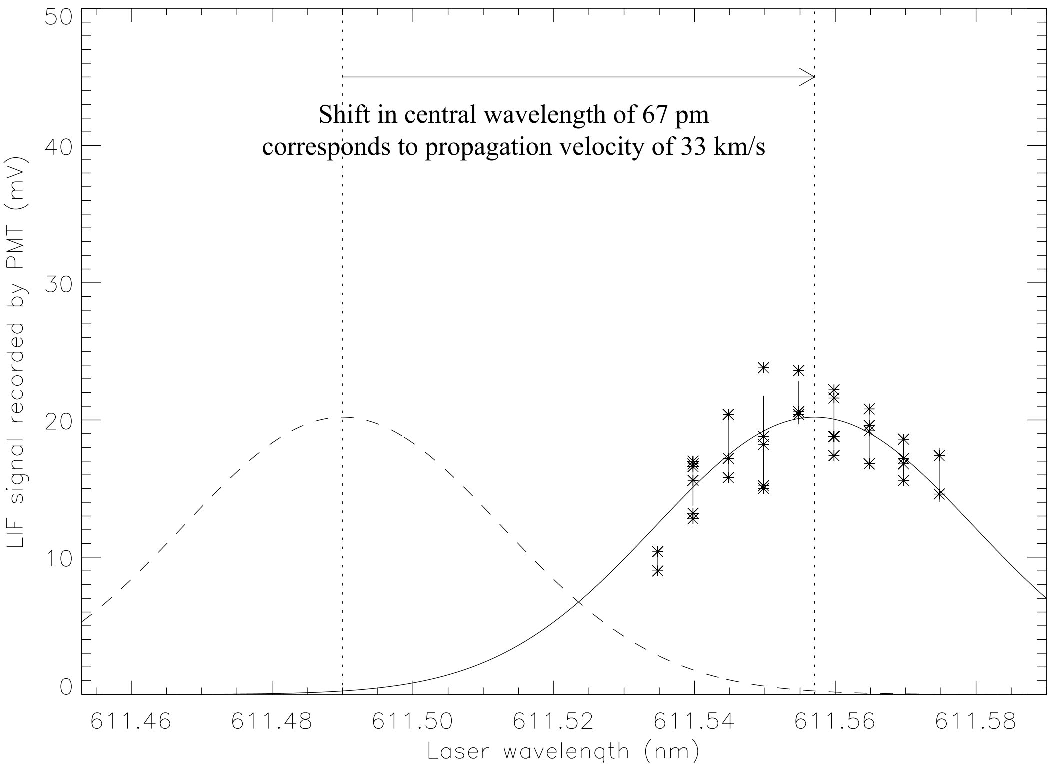

Figure 4.17. Propagation velocity corresponding to the shift in observed central wavelength of the ion distribution function for the data shown in Figure 4.16.

proximately 25.4 cm in front of the planar gun. The overall length of the vacuum chamber is 2 m, resulting in the laser making an angle of ~10º with respect to the spheromak axis, as illustrated in Figure 4.15.

4.5.2 Fitting to Theoretical Model

The plasmas probed in this experiment have been produced with slightly different control settings on the plasma generating equipment. The peak I_{GUN} is ~100 kA and ~1.5 mWb of poloidal stuffing flux has been applied, resulting in $\alpha_{GUN} \approx 80\ m^{-1}$. The emitted light signal level recorded at the LeCroy digitizer is frequently observed to exceed the -750 mV limit, so an additional 3 dB of coaxial attenuation has been added, for a total of 18 dB.

Fitting the collected LIF data to the Doppler broadening model returns an estimated ion propagation rate of ~33 km/s and ion temperature of 52±6 eV. The Stark broadening model indicates an ion density of $\sim 1.4 \cdot 10^{23}\ m^{-3}$. Finally, the Voigt profile returns ion parameter estimates of ~33 km/s propagation velocity, 47±9 eV ion temperature, and $\sim 1.1 \cdot 10^{22}\ m^{-3}$ ion density.

4.5.3 Imacon Camera Images

The laser induced fluorescence experiments described in this chapter have benefitted from the use of the Imacon 200 high speed framing camera. One application for the camera is to provide a rough approximation of the ion propagation velocity in the axial direction as the plasma moves away from the coplanar gun. By orienting the Imacon perpendicular to the spheromak axis and following the displacement of a particular region of plasma as a function of time, an average velocity can be calculated. A sequence of 16 images taken by the Imacon in this perpendicular orientation is shown in Figure 4.18; the time between frames is 1 μs. The most easily identifiable feature of the plasma to follow is the leading edge of the large bright region as the plasma travels from right

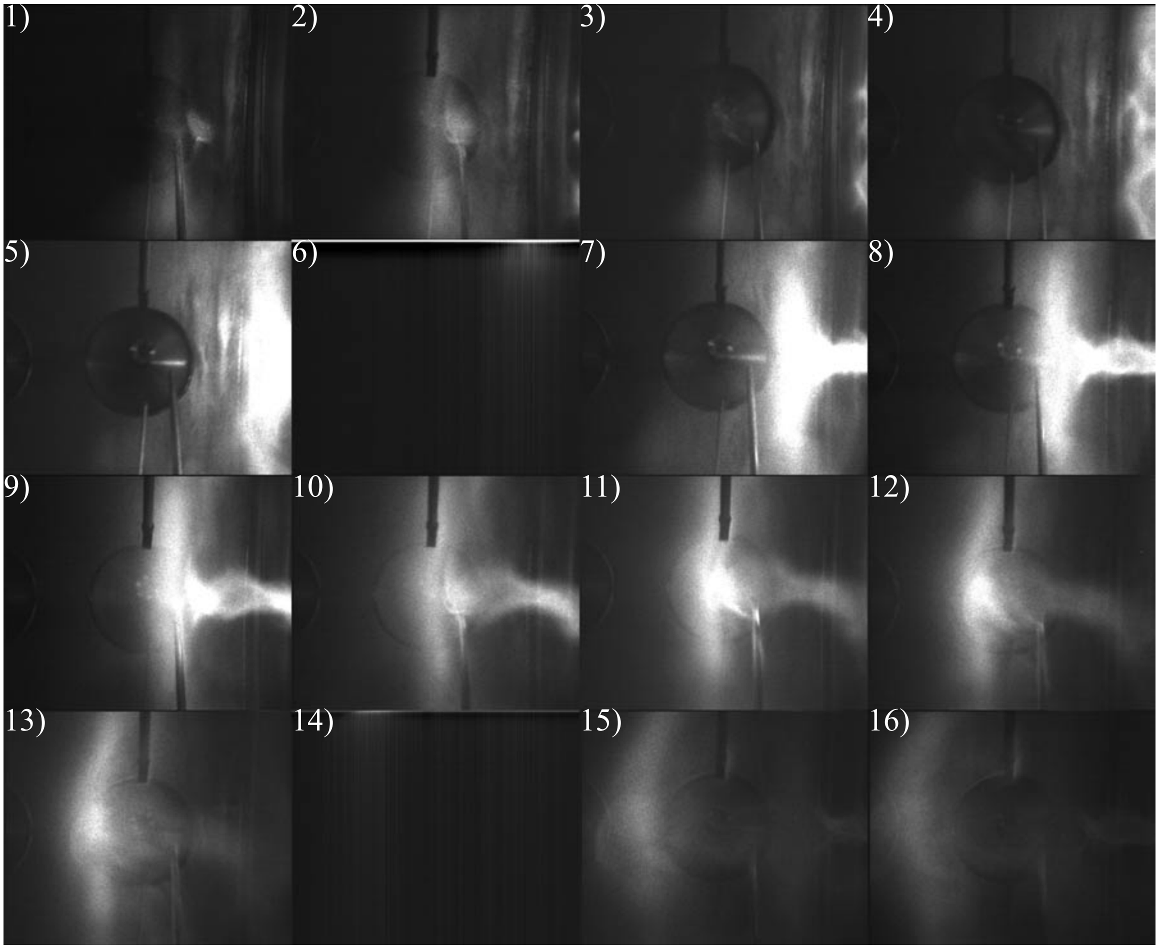

Figure 4.18. Imacon framing camera photo sequence of plasma propagation, with 1 μs separation between frames. The edge of the bright plasma region moves ~11.4 cm in 6 μs between frame 7 and frame 13, corresponding to an average propagation rate of ~20 km/s. (Frames 6 and 14 do not contain image data due to a camera malfunction at the time of the experiment.)

to left through the sequence of images. A reference for measurement is provided by the 10” vacuum port visible in the background of the images, for which the diameter of the interior of the port is known to be 9”. The plasma is observed to reach the right edge of this port in frame 7 of the sequence and the left edge in frame 13, for a total elapsed time of 6 μs. The plasma is only half as far from the camera as the port in the background, however, so the distance travelled by the plasma in this time is not 9”, but only 4.5” (11.4 cm). This yields a rough estimate for the plasma propagation velocity of ~20 km/s, which differs from the LIF-calculated value by a constant of order unity.

4.5.4 Comparison to Perpendicular Orientation Measurements

With the exception of ion temperature, the ion parameter values calculated in this experiment are in reasonable agreement with those calculated in the experiments in which the laser is directed perpendicular to the spheromak axis. The larger ion temperature estimate in the on-axis experiment may be due in part to the quality of the experimental data collected, which contains fewer data points per laser wavelength. This is symptomatic of a larger problem with the LIF experimental equipment that is discussed in the next section.

4.6 Loss of LIF Signal

Over the course of the investigations described in this chapter, it became progressively more difficult to observe an LIF signal from spheromak plasmas produced by the coplanar device. At first, nearly every plasma discharge produced a well-defined LIF signal, comparable in quality to that depicted in Figure 4.10. However, by the time of the experiments performed with the laser oriented parallel to the axis of the spheromak, for every successful detection of an LIF signal, as many as 15–20 consecutive shots would produce spontaneous light emission at the 460.96 nm line but exhibit no induced fluorescence above that background level. This inability to detect an LIF signal has grown to the extent that signals are no longer observed for experimental control settings that previously produced strong signals, even after hundreds of attempts. The only known change to the experimental apparatus prior to the onset of this problem was a modification to the exterior copper tubing that connects the gas puff valves to the gas supply cylinders; it seems unlikely that this should have caused the ion parameters of the plasma to shift beyond the ability of the LIF diagnostic to measure. An investigation into the cause of this problem will be discussed in Chapter 5.

4.7 Discussion

The laser induced fluorescence experimental technique developed on the earlier coaxial spheromak gun has been successfully adapted for use with the new coplanar spheromak device. Independent sets of measurements performed on Ar II plasmas produced with the same experimental control settings yield virtually identical calculated ion parameters, suggesting reasonable plasma reproducibility. Measurements have been performed with the probing laser oriented either perpendicular to or parallel to the spheromak's axis of symmetry; the ability to make measurements in either orientation is significant, as it suggests one possible course for future expansion of the experiment. In addition, parameter estimates derived from data provided by both passive spectroscopy and visible light photography are in reasonable agreement with the ion densities and propagation rates calculated from the LIF measurements performed in this work.

Unfortunately, the success of the experiment cannot be characterized as complete. The increasing difficulty encountered in detecting an induced fluorescence signal must be investigated and resolved. Even when the signal is present and can be reproduced reliably, the rate at which data can be obtained from the experiment in its present configuration makes the collection of sufficient data to lead to meaningful physical interpretation of the results a challenge. Finally, while induced fluorescence measurements have been made for experiments involving the laser beam positioned in various orientations, the system still lacks a certain level of freedom in the configuration of equipment; for instance, plasma close to the gun electrodes (most notably the spider legs) cannot be diagnosed with the laser oriented perpendicular to the axis of the spheromak, as there are no vacuum chamber ports at the necessary location.

Of these negative points, the loss of signal clearly poses the greatest obstacle to the future success of LIF experiments on the coplanar spheromak. Chapter 5 presents a discussion of the steps that have been taken to assess and to attempt to resolve this problem.

4.8 References

J.A. Aparicio, M.A. Gigosos, V.R. González, C. Pérez, M.I. de la Rosa, and S. Mar, "Measurement of Stark broadening and shift of singly ionized Ar lines," *J. Phys. B: At. Mol. Opt. Phys.*, **31**, 1029 (1998).

P.M. Bellan, *Spheromaks* (Imperial College Press, 2000).

P.M. Bellan, "Why current-carrying magnetic flux tubes gobble up plasma and become thin as a result," *Phys. Plasmas*, **10(5)**, 1999 (2003).

S.D. Bruce, J. Higinbotham, I. Marshall, and P. Beswick, "An analytical derivation of a popular approximation of the Voigt function for quantification of NMR spectra," *J. Mag. Res.*, **142**, 57 (2000).

S.C. Hsu and P.M. Bellan, "A laboratory plasma experiment for studying magnetic dynamics of accretion discs and jets," *Mon. Not. R, Astron. Soc.*, **334**, 257 (2002).

S.C. Hsu and P.M. Bellan, “On the jets, kinks, and spheromaks formed by a planar magnetized coaxial gun,” *Phys. Plasmas*, **12**, 032103 (2005).

J.F. Kielkopf, “New approximation to the Voigt function with applications to spectral-line profile analysis,” *J. Opt. Soc. Amer.*, **63(8)**, 987 (1973).

R. Stern, private communication.

G.K. Wertheim, M.A. Butler, K.W. West, and D.N.E. Buchanan, “Determination of the Gaussian and Lorentzian content of experimental line shapes,” *Rev. Sci. Instrum.*, **45(11)**, 1369 (1974).

E.E. Whiting, “An empirical approximation to the Voigt profile,” *J. Quant. Spectrosc. Radiat. Trans.*, **8**, 1379 (1968).

J. Yee and P.M. Bellan, “Taylor relaxation and λ decay of unbounded, freely expanding spheromaks,” *Phys. Plas.*, **7(9)**, 3625 (2000).

S. You, G.S. Yun, and P.M. Bellan, “Dynamic and stagnating plasma flow leading to magnetic-flux-tube collimation,” *Phys. Rev. Let.*, **95**, 045002 (2005).

G. Yun, private communication.

Chapter 5
Portable Plasma Device

5.1 Introduction

This chapter describes the design and operation of a portable plasma generation device intended to serve as a means of investigating problems encountered in LIF signal detection in the Caltech spheromak experiments.

5.1.1 Loss of LIF Signal

The experiments described in Chapters 3 and 4 have demonstrated that it is possible to calculate ion temperatures, velocities, and densities from LIF measurements of argon plasmas produced in a spheromak confinement configuration. However, these experiments have been affected by occasional difficulties in maintaining a repeatable LIF signal. The most common manifestation of this phenomenon is that for two otherwise identical plasma discharges—same charging voltages applied to capacitor banks, same experimental time delays, same laser wavelength—a distinct LIF signal is seen in one discharge, while the other does not exhibit any induced fluorescence. Plasma discharges that failed to produce detectable induced fluorescence became more common toward the end of the investigations described Chapter 4.

Two possible explanations for this effect present themselves: either the plasma has changed such that its ion parameters are significantly different from those that were measured previously, or some element of the experimental apparatus used to diagnose the plasma has changed. Diagnostic equipment monitoring other aspects of the spheromak experiment does not show any appreciable change in such parameters as the time between the discharge of the capacitor bank connected to the gun electrodes and the onset of plasma breakdown, the current I_{GUN} driven through the gun electrodes, or the visual appearance of the plasma as observed in Imacon camera photographs. The only modification made to the spheromak formation apparatus prior to the onset of the loss of signal problem was a minor reconfiguration of the copper tubing connecting the gas puff valves to the argon gas bottle; however, as this change should not have altered the amount of argon present in the plenum of the gas valves at the time the valve coils are pulsed, it does not seem a likely candidate to explain the change in the fluorescence signal recorded by the photomultiplier.

A logical next step is to investigate the possibility that a change has occurred either in the laser system or in the photomultiplier light collection system.

5.1.2 Encore Tokamak

Several LIF experiments have been performed at Caltech on the Encore tokamak device; among these are ion heating studies by McChesney, Stern, and Bellan (1987) and the planar LIF experiments of Bailey, Stern, and Bellan (1993). One characteristic of Encore that makes it an attractive candidate for LIF experiments is its ability to generate 15 plasma discharges per second. This high repetition rate allows the process of sweeping the probing laser wavelength across the resonant portion of the ion distribution function to be performed in a matter of minutes, as compared with the much slower process associated with spheromak experiments. Consequently, the first test chosen to analyze the functionality of the laser and photomultiplier systems is to attempt to detect an induced fluorescence signal in an Encore argon plasma using the same equipment. For argon plasmas produced under typical experimental conditions of B_φ=300 G toroidal magnetic field and I_P=1 kA plasma current, a distinct LIF signal is indeed seen, as shown in Figure 5.1. To produce this signal, the probing laser has been tuned to wavelengths that are in good agreement with those used in prior Encore experiments. The fact that an induced fluorescence signal has been produced and detected confirms that the laser and photomultiplier are in good working condition.

An important difference between the experimental setup used in this test and

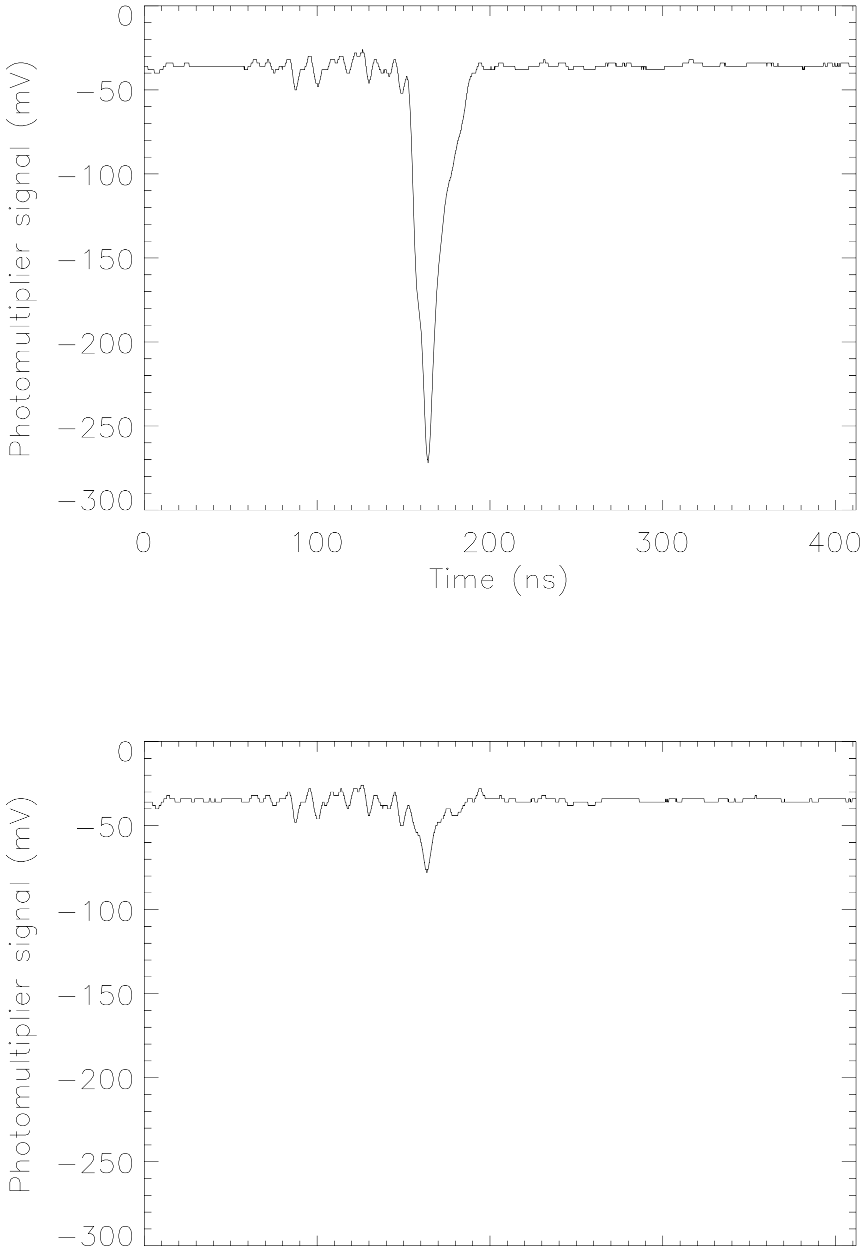

Figure 5.1. LIF signals detected in Ar II plasmas generated by the Caltech Encore tokamak. The strong signal at top is produced with the probing laser wavelength set to 611.455 nm, while the bottom signal is obtained at 611.555 nm. All other experimental conditions are identical for the two plasma discharges. The detection of an LIF signal from the tokamak plasma confirms that both the laser and photomultiplier are functioning normally, eliminating these as possible causes for the lack of signal in the spheromak LIF experiment.

that of the spheromak LIF experiments is the optical fiber used to transmit the laser to the spheromak vacuum chamber. The laser is typically directed into the tokamak via a series of mirrors rather than through a fiber, as the laser system is located adjacent to the tokamak, although optical fiber laser transmission has also been used in previous Encore LIF experiments. While it is possible to extract the 55 m length of optical fiber used in the spheromak experiments from the cable tray in which it is located, there is a risk of damaging the fiber in the process. (The fiber was damaged when it was first installed and required repair prior to proceeding with experiments on the spheromak plasmas.)

Since it is impractical to move the optical fiber to another plasma for testing of the LIF equipment, an alternative approach is to devise a method for bringing a second plasma source to the fiber. Encore itself is too cumbersome to be relocated, but a new plasma device, designed to be portable and to have a sufficiently high repetition rate so as to allow for rapid sweeping of the probing laser wavelength in an LIF experiment, should make it possible to assess the functionality of the optical fiber.

5.2 Portable Plasma Device Apparatus

5.2.1 Design Considerations

While the primary motivation for the construction of the portable plasma device is to provide a testbed for diagnosing the laser light output from the optical fiber, the design should be kept as flexible as possible in anticipation of potential future uses for such a device. The design should therefore use standard vacuum components and be modular, to allow for quick hardware changes or additions. Since the optical fiber assembly in the spheromak experiment is mounted on a 2.75” vacuum port, it is logical to adopt this dimension as the standard port size for vacuum hardware components used in construction of the portable device. The device must provide adequate optical access for both the laser as well as the photomultiplier, and the device should be controlled by the same time delay sequencers used in the spheromak experiments.

5.2.2 Mechanical

The portable plasma device has been assembled in the shape of a five-way cross, as shown in Figure 5.2. The cross design establishes mutual orthogonality of the laser beam, the direction of photomultiplier viewing, and the direction of plasma current. The relative orientation of these three directions in the portable device will thus mimic the geometry of their analogues in the larger spheromak experiment. Glass viewports are mounted at two opposing ends of the cross to permit the laser beam to enter the device, interact with the plasma, and then exit through the opposite side of the chamber. A third window allows light emitted from the plasma to exit the chamber for collection by the photomultiplier.

The portable device is pumped down to <1 mTorr through a Swagelock fitting connected by 1/4” tubing to a Tribodyn vacuum pump. This same fitting also allows for injection of the gas that will be ionized; a thermocouple tube permanently attached to the portable device permits the chamber to be filled to a desired pressure.

The two ports of the five-way cross that do not have windows attached are electrically isolated from the remainder of the vessel by ceramic breaks; these ports are connected via high voltage cable to a pulsed capacitor power supply capable of producing voltages of up to 1.6 kV. To force plasma breakdown to occur in the center of the device, such that the probing laser can pass through the plasma, 1/8” diameter steel rods are attached to the interior surface of each flange to yield a final interelectrode spacing at the center of the device of approximately 2 cm, as shown in the bottom right photograph in Figure 5.2. The insulating alumina sheath seen surrounding one of these rods was added to the device in an early attempt to force breakdown between the electrode tips when only one 2.75” ceramic break was present; the later installation of the second ceramic break has rendered this additional insulation obsolete.

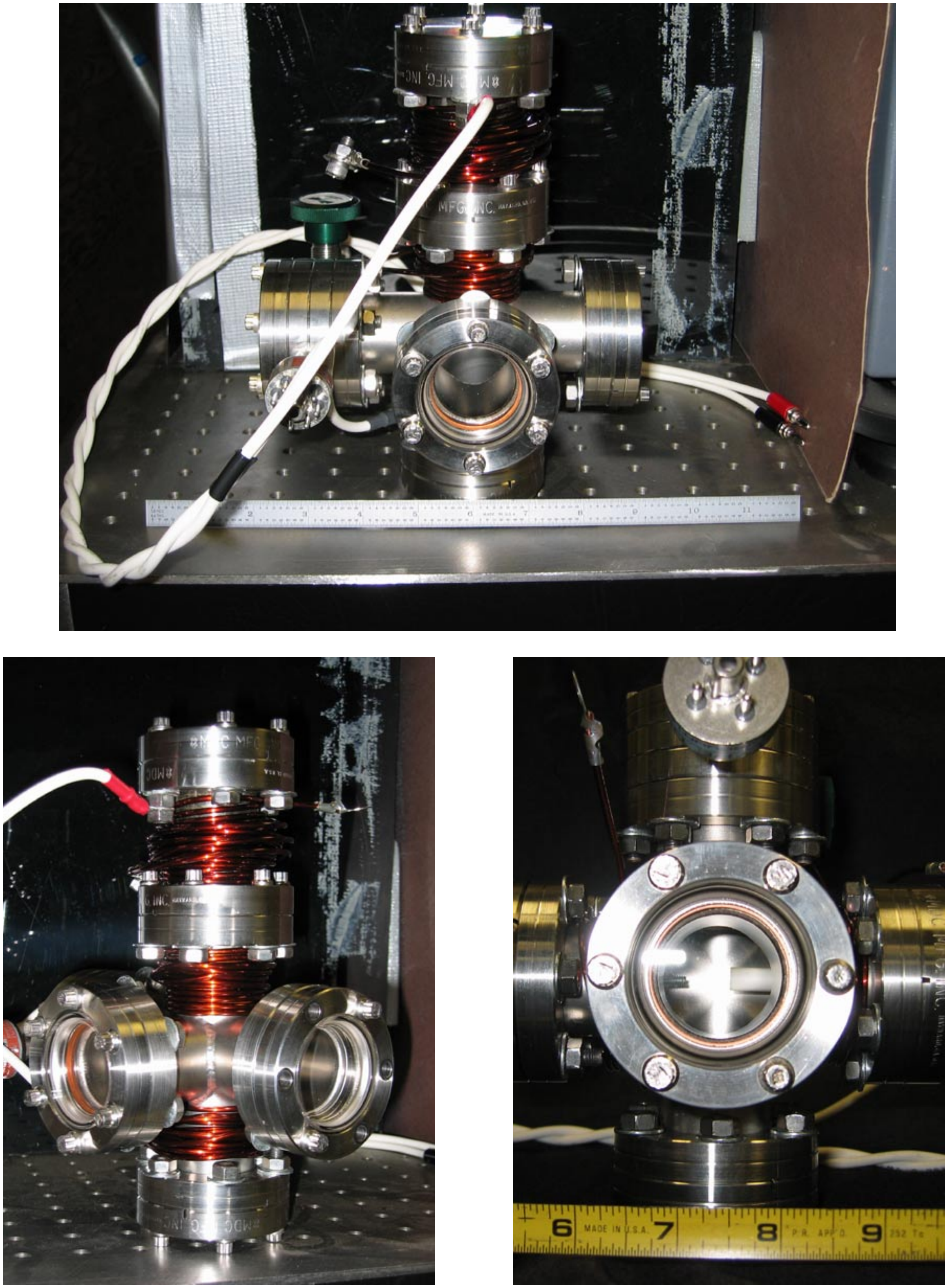

Figure 5.2. Portable plasma device. The electrodes used for plasma breakdown are seen in the bottom right photograph.

5.2.3 Electrical

Plasma is created in the portable device by electrostatic breakdown initiated by the capacitor bank attached to the device electrodes. The Paschen criterion holds that the minimum voltage required to break down gas in this experimental configuration is a function of the distance between electrodes and the gas fill pressure. The exact functional form of the relationship between these quantities can vary, but a common form as identified by Von Engel (1965) is

$$V_{\min} = \frac{B \cdot pd}{C + \ln(pd)} \tag{5.1}$$

where p and d are the gas pressure and electrode separation, respectively, and $V_{\min}$ is the minimum voltage required for breakdown. B and C are empirically determined constants for a given gas and electrode material. The function defined by Equation 5.1 is often called the Paschen curve; one such curve for argon gas is shown in Figure 5.3. For a given pd product, argon will break down at voltages above the curve but not for values below it.

Von Engel's discussion of the Paschen curve for argon gas identifies an absolute minimum breakdown potential for iron electrodes of 265 V, achieved at a pd product of 1.5 Torr-cm. The interelectrode spacing in the portable plasma device is ~2 cm; therefore, the gas pressure required for breakdown at 265 V is approximately 750 mTorr. The portable device electrodes are composed of steel, not iron, but this should only cause a minor change in the optimal pd value.

Since it is advantageous to ionize as much of the argon gas in the portable device as possible—to yield a stronger LIF signal—the breakdown capacitor is typically charged to voltages in the range of 1–1.6 kV. Also, operation of the device at a fill pressure of 750 mTorr is observed to result in qualitatively erratic breakdown behavior. More modest pressures of 400–500 mTorr are found to yield better plasma reproducibility.

The shape of the five-way cross lends itself to the use of a Helmholtz coil to provide a bias magnetic field to aid in collimation of the plasma discharge along the axis

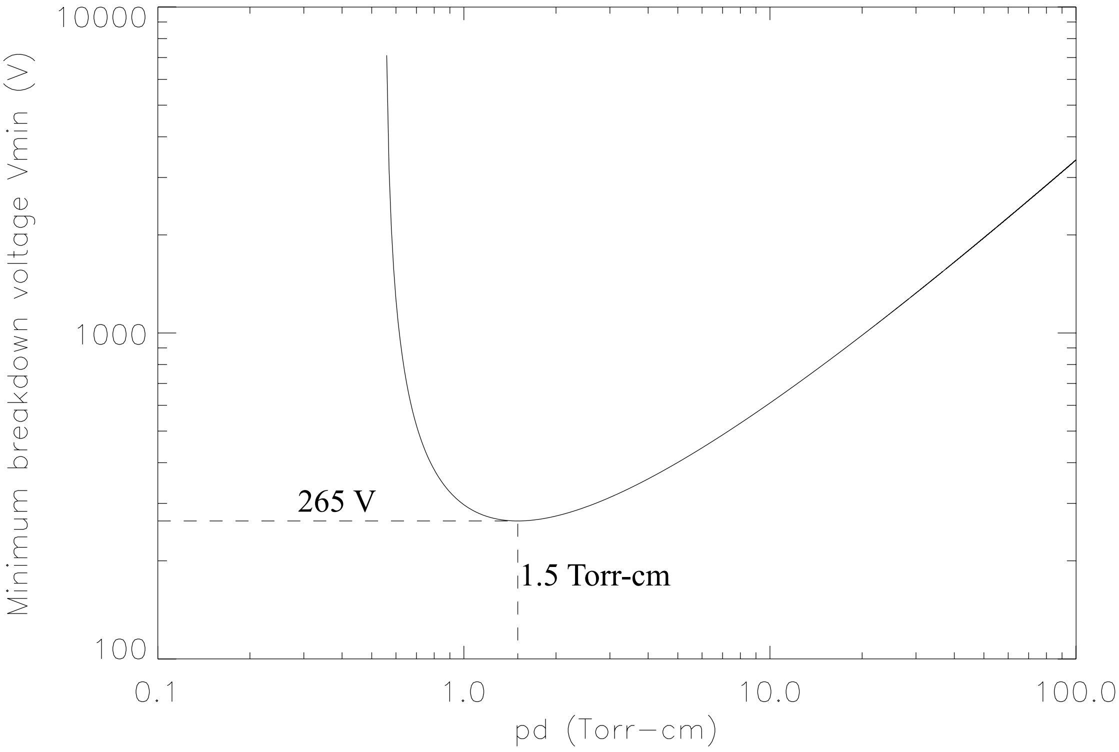

Figure 5.3. The Paschen curve describes the relationship between the minimum voltage V_{min} required to break down a gas at pressure p between two electrodes separated by a distance d. The numerical values shown correspond to those provided by Von Engel for argon gas and iron electrodes.

defined by the electrodes. Coils have been placed around the arms of the five-way cross that contain the electrodes used in plasma breakdown; this configuration will not be an ideal Helmholtz coil, as the distance between coils is twice the radius of a coil, but the magnetic field near the central axis of the chamber will still be nearly parallel to the electrodes. Electric current for the coils is provided by the discharge of an 1800 μF capacitor that is typically charged to 30–40 V.

5.2.4 Experimental Timing and Data Acquisition

Experimental timing for the portable device experiment is controlled by the same CAMAC timing sequencers used in the spheromak experiments. During testing of the portable device, timing signals have been provided by the eight-channel CAMAC module that also controls laser timing. The Helmholtz coil is found to achieve peak magnetic field strength approximately 0.5 ms after the discharge of the capacitor bank providing current to the coil. The timing signal to trigger plasma formation should therefore be adjusted such that breakdown will take place 0.5 ms after the Helmholtz coil is energized. A second flip-flop circuit, identical to the one used in the spheromak experiments, has been built to accomplish this synchronization. The output of one flip-flop circuit is split to trigger the Helmholtz coil and to act as the input to the second flip-flop that will then trigger the capacitor bank used for plasma breakdown. Separate channels of the eight-channel CAMAC delay sequencer provide clock pulses to the two flip-flops, with the clock signal for the breakdown capacitor circuit delayed by the needed 0.5 ms. While other means of generating the necessary timing signals are possible, the construction of a second flip-flop enjoys the additional advantage of furnishing a spare for use in the spheromak experiment should the original ever be damaged, or if future enhancements to that experiment would benefit from the incorporation of a second such device. Table 5.1 lists the time delays used in the operation of the portable plasma device relative to the firing of the YAG laser flashlamps.

Event	Time
YAG flashlamps fire	---
Helmholtz coil energized	266 μs
Maximum applied magnetic field	766 μs
Breakdown capacitor discharges	766 μs
Oscilloscope acquisition begins	766 μs
YAG Q-switch triggered	768.4 μs

Table 5.1. Experimental timing delays for operation of the portable plasma device, relative to the firing of the YAG laser flashlamps.

5.3 Experiments

This section reports observations made in experiments designed to produce an LIF signal in Ar II plasmas generated in the portable plasma device.

5.3.1 Spectroscopy

Before searching for an LIF signal in argon plasmas produced by the portable device, it should first be confirmed that Ar II is present. Spontaneous emission from the plasma has been directed into a Jobin Yvon SPEX 1000M spectrometer for analysis. The emission spectrum about 460.96 nm, the Ar II wavelength of interest in the spheromak experiment, is shown in Figure 5.4. The spectrum exhibits strong emission at 458.99 nm and 460.96 nm, both of which are Ar II lines. Ar I lines at 459.61 nm and 462.84 nm are not seen, suggesting that the plasma is nearly fully ionized. A line observed at 463.05 nm is suspected to originate from N II; it is likely that some nitrogen is present in the vessel due to small vacuum leaks.

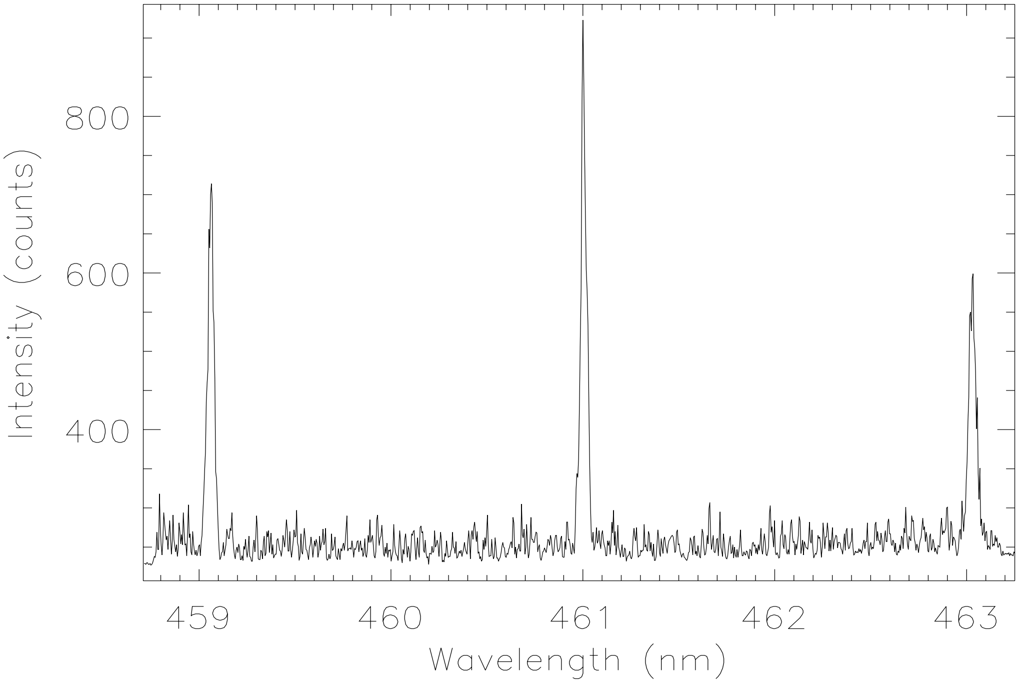

Figure 5.4. Emission spectrum for argon plasma produced by the portable plasma device. The lines at 458.99 nm and 460.96 nm are from Ar II. Neutral argon lines at 459.61 nm and 462.84 nm are not seen. The 463.05 nm line is believed to come from N II present in the chamber.

5.3.2 Plasma Current and Magnetic Confinement

Two important experimental parameters monitored during plasma discharges in the portable device are the current driven through the Helmholtz coil and the current flowing from the breakdown capacitor to the electrodes of the portable device. The former is proportional to the magnetic field inside the chamber, assuming normal Helmholtz coil behavior, while the latter provides an upper bound on an estimate of I_p, the current flowing through the plasma itself. The estimate of I_p should be considered an upper bound, since the main body of the portable device is electrically isolated from all external power supplies; it is reasonable to assume that the nearly all of the current flowing between terminals of the capacitor must therefore be carried by the plasma and not through the body of the chamber itself.

With the plasma current and the magnetic field in the device, it is possible to calculate the ratio of these two quantities, recalling the α parameter that has previously been cited as important in the understanding of spheromak evolution. Of course, it has not been established that the plasma inside the portable device is in a force-free state, so an α value may not have the same physical signficance as it does for plasmas formed in the larger spheromak device.

Ion Physics current monitors are used to measure the current output of the breakdown capacitor circuit and the current driven through the Helmholtz coil. Figure 5.5 displays currents that have been measured by these monitors. The magnetic field at the center of the chamber will follow from the Helmholtz formula, modified to account for the 1:2 ratio of coil radius to distance between coils.

$$B = \left(\frac{1}{2}\right)^{\frac{3}{2}} \frac{\mu_0 n I}{R} \tag{5.2}$$

Here, I is the current flowing through the Helmholtz coil, n is the number of turns in one coil (n=45 in the present design), and R is the radius of a coil (R=3/4”, the radius of a branch of the five-way cross).

To measure the actual magnetic field created inside the chamber by the Helmholtz coil, a 1/4” diameter magnetic pickup coil is inserted into the portable device with the chamber at atmospheric pressure, and the voltage induced in this pickup coil is recorded when the Helmholtz coil is energized. Faraday’s law describes the expected relationship between this induced voltage and the magnetic flux produced by the Helmholtz coil.

$$V = -\frac{d\Phi}{dt}, \Phi = \int N\mathbf{B} \cdot d\mathbf{A} \tag{5.3}$$

$$V = -NA\frac{dB}{dt} \tag{5.4}$$

$$B = -\frac{1}{NA}\int V dt \tag{5.5}$$

where A is the cross-sectional area of one turn of the pickup coil and N is the number of turns (N=10 for the pickup coil used in the present experiment). For a sufficiently small pickup coil area, B should not vary significantly as a function of position, so the magnitude of B in these equations may be considered the average magnetic field strength. As both N and A of the pickup coil are known quantities, the average magnetic field strength at the center of the portable device can be calculated from a measurement of V.

Figure 5.6 displays the voltage induced in the pickup coil when the Helmholtz coil is pulsed. The data shown has been produced with the capacitor bank that provides current to the Helmholtz coil charged to 40 V, its maximum setting in the present experimental configuration. After integrating the induced voltage as a function of time and dividing the result by –NA, the peak magnetic field B passing through the pickup coil is found to be approximately 400 Gauss. By comparison, the field predicted by Equation 5.2, the modified Helmholtz formula, is ~250 Gauss, within a factor of unity of the measured field. The discrepancy between the two values is most likely due to imperfections in coil shapes and small errors in coil area estimates.

For the measured plasma current I_p=130 A and magnetic field 400 Gauss, the α parameter is estimated to be $\alpha \approx 3.5\ m^{-1}$, assuming the magnetic field to be uniform over the cross-sectional area of one branch of the portable device. This α is roughly a factor of 20 less than that typically found in the coplanar spheromak, due primarily to the much

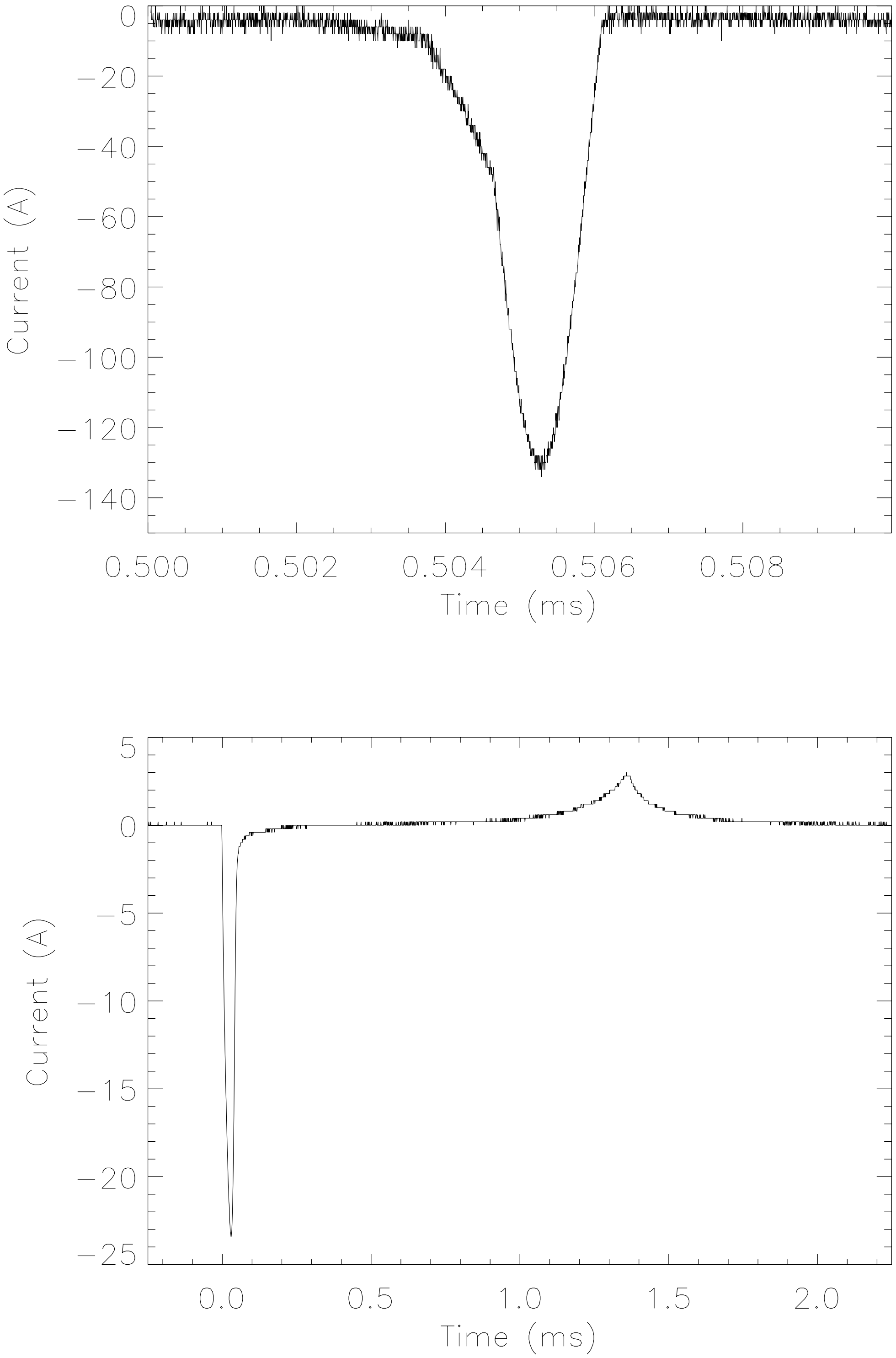

Figure 5.5. (Top) Current flowing through the capacitor bank connected to the portable plasma device electrodes. (Bottom) Current flowing through the Helmholtz coil circuit.

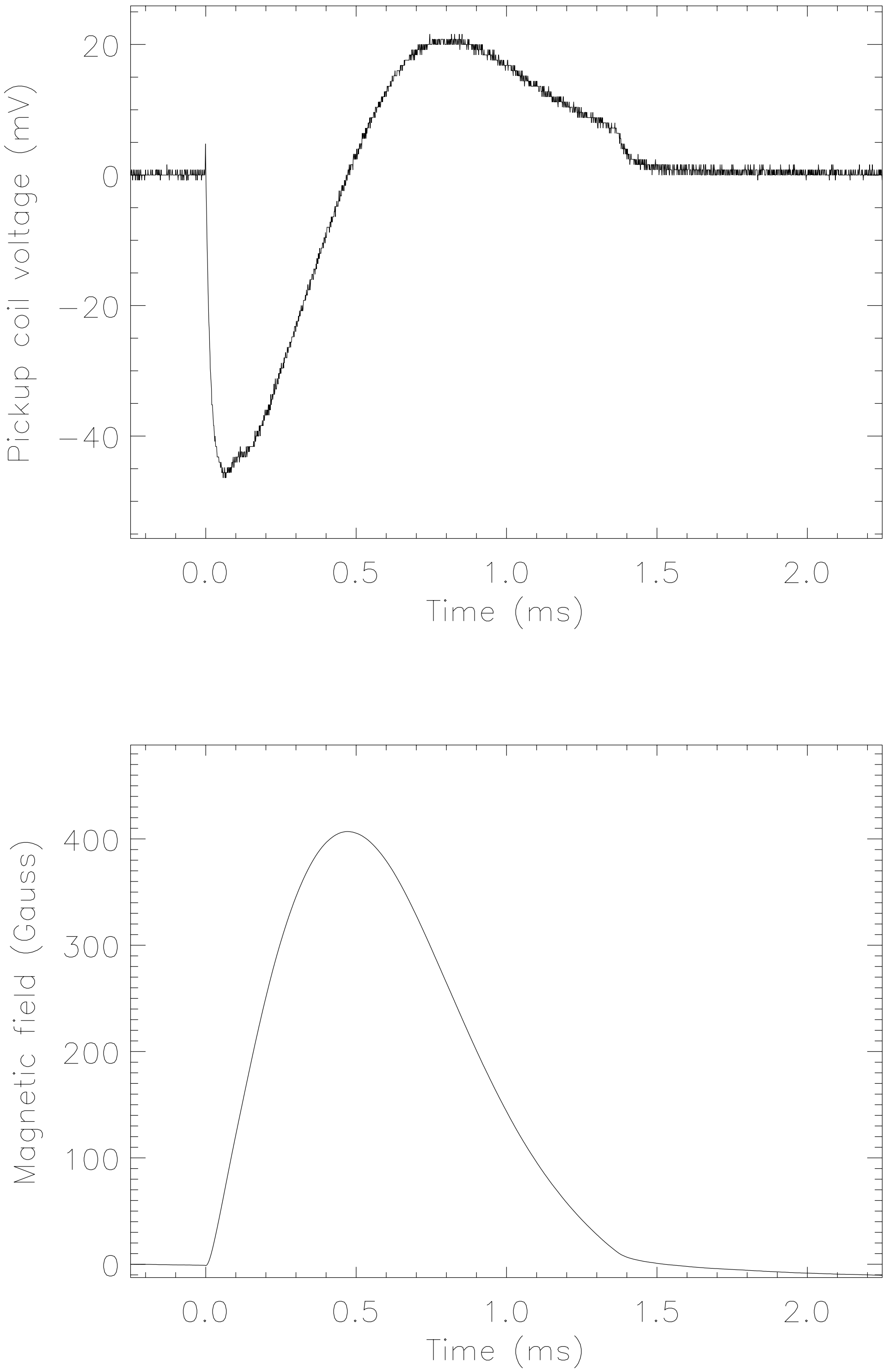

Figure 5.6. (Top) Voltage induced in the pickup coil by the magnetic field produced by the Helmholtz coil. (Bottom) Magnetic field calculated from the induced voltage.

smaller plasma current used in the portable device. As a reminder, α has physical meaning only when the plasma may be assumed to be in a force-free state, which has not been established for plasmas produced in the portable device.

5.3.3 Imacon Photography

In the first assembled version of the portable plasma device, before the second 2.75” ceramic break was added, a bright flash of light could be observed inside the chamber when the breakdown capacitor was discharged, but it was unclear whether this light was the result of plasma formation between electrodes or the result of arcing from one electrode to the vessel wall, which at that time was held at the same potential as one of the electrodes. Images recorded by the Imacon 200 camera can provide information regarding where breakdown is occurring.

As shown in Figure 5.7, a bright flash is seen at the edge of the device window, but not in the center, when only one ceramic break is used. This is not entirely unexpected, as the 2 cm distance between electrode tips is roughly the same as that between the electrode and the chamber wall. With the second ceramic break attached, isolating the central five-way cross from the electrodes, a narrow region of intense emission is seen between the electrode tips, as displayed in Figure 5.8. This observation suggests that plasma is present in the center of the device, where the laser will be directed in LIF experiments.

5.3.4 LIF Signal Detection

The photomultiplier from the spheromak experiments is used to collect emitted light from argon plasmas produced by the portable device and to monitor for the presence of an LIF signal. The compact size of the portable device makes it possible to situate the photomultiplier arbitrarily close to the 2.75” viewport; in practice, a separation of a few centimeters is maintained for safety, to prevent the metal casing of the photomultiplier from accidentally coming into contact with the plasma device.

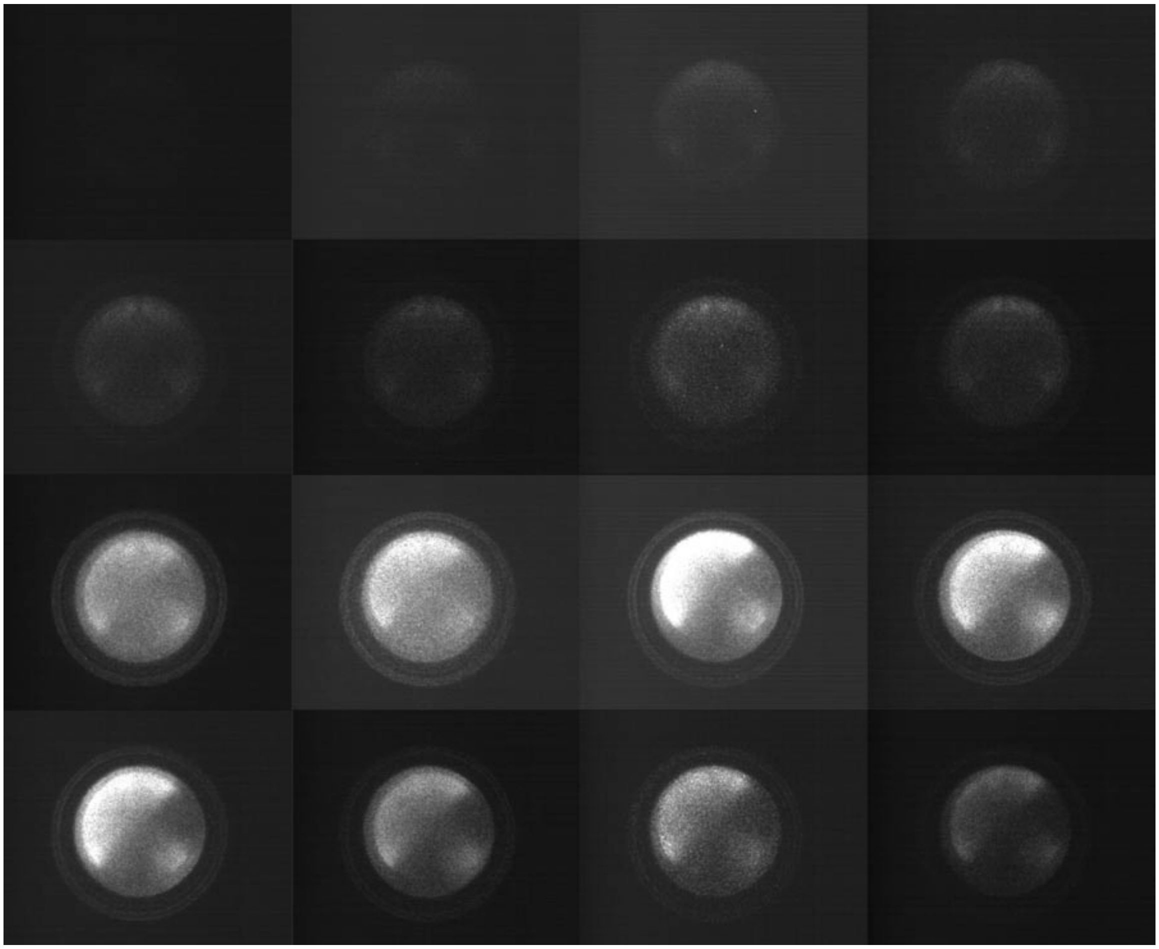

Figure 5.7. Imacon photography of plasma breakdown in the portable device when only one ceramic break is used. Plasma emission is seen at the edges of the window, but not in the center of the device.

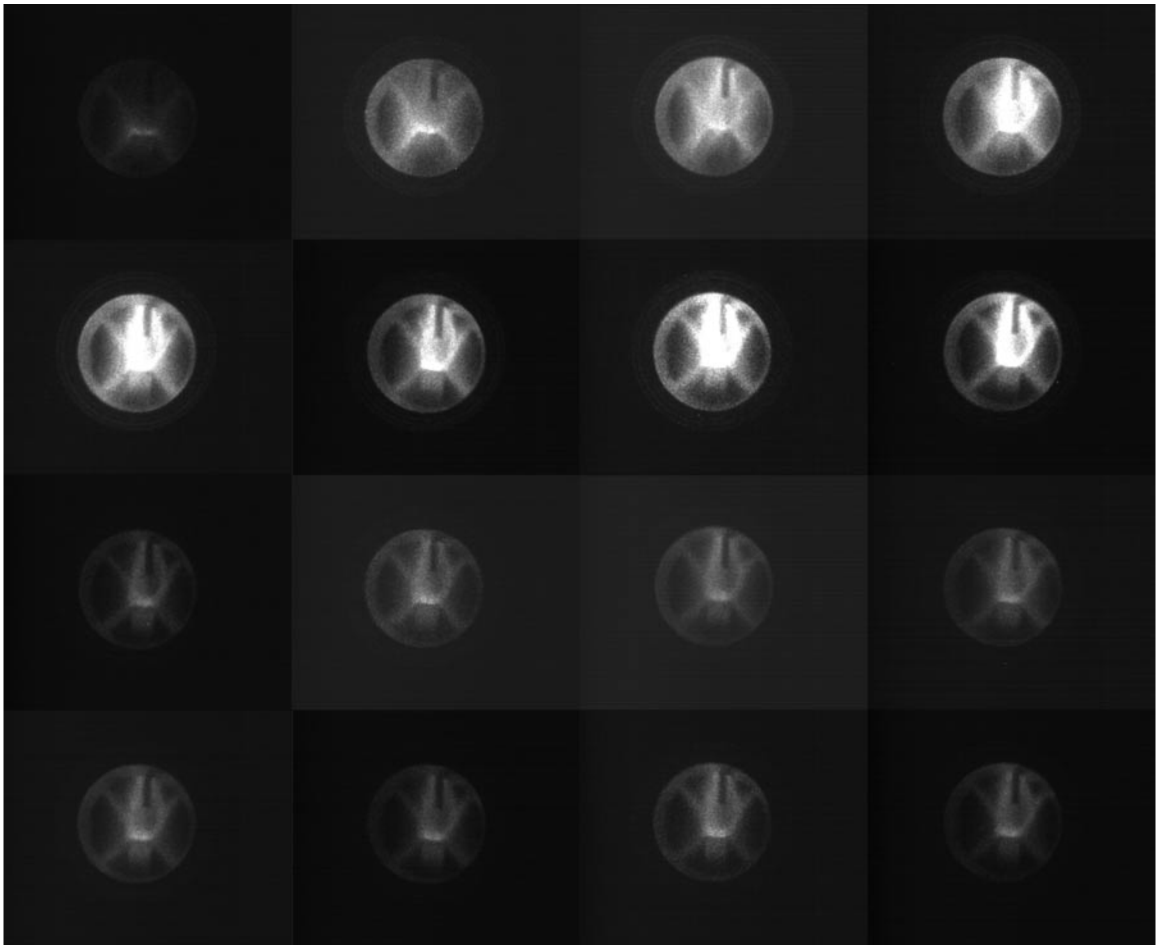

Figure 5.8. Imacon photography of plasma breakdown in the portable device when two ceramic breaks are used, along with the 1/8” diameter electrode tips. Intense plasma emission is seen in the center of the device, where the laser will pass during LIF experiments.

The photomultiplier detects an appreciable signal of spontaneous emission at 460.96 nm when the portable device is operated with typical experimental parameters of 40 V on the Helmholtz coil power supply and 1.6 kV on the breakdown capacitor connected across the device electrodes. The probing laser is directed through the two windows of the portable device that are perpendicular to the window through which the photomultiplier views the plasma. The appropriate time delay between plasma formation and laser firing has been identified empirically; the photodiode used for this same purpose in the spheromak experiment is placed just outside the window through which the laser exits the portable device. Appropriate adjustments are then made to synchronize the laser's transit through the chamber with a desired time during the plasma discharge.

The wavelength of the dye laser is first tuned to 611.49 nm, the natural resonant wavelength of the Ar II transition of interest. No induced fluorescence is observed from the plasma at this setting, and the experiment proceeds with the laser wavelength changed in 3 pm increments. However, even at wavelengths up to ±100 pm away from the central 611.49 nm, no LIF signal can be seen. Subsequent experiments using different values for experimental timing and voltages, as well as experiments performed with the dye laser operating in a broadband LIF mode, have failed to produce a detectable LIF signal.

5.4 Discussion

The portable plasma device was assembled for the purpose of providing a mobile plasma source that could assess the functionality of the optical fiber used for LIF experiments. Unfortunately, no induced fluorescence has yet been seen in Ar II plasmas produced in the device. If a signal is present, it may be at too weak of a signal level to be detected above the noise level present in the photomultiplier. One possible explanation for a weak signal would be a lack of sufficient target plasma ions present in the device. A rough estimate of particle density prior to breakdown can be provided by the ideal gas law, PV=nRT, as argon gas is being used. The pressure P has been set at 500 mTorr, while the internal volume of the portable device is approximately $4 \cdot 10^{-4}$ m^{-3}. At room temperature, these values suggest that n=10^{-5} mol=$6 \cdot 10^{18}$ gas molecules are present in the device. Thus, the particle density is ~10^{22} m^{-3}, close to ion densities found in the spheromak experiment. Nevertheless, the number of particles present in the narrow region where plasma emission is observed in the photographs in Figure 5.9 might still be insufficient to produce a detectable LIF signal. In addition, if the ion temperature is low, emission line broadening due to Doppler considerations may also be negligible, such that the ion distribution function has an extremely narrow line width.

Nevertheless, the fact that the first generation portable device has produced Ar II plasmas that spontaneously emit at the desired 460.96 nm wavelength suggests that generating plasmas from which LIF signals can be detected may only be a matter of scaling up the device parameters. The pd product presently used in the device is approximately 1 Torr-cm, close to the minimum of the Paschen curve. A tenfold increase in pressure should increase the number of ions present in the plasma while still leaving the voltage V_{min} required for breakdown well within the capabilities of the discharge capacitor bank. Of course, in any future enhancement of the portable device, it would be important to maintain the device's portability, recalling its primary purpose of providing a means to assess LIF equipment used in various locations.

5.5 References

A. Von Engel, *Ionized Gases* (Clarendon Press, 1965).

A.D. Bailey III, R.A. Stern, and P.M. Bellan, "Measurement of coherent drive-eave ion-fluid velocity field when ion dynamics are stochastic," *Phys. Rev. Let.*, **71(19)**, 3123 (1993).

J.M. McChesney, R.A. Stern, and P.M. Bellan, “Observations of fast stochastic ion heating by drift waves,” *Phys. Rev. Let.*, **59(13)**, 1436 (1987).

Chapter 6
Summary and Discussion

6.1 Introduction

This chapter summarizes the experimental results that have been obtained in laser induced fluorescence experiments performed on plasmas produced in the Caltech coaxial and coplanar spheromak devices. Some of the remaining obstacles that serve to limit the usefulness of the LIF diagnostic as applied to these devices are discussed, including suggestions for how these problems might best be addressed. Recommendations for future expansion of this course of investigation are also proposed.

6.2 Experimental Results

The ordinarily separate fields of spheromak research and laser induced fluorescence have been combined successfully in the investigations described in this thesis. While most previous spheromak experiments have focused on the study of hydrogen plasmas, the nature of laser induced fluorescence necessitated that the present work follow a different path. Argon plasmas have been produced in a spheromak confinement configuration, with the observed evolution of plasma topology consistent with the expected relaxation to a minimum energy Taylor state. Laser induced fluorescence signals have been observed in these argon spheromak plasmas, and the ion parameters calculated from these measurements are in reasonable agreement with estimates obtained from additional independent diagnostics.

6.3 Challenges

Arguably the most limiting characteristic of the present implementation of the LIF diagnostic technique is the slow rate at which experiments can be performed and data collected. LIF experiments performed at Caltech on the Encore tokamak enjoyed the advantage of producing 15 plasma discharges per second for study (Sanders 1998, among others). In comparison, the average time between plasma discharges in both the coaxial and coplanar spheromak experiments is on the order of one minute. Any method that can increase data throughput will improve an LIF experiment by reducing the statistical noise observed for a given set of observations and by permitting the inclusion of measurements performed under a variety of experimental conditions, rather than just a select few. Changing the rate at which plasma discharges are generated in the present spheromak experiment is impractical; a limit on the firing rate is imposed by the time required for recharging of the stuffing flux and gas valve capacitor banks, and as such the experiment itself cannot be performed at an appreciably faster rate.

However, there are ways in which more LIF data might be obtained for each individual plasma discharge. Probing the spheromak plasmas with a CW laser, rather than one operating on a pulsed power supply, should greatly expedite the measurement of ion parameters as a function of time into the plasma discharge. For a pulsed laser to probe the ~25 μs duration of an argon plasma produced by the coplanar device in 0.5 μs steps, a total of 50 sets of data comparable to one of those presented in this thesis would be required. With all experimental apparatus functioning normally, such an undertaking would require several months, during which time experimental conditions would need to be kept as constant as possible. By contrast, the use of a CW laser would allow for the same set of measurements to be performed in just two experimental runs, one with the laser turned on and one with the laser off to provide the background spontaneous light emission level.

Another possible means for increasing data throughput would be to have multiple intersections of the laser beam and plasma during an individual plasma discharge. This procedure has been attempted on plasmas produced in the coplanar spheromak device, using optics mounted outside the vacuum chamber to refocus and redirect the laser beam back to the plasma, as shown in Figure 6.1. The laser first intersects the plasma with the beam perpendicular to the axis of the spheromak, in the same manner as in the experi-

Side view

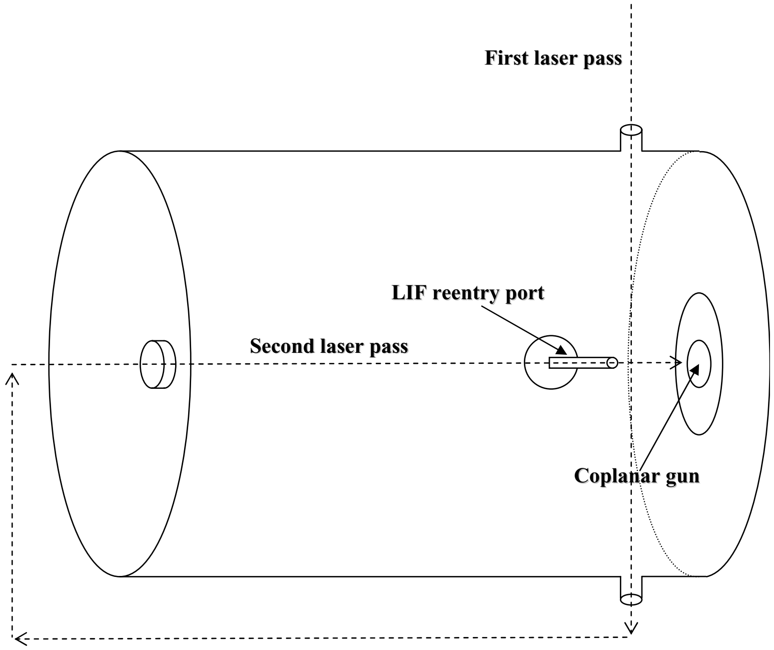

Top view, second laser pass

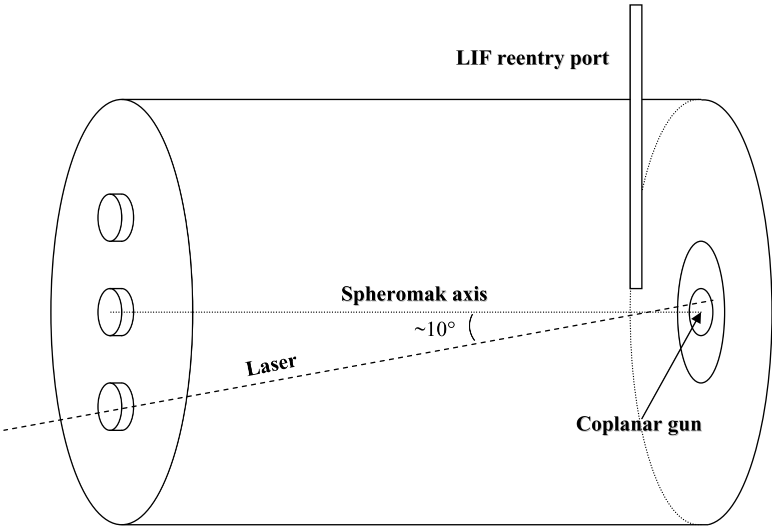

Figure 6.1. Experimental configuration to produce two LIF signals per plasma discharge in the coplanar spheromak experiment. The laser first intersects the plasma with the beam traveling perpendicular to the spheromak axis. After the beam exits the vacuum chamber through a viewport, it is redirected by a series of mirrors back into the chamber to intercept the plasma again, this time with the beam nearly parallel to the spheromak axis.

ments detailed in Section 4.4. After this first intersection, the laser exits the vacuum chamber via a window on the opposite side of the chamber. A series of mirrors then redirects the beam to reenter the vacuum chamber along the same path used for the on-axis LIF measurements described in Section 4.5. The laser travels ~9 m between the two intersections with the plasma; the ~30 ns required for light to traverse this distance is in fact a necessary delay, so that the two LIF signals (each of which is expected to last ~20–30 ns) may be distinguished by the photomultiplier. Unfortunately, only one LIF peak has been observed in this experimental configuration to date; this signal is believed to be induced fluorescence associated with the first pass of the laser, based upon the time at which the peak is observed. A second peak may be present but at a diminished level that cannot be detected above the ~10 mV noise level recorded by the photomultiplier. Such a diminished signal amplitude might be caused by the depletion of target ions in the region of interest after the first laser pass or by decreased laser energy due to beam divergence over the longer path traveled in the second laser pass. However, in time it should be possible to develop a multiple beam pass configuration that detects multiple LIF signals and thus increases the rate of data collection.

6.4 Suggestions for Future Work

6.4.1 LIF Optical Probe

The present work has only studied plasmas that have propagated a considerable distance from the spheromak device electrodes. As a result, significant changes in plasma morphology—including the merger of the spider legs to form the central column in the coplanar experiment—have already occurred by the time LIF measurements are made. This limitation is unavoidable so long as the laser and photomultiplier are located outside the vacuum chamber and forced to interact with the plasma through one of the available fixed-position viewports.

Palmer, Gekelman, and Vincena (2005) have assembled a probe that allows for the laser and emitted light viewing optics to be placed inside the vacuum chamber and arbitrarily close to the region of plasma to be studied, reducing the amount of background spontaneous emission through which an LIF signal must otherwise be viewed. An optical fiber within the body of the probe directs the laser into the plasma, while another fiber transmits emitted fluorescent light back to the photodetection system. The use of such a probe in Caltech spheromak experiments should enable the study of specific locations of interest with the spheromak plasma, including areas close to the gun electrodes, as well as provide the benefit of reducing the amount of background fluorescent light collected.

6.4.2 LIF Experiments on Plasmas Composed of Mixtures of Gases

Plasmas composed of a mixture of gases have been generated in the coplanar spheromak device by You, Yun, and Bellan (2005). In these experiments, neon gas is injected through the 1/4” apertures on the anode, while nitrogen enters through the cathode. Plasma breakdown and evolution is observed to follow the same sequence of events as described in Section 4.2. Imacon camera photography allows for differentiation of the two gases within the plasma flow via the use of narrow bandwidth line filters centered on wavelengths found in the emission spectrum of nitrogen.

The You experiment suggests a possible means for applying the LIF diagnostic technique to the study of ionized hydrogen plasmas, not possible under normal circumstances as LIF requires the presence of at least one electron in an orbital associated with the plasma ion. If a plasma composed of a mixture of hydrogen and another gas can be formed, LIF could be used to calculate estimates of the ion parameters of the second gas. If the two species may be assumed to be confluent, then the ion parameters of hydrogen should be approximately the same as those of the other gas. The validity of this assumption will be highly dependent upon the choice of the second gas species, which should have a molecular mass as close to that of hydrogen as possible. Helium is the obvious choice, and one for which numerous LIF transition schemes are known, although other light gases may also yield meaningful results.

6.5 Concluding Thoughts

As the use of plasma-based technology becomes more ubiquitous in the modern world—whether in semiconductor manufacturing, spacecraft propulsion, home electronics, or perhaps one day electrical power produced via nuclear fusion—it will always be necessary to have a reliable set of tools with which any given plasma may be measured. The present work has only begun to apply the versatile tool of laser induced fluorescence to the study of spheromak plasmas, and there should be no doubt that future study will reap the rewards of an even greater understanding of this simple yet promising confinement concept.

6.6 References

N. Palmer, W. Gekelman, and S. Vincena, "Measurement of ion motion in a shear Alfvén wave," *Phys. Plas.*, **12**, 072102 (2005).

S.J. Sanders, "Plasma ion dynamics in large-amplitude drift waves: stochasticity, collisions, orbit loss, and recycling," (Ph.D. dissertation, California Institute of Technology, 1998).

S. You, G.S. Yun, and P.M. Bellan, "Dynamic and stagnating plasma flow leading to magnetic-flux-tube collimation," *Phys. Rev. Let.*, **95**, 045002 (2005).